Scattering Amplitudes Beyond the Planar Limit of Quantum Chromodynamics

Giulio Gambuti

New College
University of Oxford

A thesis submitted for the degree of
Doctor of Philosophy

Trinity 2024

Abstract

Scattering amplitudes provide insight into the all-orders structure of gauge theories. Particularly rich is their non-planar sector, where new and interesting physical phenomena appear. This thesis aims to push the boundaries of perturbative scattering amplitudes, with special emphasis on calculations in massless Quantum Chromodynamics. We review the colour and helicity decomposition of gauge theory amplitudes, as well as the structure of their ultraviolet and infrared divergences. We then discuss the application of state-of-the-art methods to the computation of all four-point three-loop scattering amplitudes in Quantum Chromodynamics. As an immediate consequence we both verify the structure of infrared divergences and extract the gluon Regge trajectory at the corresponding perturbative order. We further describe the computation of five-gluon scattering at the two-loop order, with special emphasis on the multi-scale complexity of this process. Finally, we explore the idea of simplifying the integrand representation of gauge theoretic scattering amplitudes by leveraging their highly-constrained infrared structure. We provide a proof-of-concept application to two-loop four-gluon scattering amplitudes.

Scattering Amplitudes Beyond the Planar Limit of Quantum Chromodynamics

Giulio Gambuti

New College

University of Oxford

A thesis submitted for the degree of

Doctor of Philosophy

Trinity 2024

Acknowledgements

Personal

This journey would not have been possible without my supervisors Fabrizio and Lorenzo. On top of being brilliant scientists they have both proved to be excellent teachers and friends. I consider myself very lucky for having had the opportunity of sharing these four years with them. Having started my DPhil adventure with him, a special thanks goes to Lorenzo.

I am also thankful to my collaborators Amlan Chakraborty, Andreas von Manteuffel, David Kosower, Federica Devoto, Federico Buccioni, Piotr Bargiela and Pavel Novichkov. Doing research with them has been an incredibly instructive experience and a great pleasure. Among them, I would like to especially thank Federica and Federico, with whom I have worked side by side for more than a year now.

I am also grateful for the countless opportunities to discuss physics with other members of the department. They have invariably stimulated me to broaden my knowledge. In particular, I would like to extend my gratitude to my office-mate and friend Thomas Harvey for his contagious excitement about all things physics and his atomic-clock precision in reminding me of the 11 am coffee.

Outside of the theoretical physics world, I particularly cherish the time spent in Oxford with my friend Patrick Murton, who was my housemate for two years.

I would like to express my deepest gratitude to my partner Sara, with whom I shared my life all the way from our undergraduate years to now. She has been an infinite source of support, love and happiness and made it all worth it. I thank her for putting up with these four years split between London and Oxford and I very much look forward to sharing every day with her from now on.

Finally, I would like to thank my parents, to which I am eternally grateful for being the foundation upon which all this was built and for representing a guiding light throughout the years.

Institutional

My graduate research was supported by the Royal Society, by the Science and Technology Facilities Council (STFC) and by the Oxford Physics department.

Abstract

Scattering amplitudes provide insight into the all-orders structure of gauge theories. Particularly rich is their non-planar sector, where new and interesting physical phenomena appear. This thesis aims to push the boundaries of perturbative scattering amplitudes, with special emphasis on calculations in massless Quantum Chromodynamics. We review the colour and helicity decomposition of gauge theory amplitudes, as well as the structure of their ultraviolet and infrared divergences. We then discuss the application of state-of-the-art methods to the computation of all four-point three-loop scattering amplitudes in Quantum Chromodynamics. As an immediate consequence we both verify the structure of infrared divergences and extract the gluon Regge trajectory at the corresponding perturbative order. We further describe the computation of five-gluon scattering at the two-loop order, with special emphasis on the multi-scale complexity of this process. Finally, we explore the idea of simplifying the integrand representation of gauge theoretic scattering amplitudes by leveraging their highly-constrained infrared structure. We provide a proof-of-concept application to two-loop four-gluon scattering amplitudes.

Contents

1 A Primer in Quantum Chromodynamics **1**

1.1 Introduction 1

1.2 The QCD Lagrangian 3

1.3 Feynman Rules 6

1.4 Renormalisation 7

1.5 Scattering Amplitudes and LSZ Reduction 12

2 The Structure of Scattering Amplitudes **15**

2.1 Helicity Amplitudes 18

2.1.1 Spinor Helicity Formalism 21

2.1.2 Tensor Projection 23

2.2 Colour Decomposition 24

2.3 Feynman Integrals 28

2.3.1 Representations 28

2.3.2 Integration-by-parts Relations 32

2.3.3 Other Integral Relations 33

2.3.4 The Laporta Algorithm 35

2.3.5 Differential Equations and Iterated Integrals 36

2.3.6 Divergences of Feynman Integrals 39

2.4 Divergences of Scattering Amplitudes 45

2.4.1 Renormalisation of UV Divergences 45

2.4.2 Factorisation of IR Divergences 47

3 Three-Loop Four-Point Scattering **52**

3.1 Introduction . . . 52
3.2 Colour and Helicity Decomposition . . . 53
3.3 Loop Integrals . . . 59
3.4 Analytic Continuation . . . 62
3.5 Crossed Channels and Equal Flavour Amplitudes . . . 66
3.6 Infrared Structure and Quadrupole Radiation . . . 67
3.7 Analytic Results and Numerical Evaluation . . . 69
3.8 The Gluon Regge Trajectory . . . 72

4 Two-Loop Five-Gluon Scattering **79**

4.1 Introduction . . . 79
4.2 Colour Decomposition . . . 80
4.3 Helicity Amplitudes . . . 82
4.4 Loop Integrals . . . 87
4.5 Results . . . 92

5 Infrared-Finite Integrals **95**

5.1 Introduction . . . 95
5.2 Dimension-Independent Integral Relations . . . 97
5.3 IR-finite Feynman Integrals . . . 100
5.3.1 Ideals of IR-finite Integrals . . . 102
5.3.2 IR Power Counting . . . 102
5.3.3 Example: Massless Box . . . 105
5.3.4 Evanescent Integrands . . . 109
5.3.5 Example: Massless Pentagon . . . 111
5.4 Examples of Finite Ideals . . . 112
5.4.1 Planar Double Box . . . 112
5.4.2 Ladder Integrals: an All-Loops Conjecture . . . 119
5.4.3 Non-Planar Double Box . . . 121
5.4.4 Two-Loop Beetle . . . 124

5.4.5 Two-Loop Four-Gluon Helicity Amplitudes 125

6 Conclusions and Outlook **128**

Appendices

A Constants **131**

A.1 Cusp and Collinear Anomalous Dimensions in QCD 131

A.2 Impact Factors for the High-Energy Limit 132

B Spinor Helicity Formulas and Conventions **135**

C Rational Coefficients of the All-Plus Amplitude **137**

References **139**

1

A Primer in Quantum Chromodynamics

Contents

1.1 Introduction 1
1.2 The QCD Lagrangian 3
1.3 Feynman Rules 6
1.4 Renormalisation 7
1.5 Scattering Amplitudes and LSZ Reduction 12

1.1 Introduction

The dynamics of the strong force, at high energies, are described by a quantum field theory whose fundamental degrees of freedom are quarks and gluons. Quarks are spin-1/2 fermions, while gluons are spin-1 bosons which mediate strong interactions. They are packaged together in a non-abelian gauge theory with a $SU(N_c)$ symmetry group which endows them with an extra quantum number, the colour charge. This theory is referred to as Quantum Chromodynamics, or QCD.

The non-abelian nature of QCD, *i.e.* the fact that its force-carrying particles are themselves charged under the same interaction, leads to interesting and complex dynamics. One of its most remarkable effects is *confinement*, the fact that asymptotic states of QCD are bound states of quarks and gluons with no overall colour charge.

Roughly speaking, the strong force among quarks and gluons increases with their distance, so that configurations with widely separated coloured states are highly unfavoured. Another important feature of QCD is *asymptotic freedom*. It predicts that at very short distances the intensity of the strong force should decrease, allowing quarks and gluons to be treated as weakly coupled quantum fields. Asymptotic freedom ultimately enables us to study the high-energy dynamics of QCD via perturbative calculations and is at the basis of the success of scientific programs such as the Large Hadron Collider (LHC) in comparing first-principle theoretical predictions with experimental data.

The bridge which connects theory and experiment is *differential cross sections*, which represent the probability of given processes to take place. At the core of cross sections lie scattering amplitudes, which describe the high-energy quantum mechanical interactions among fundamental fields. Though originally introduced in the context of particle physics phenomenology, scattering amplitudes, or more generally correlation functions in QFT, turned out to be interesting objects of intrinsic mathematical interest. They serve as a testing ground for ideas in complex analysis, group and graph theory as well as computer science, to name a few. Green's functions in QFT can be extremely complex or beautifully simple depending on their representation and are connected by inter-theory relations, many of which are yet to be understood. In short, they offer the opportunity of tackling a physically meaningful problem while delving into the mathematics of QFT.

It is the goal of this thesis to review, apply and extend some of the mathematical methods required for the computation of scattering amplitudes, with special emphasis on analytic QCD computations. The remainder of this chapter contains a brief review of QCD and related concepts which will be used in the rest of the thesis. In chapter 2 we review in more detail the analytical methods employed in the computation of gauge theory scattering amplitude. Chapters 3 and 4 describe

state-of-the-art applications of these methods in the context of four-point three-loop and five-point two-loop QCD scattering amplitudes respectively. Chapter 5 explores the possibility of better exposing infrared factorisation of massless gauge theory amplitudes at the level of the loop integrand. We conclude with some final comments in chapter 6.

1.2 The QCD Lagrangian

We start our review of QCD by looking at its symmetry group $SU(N_c)$, the group of unitary matrices with unit determinant. A transformation $U(\alpha) \in SU(N_c)$ can always be expressed in terms of a set of real coordinates α_a as

$$U(\alpha) = \exp(i\alpha_a T^a)\,, \tag{1.1}$$

where the T^a are a basis of $N_c^2 - 1$ traceless hermitian matrices which satisfy the algebra

$$[T^a, T^b] = i\, f^{abc}\, T^c\,, \tag{1.2}$$

and can be chosen such that the structure constants f^{abc} are a real and fully antisymmetric tensor. Using T_R^a to denote the generators in a representation R, it is always possible to find a basis with the property

$$\mathrm{Tr}[T_R^a T_R^b] = C_1(R)\delta^{ab}\,. \tag{1.3}$$

Here we fix the normalisation of the basis elements in the fundamental representation by requiring that

$$C_1(F) = \mathrm{Tr}[T_F^a T_F^b] = \frac{1}{2}\,\delta^{ab} \implies C_1(F) = \frac{1}{2}\,. \tag{1.4}$$

This fixes $C_1(R)$ for all representations, and in particular in the adjoint representation, for which $(T_A^a)_{bc} = if^{abc}$, we find $C_1(A) = N_c$. Another important quantity is the quadratic Casimir operator $T_R^a T_R^a$ which commutes with all generators and by Schur's Lemma is proportional to the identity

$$T_R^a T_R^a = C_2(R)\,\mathbb{I}_R\,. \tag{1.5}$$

Due to the normalisation choice made in eq. (1.4), we find

$$C_2(F) \equiv C_F = \frac{N_c^2 - 1}{2N_c}\,, \qquad C_2(A) \equiv C_A = N_c\,. \tag{1.6}$$

Having fixed the group-theoretic notation, we turn to the QCD lagrangian. To represent the different quark flavours, we introduce n_f copies of the Dirac field Ψ, transforming under the fundamental representation of $SU(N_c)$, as well as the covariant derivative $\mathcal{D}_\mu$ defined by requiring that the Dirac lagrangian

$$\mathcal{L}_{Dirac} = \sum_{f=1}^{n_f} i\overline{\Psi}_f \left(\not{\mathcal{D}} - m_f\right) \Psi_f \tag{1.7}$$

is invariant under the local transformation

$$\psi(x) \to U(x)\psi(x), \qquad \text{with} \quad U(x) = \exp\left(i\alpha_a(x)T^a\right). \tag{1.8}$$

Above we defined $\not{\mathcal{D}} = \mathcal{D}^\mu\gamma_\mu$, where the Dirac gamma matrices satisfy the Clifford algebra $\{\gamma_\mu, \gamma_\nu\} = 2g_{\mu\nu}$. We also defined the quark masses m_f. At the typical energy scales of LHC partonic interactions, one can approximately set the masses of the five lightest quarks to zero, while the mass of the top quark $m_t \approx 170$ GeV cannot be neglected.

Instead, below the center-of-mass energy threshold for top-quark production ($\sqrt{s} \leq 2m_t$), one can expand observables in the ratio $s/4m_t^2 < 1$. For small enough energies, the first order in the expansion is provides a good approximation, [1] which we adopt in this thesis.

As a result we will consider massless QCD with five active quarks, but nevertheless retain the full dependence on the number of quark flavours n_f, setting $n_f = 5$ only when numerical evaluations are required.

Local gauge invariance of eq. (1.7) can be achieved by asking that $\mathcal{D}^\mu U(x) = U(x)\mathcal{D}^\mu$, which in turn is obtained by writing the covariant derivative in terms of a gauge connection $A^\mu = A^\mu_a T^a$, also known as gluon field. In particular we write

$$\mathcal{D}_\mu = \mathbb{I}_R\partial_\mu + igT^a_R A^a_\mu\,, \tag{1.9}$$

[1] For instance at $\sqrt{s} \sim 100$ GeV one has $s/4m_t^2 \sim 0.1$.

where the representation R depends on what the derivative is acting on. This fixes the transformation of the gluon field to

$$A^\mu(x) \to U(x)A^\mu(x)U^{-1}(x) + i\,g\,U(x)\partial^\mu U(x)^{-1}\,. \tag{1.10}$$

The most general renormalisable lagrangian density satisfying locality and symmetric under eqs. (1.8) and (1.10) reads

$$\mathcal{L} = -\frac{1}{2}\mathrm{Tr}F^{\mu\nu}F_{\mu\nu} + \sum_{f=1}^{n_f} i\overline{\Psi}_f \not{\mathcal{D}}\Psi_f + \theta\frac{g^2}{32\pi^2}\epsilon_{\mu\nu\rho\sigma}\mathrm{Tr}F^{\mu\nu}F^{\rho\sigma}\,, \tag{1.11}$$

where we defined the gluon field strength

$$F^{\mu\nu} \equiv T^a F_a^{\mu\nu} = [\mathcal{D}^\mu, \mathcal{D}^\nu] \implies F_a^{\mu\nu} = \partial^\mu A_a^\nu - \partial^\nu A_a^\mu - g f_{abc} A_b^\mu A_c^\nu \tag{1.12}$$

and introduced the dimensionless parameter θ. In the path integral approach to QFT, one has to eliminate the gauge redundancy of the lagrangian in eq. (1.11) before the sum over field configurations can be meaningfully performed. The redundancy can be removed[2] by following the Faddeev-Popov gauge fixing procedure [2]. In the presence of non-abelian gauge fields one is required to introduce interacting Grassman-valued *ghost* fields η_a (see *e.g.* [3]). Using a covariant gauge-fixing condition, the result is the gauge-fixed massless QCD lagrangian

$$\mathcal{L}_{QCD} = \mathcal{L}_{YM} + \mathcal{L}_{Dirac} + \mathcal{L}_{g.f.} + \mathcal{L}_{ghost} + \mathcal{L}_\theta\,, \tag{1.13}$$

whose terms are defined as

$$\begin{aligned}
\mathcal{L}_{YM} &= -\frac{1}{2}\mathrm{Tr}F^{\mu\nu}F_{\mu\nu} = -\frac{1}{4}F_a^{\mu\nu}F^a_{\mu\nu}\,,\\
\mathcal{L}_{Dirac} &= \sum_{f=1}^{n_f} i\overline{\Psi}_f \not{\mathcal{D}}\Psi_f\,,\\
\mathcal{L}_{g.f.} &= -\frac{1}{2\xi}(\partial_\mu A_a^\mu)^2\,,\\
\mathcal{L}_{ghost} &= -(\partial_\mu\eta_a)^\dagger \mathcal{D}^\mu_{ab}\eta_b\,,\\
\mathcal{L}_\theta &= \theta\frac{g^2}{32\pi^2}\epsilon_{\mu\nu\rho\sigma}\mathrm{Tr}F^{\mu\nu}F^{\rho\sigma}\,.
\end{aligned} \tag{1.14}$$

[2]Apart from the Gribov ambiguity [1], which however plays no role in perturbative computations.

The QCD lagrangian (1.13) depends on five parameters: the strong coupling g, the dimension of the gauge group N_c, the number of quark flavours n_f, the covariant gauge fixing parameter ξ and the θ-parameter.

The $\mathcal{L}_\theta$ contribution to the QCD lagrangian breaks parity invariance (P) as well as time reversal symmetry (T $\equiv$ CP). However, experimental evidence [4, 5] for strong interactions sets the upper bound $\theta \leq 10^{-10}$. The observed, but unexplained, smallness of the θ-parameter takes the name of *strong CP problem* and constitutes a currently active area of research.

Nevertheless, in this thesis we will only be concerned with perturbation theory and will ignore the CP violating θ-term. In fact it possible to write it as a total derivative

$$\epsilon_{\mu\nu\rho\sigma} F_a^{\mu\nu} F^{a,\rho\sigma} = 4\partial_\mu \epsilon^{\mu\nu\rho\sigma} A_\nu^a \left(\partial_\rho A_\sigma^a - \frac{2}{3} g f^{abc} A_\rho^b A_\sigma^c \right) , \tag{1.15}$$

which does not contribute to the Feynman rules. Because $\mathcal{L}_\theta$ is a total derivative, its space-time integral $\int \mathrm{d}^4x \mathcal{L}_\theta(x)$ only depends on boundary information and is usually referred to as topological. Furthermore, working in a theory with massless fermions, the θ parameter can always be shifted away via field redefinitions [3].

1.3 Feynman Rules

The lagrangian (1.13) provides us with Feynman rules, a powerful tool to perform perturbative calculations in QCD. Denoting gluons with curly lines, quarks with solid lines and ghosts with dashed lines we find the propagators

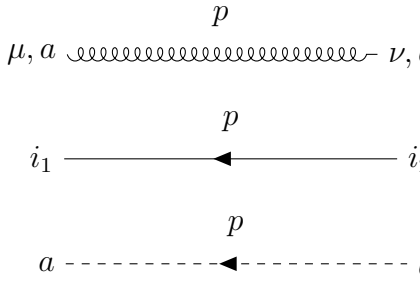

$$\begin{aligned} &= \frac{i\,\delta_{ab}}{p^2 + i\varepsilon} \left(-g_{\mu\nu} + (1-\xi)\frac{p_\mu p_\nu}{p^2} \right) , \\ &= \frac{i\,\delta_{i_1 i_2}\, \not{p}}{p^2 + i\varepsilon} , \\ &= \frac{i\,\delta^{ab}}{p^2 + i\varepsilon} , \end{aligned} \tag{1.16}$$

the three-point vertices

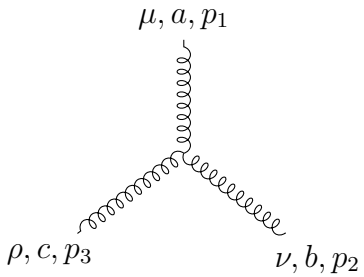

$$= g\, f^{abc}\, [g^{\mu\nu}(p_2 - p_1)^\rho + g^{\nu\rho}(p_3 - p_2)^\mu + g^{\rho\mu}(p_1 - p_3)^\nu] \,,$$

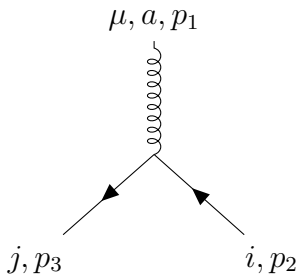

$$= i\, g\, \gamma^\mu (T^a)_j{}^i \,,$$

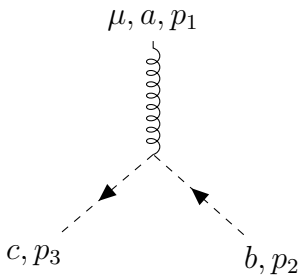

$$= g\, f^{abc} p_3^\mu \,, \tag{1.17}$$

and the four-point gluon vertex

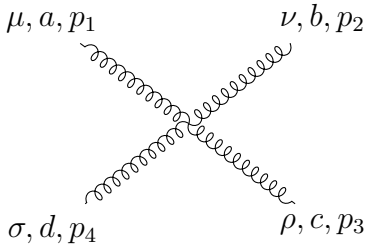

$$\begin{aligned} = -i\, g^2 \Big[& f^{abe} f^{cde} (g^{\mu\rho} g^{\nu\sigma} - g^{\mu\sigma} g^{\nu\rho}) + \\ & f^{ace} f^{bde} (g^{\mu\nu} g^{\rho\sigma} - g^{\mu\sigma} g^{\nu\rho}) + \\ & f^{ade} f^{bce} (g^{\mu\nu} g^{\rho\sigma} - g^{\mu\rho} g^{\nu\sigma}) \Big] . \end{aligned} \tag{1.18}$$

Above all momenta in eqs. (1.17) and (1.18) are taken to be incoming, so that for any vertex the sum of external momenta vanishes.

1.4 Renormalisation

In order to use QCD, or any other QFT aiming to describe Nature, to make empirical predictions it is mandatory to first fix the parameters of the lagrangian by comparison to (some) experimental data. Stated differently, one wishes to connect the parameters of the theory to observables. In general, in a quantum theory this could be subtle, especially if the theory develops, through quantum corrections, sensitivity to very short distance physics. This can be formally achieved via the procedure of renormalisation, whereby the parameters in the lagrangians are rewritten in terms of a set of *reference observables*. The theory is said to be

renormalisable if only a finite number of reference observables is needed to fix all of its free parameters. QCD and more in general gauge theories are renormalisable QFTs [6].[3] More concretely, one can usually fix all parameters of the lagrangian at some reference scale μ_R, usually called *renormalisation* scale, by rewriting them in terms of the reference observables measured at that scale. It turns out that in QCD the *bare* fields and coupling appearing in eq. (1.13) (which in a slight change of notation will be denoted by a 0 subscript) can be written in terms of multiplicative renormalisation factors and renormalised quantities:

$$g_0 = \sqrt{Z_g} g\,, \quad A_0 = \sqrt{Z_A} A\,, \quad \psi_0 = \sqrt{Z_\psi}\psi\,, \quad \eta_0 = \sqrt{Z_\eta}\eta\,, \tag{1.19}$$

where all indices have been left implicit. The renormalisation factors Z_i indirectly carry information on the reference observables and renormalisation scale and effectively define the renormalised fields and coupling. The QCD lagrangian, expressed in terms of renormalised quantities (and at $\theta = 0$) reads

$$\begin{aligned}\mathcal{L}_{QCD} = &\\ &-\frac{1}{4}Z_A(\partial^\mu A^\nu_a - \partial^\nu A^\mu_a)^2 + \sqrt{Z_g}Z_A^{3/2} g f_{abc}(\partial^\mu A^\nu_a)A^\mu_b A^\nu_c - \frac{1}{4}Z_g Z_A^2 g^2 f_{abe} f_{cde} A^\mu_a A^\nu_b A^\mu_c A^\nu_d \\ &+ iZ_\psi \overline{\Psi}\partial\!\!\!/\Psi - \sqrt{Z_g Z_A}Z_\psi g A^\mu_a \overline{\Psi} T^a \gamma_\mu \Psi - Z_\eta(\partial_\mu \eta_a)^\dagger \partial^\mu \eta_a - i\sqrt{Z_g}Z_\eta g A^\mu_a f^{abc}(\partial_\mu \eta_b)^\dagger \eta_c \\ &- \frac{1}{2\xi}Z_A(\partial_\mu A^\mu_a)^2\,.\end{aligned} \tag{1.20}$$

Practically, the structure of the renormalised lagrangian tells us which combination of correlation functions is needed to fully determine the renormalisation factors. Importantly, the renormalisation procedure described above can be carried out perturbatively, truncating correlators up to a given loop order.

Nevertheless, any prediction provided by the theory should not depend on the choice of μ_R, which is entirely arbitrary.[4] In QCD, this is reflected in the fact that the renormalised coupling g, develops a dependence on μ_R, a phenomenon known as *running coupling*. It ensures consistency of the predictions by exactly compensating for the explicit dependence on μ_R of the perturbative coefficients.

[3] Renormalisability of QCD was proven by exploiting the quantum-level BRST symmetry [7, 8] of $\mathcal{L}_{QCD}$.

[4] Apart from having to be within the range of validity of the theory.

As we will discuss in the next chapter, QCD scattering amplitudes and observables, when expressed in terms of the bare parameters, develop singularities associated with short-distance or *ultra-violet* (UV) degrees of freedom. They are called UV divergences and perturbatively they appear as infinities arising from the integration over unbounded loop momenta. Indeed, the presence of UV divergences reinforces the idea that the lagrangian $\mathcal{L}_{QCD}$ does not describe a sensible quantum field theory, taken at face value. Fortunately, renormalisation automatically accounts for UV divergences, because it allows us to only talk about relative quantities, in which UV divergences never appear.

Practically, in order to perform calculations, for example the ones needed to fix the renormalisation factors Z_i, one needs to first regulate UV divergences. A physically intuitive way of doing this is to simply limit the integration over the loop momenta by introducing a cut-off scale Λ_{UV}. However this method breaks Lorentz as well as gauge invariance and is not well suited for current state-of-the-art calculations. A less intuitive but more effective way to regulate UV divergences is *dimensional regularisation* [6], where calculations are performed in $d \in \mathbb{C}$ space-time dimensions.

More specifically, integrals in dimensional regularisation are defined by the following axioms

- linearity

$$\int \mathrm{d}^d x \, (\alpha f(x) + \beta g(x)) = \int \mathrm{d}^d x \, \alpha f(x) + \int \mathrm{d}^d x \, \beta g(x) \,, \quad \alpha, \beta \in \mathbb{C} \,, \tag{1.21}$$

- translation invariance

$$\int \mathrm{d}^d x \, f(x + x_0) = \int \mathrm{d}^d x \, f(x) \,, \tag{1.22}$$

- scaling

$$\int \mathrm{d}^d x \, f(\lambda x) = \lambda^{-d} \int \mathrm{d}^d x \, f(x) \,, \quad \lambda \in \mathbb{C} \,. \tag{1.23}$$

They are also defined so that whenever an integral is convergent in $d_0 \in \mathbb{N}^+$ it should coincide with the standard integration in d_0 dimensions.

Writing $d = 4 - 2\epsilon$, UV divergences in the regulated theory manifest themselves as (multiple-)poles in ϵ. An important effect of dimensional regularisation is that the strong coupling acquires a mass dimension $[g] = \epsilon$. This can be made explicit in the renormalised lagrangian[5] by defining the dimensionless renormalised coupling $\overline{g}$ as

$$g \equiv \mu^{\epsilon}\, \overline{g}(\mu)\,, \tag{1.24}$$

where μ is an arbitrary energy scale. We also introduce the standard coupling $\alpha_s(\mu) = \overline{g}^2(\mu)/4\pi$ and the β-function together with its perturbative expansion

$$\mu\frac{d\alpha_s(\mu)}{d\mu} = \beta(\alpha_s(\mu)) - 2\epsilon\alpha_s(\mu)\,, \qquad \beta(\alpha_s) = -2\alpha_s \sum_{n=0} \beta_n \left(\frac{\alpha_s}{4\pi}\right)^{n+1}\,. \tag{1.25}$$

Because measured quantities are finite, it immediately follows that the renormalised lagrangian (1.20) should provide UV-finite observables. However this only fixes the renormalisation factors up to a finite shift, the finite terms are instead determined by our definition of the renormalised fields and coupling. The way in which this freedom is fixed is referred to as *renormalisation scheme*. Different schemes may be useful for different purposes and in the context of perturbative calculations in massless QCD the modified minimal-subtraction ($\overline{\text{MS}}$) scheme is a popular one and is the one which will be employed in this thesis. The standard minimal-subtraction (MS) scheme states that the renormalisation factors Z_i should be chosen as purely UV divergent terms, *i.e.* the corresponding counterterms should have no finite parts in ϵ. The $\overline{\text{MS}}$ scheme differs from the MS scheme by absorbing into the coupling renormalisation the extra factor $S_\epsilon = (e^{-\gamma_E}/4\pi)^\epsilon$ which can be ascribed to the d-dimensional loop integration. This can be summarised by defining $Z_g^{\overline{\text{MS}}}$ so that

$$\alpha_{s,0} S_\epsilon^{-1} = \alpha_s(\mu)\mu^{2\epsilon} Z_g^{\overline{\text{MS}}}\left[\alpha_s(\mu)\right]\,, \tag{1.26}$$

where $\alpha_{s,0} = g_0^2/4\pi$ and is independent of the arbitrary scale μ. Then $Z_g^{\overline{\text{MS}}}$, $Z_A^{\overline{\text{MS}}}$, $Z_\psi^{\overline{\text{MS}}}$ and $Z_\eta^{\overline{\text{MS}}}$ are fixed by requiring that their perturbative corrections have no finite parts in ϵ. Since $\overline{\text{MS}}$ is the only renormalisation scheme used in this thesis we

[5] By renormalised lagrangian we still mean the QCD lagrangian, but explicitly written in terms of renormalised quantities.

will drop the superscript from now on.

Differentiating both sides of eq. (1.26) with respect to $\log(\mu)$ and solving for Z_g order by order in α_s with the condition $Z_g = 1$ at $\alpha_s = 0$ allows us to write the coupling renormalisation factor in terms of the β-function. Up to third order in the coupling we find

$$Z_g[\alpha_s] = 1 - \left(\frac{\alpha_s}{4\pi}\right)\frac{\beta_0}{\epsilon} + \left(\frac{\alpha_s}{4\pi}\right)^2\left(\frac{\beta_0^2}{\epsilon^2} - \frac{\beta_1}{2\epsilon}\right) - \left(\frac{\alpha_s}{4\pi}\right)^3\left(\frac{\beta_0^3}{\epsilon^3} - \frac{7}{6}\frac{\beta_0\beta_1}{\epsilon^2} + \frac{\beta_2}{3\epsilon}\right) + \mathcal{O}(\alpha_s^4)\,. \tag{1.27}$$

The QCD β-function coefficients β_i have currently been computed up to five loops [9–14], but in this thesis we will only need the coefficients up to three loops:

$$\begin{aligned}
\beta_0 &= \frac{11}{3}C_A - \frac{2}{3}\,n_f\,,\\
\beta_1 &= \frac{1}{3}\left(34\,C_A^2 - 10\,C_A\,n_f\right) - 2\,C_F\,n_f\,,\\
\beta_2 &= -\frac{1415\,C_A^2\,n_f}{54} + \frac{2857\,C_A^3}{54} - \frac{205\,C_A\,C_F\,n_f}{18} + \frac{79\,C_A\,n_f^2}{54} + C_F^2\,n_f + \frac{11\,C_F\,n_f^2}{9}\,.
\end{aligned} \tag{1.28}$$

Eqs. (1.25) and (1.28) predict the variation of the coupling with the value of the scale μ. This is a very powerful statement: given an input value of $\alpha_s(\mu_R)$ at some scale μ_R we can in principle predict the value of the coupling at any other (perturbative) scale. Of course, computing the β-function at higher perturbative orders will yield more accurate predictions. Such an "initial condition" for the value of α_s is usually given for $\mu_R = m_Z$, where $m_Z = 91.187 \pm 0.002\,\text{GeV}$ is the mass of the Z boson and the corresponding value of the coupling is [15]

$$\alpha_s(m_Z) = 0.1179 \pm 0.0009\,. \tag{1.29}$$

Because $N_c = 3$ and $n_f \leq 16$, one finds that β_0 is positive indicating that the coupling is a positive and monotonically decreasing function of μ, at least as long as $\alpha_s(\mu)$ is small enough that perturbation theory can be trusted. In turn this implies asymptotic freedom at large values of μ. As mentioned in section 1.1, asymptotic freedom corresponds to the statement that perturbation theory becomes better and

better as the energy of the interactions grows. Conversely, as μ becomes smaller the coupling grows, suggesting a breakdown of perturbation theory.

1.5 Scattering Amplitudes and LSZ Reduction

Every QFT determines a set of quantum-mechanical states and a linear operator S, the S-matrix. The evolution from infinite past to infinite future of a state $|\alpha\rangle$ is determined by $S|\alpha\rangle$, so that the probability for a state $|\beta\rangle$ to be observed in the infinite future starting from an initial state $|\alpha\rangle$ is obtained from the modulus squared of the S-matrix element

$$S_{\alpha\beta} = \langle\beta|S|\alpha\rangle\,. \tag{1.30}$$

Conservation of probabilities implies unitarity of the S-matrix, $S^\dagger S = 1$.

In the context of particle physics it is interesting to consider processes involving final and initial states which are direct products of respectively n_{out} and n_{in} non-interacting single-particle states of definite momenta $p(p')$ and polarisations $\sigma(\sigma')$:

$$S_{in,out} = \Big\langle (p_1,\sigma_1),\ \ldots,\ (p_{n_{out}},\sigma_{n_{out}})\ \Big|S\Big|\ (p'_1,\sigma'_1),\ \ldots,\ (p'_{n_{in}},\sigma'_{n_{in}})\Big\rangle\ . \tag{1.31}$$

One of the main results in QFT is the Lehman-Symanzik-Zimmermann (LSZ) formula [16, 17], which relates Green's functions to S-matrix elements. Defining momenta in the all-outgoing convention, so that

$$\{p_1,\ldots,p_{n_{out}},p'_1,\ldots,p'_{n_{in}}\} \to \{p_1,\ldots,p_{n_{out}},-p_{1+n_{out}},\ldots,-p_{n_{in}+n_{out}}\} \tag{1.32}$$

and denoting the total number of particles involved in the process by $n = n_{in} + n_{out}$, we can write the LSZ reduction formula for particles of generic spin as

$$S_{in,out} = \lim_{p_i^2\to m_i^2}\left(\prod_{i=1}^{n}\int \mathrm{d}^d x_i\, e^{ip_i\cdot x_i}\frac{\xi_i^{A_i}\,(\Box_i)_{A_iB_i}}{i\sqrt{\mathcal{Z}_i}}\right)\ \langle\Omega\left|T\left\{\Phi_1^{B_1}(x_1)\ldots\Phi_n^{B_n}(x_n)\right\}\right|\Omega\rangle\ . \tag{1.33}$$

Let us unpack the equation above:

- Ω refers to the vacuum of the interacting theory,

- ξ_i is the polarisation vector corresponding to the field Φ_i and A_i and B_i are their appropriate Lorentz indices,
- $\Box_i$ is the coefficient of the term in the lagrangian quadratic in Φ_i and independent of the other fields,
- T is the time-ordering operator,
- $\mathcal{Z}_i$ is the single-particle pole residue of the exact two-point Green's function for the field Φ_i:

$$\int \mathrm{d}^d x\, e^{ip\cdot x} \left\langle \Omega \mid T\left\{\Phi_i^A(x)\Phi_i^B(0)\right\} \mid \Omega \right\rangle = \frac{i\mathcal{Z}_i\Delta_i^{AB}(p)}{p^2 - m_i^2 + i\varepsilon} + \text{ multi-particle branch cut}\,, \tag{1.34}$$

where Δ^{AB} is the propagator numerator defined by the free-theory two-point Green's function

$$\int \mathrm{d}^d x\, e^{ip\cdot x} \left\langle 0 \mid T\left\{\Phi_i^A(x)\Phi_i^B(0)\right\} \mid 0 \right\rangle = \frac{i\Delta_i^{AB}(p)}{p^2 - m_i^2 + i\varepsilon}\,. \tag{1.35}$$

For the purposes of this thesis the Δ_i^{AB} for quarks and gluons can be read off from the propagator Feynman rules in eq. (1.16).

Finally it is convenient to split S-matrix elements as

$$S_{\alpha\beta} = \delta_{\alpha\beta} + i\mathcal{T}_{\alpha\beta}\,, \tag{1.36}$$

where $\delta_{\alpha,\beta}$ corresponds to no interaction at all. The unitarity requirement on the S-matrix then enforces the identity

$$\delta_{\alpha\beta} = \sum\!\!\!\!\!\!\int_\rho S_{\alpha\rho}S^*_{\rho\beta} \implies \left(\mathcal{T}_{\alpha\beta} - \mathcal{T}^*_{\beta\alpha}\right) = i\sum\!\!\!\!\!\!\int_\rho \mathcal{T}_{\alpha\rho}\mathcal{T}^*_{\rho\beta} \tag{1.37}$$

where we used the "integral-sum" symbol to indicate that the set of orthonormal states ρ in the theory might be labelled both by continous and discrete degrees of freedom. When $\alpha = \beta$, The equation above reduces to the optical theorem

$$2\,\mathrm{Im}\,\mathcal{T}_{\alpha\alpha} = \sum\!\!\!\!\!\!\int_\rho \mathcal{T}_{\alpha\rho}\mathcal{T}^*_{\rho\alpha}\,. \tag{1.38}$$

Finally, when working with interactions of single particle states as in eq. (1.31), it is convenient to make momentum conservation explicit by defining scattering amplitudes $\mathcal{M}_{\alpha\beta}$ via

$$\mathcal{T}_{\alpha\beta} = (2\pi)^d \, \delta^{(d)} \left(\sum_{i=1}^{n} p_i^\mu \right) \, \mathcal{M}_{\alpha\beta} \tag{1.39}$$

where $(2\pi)^d$ is a conventional normalisation factor in dimensional regularisation.

2

The Structure of Scattering Amplitudes

Contents

2.1 Helicity Amplitudes 18
2.1.1 Spinor Helicity Formalism 21
2.1.2 Tensor Projection 23
2.2 Colour Decomposition 24
2.3 Feynman Integrals 28
2.3.1 Representations 28
2.3.2 Integration-by-parts Relations 32
2.3.3 Other Integral Relations 33
2.3.4 The Laporta Algorithm 35
2.3.5 Differential Equations and Iterated Integrals 36
2.3.6 Divergences of Feynman Integrals 39
2.4 Divergences of Scattering Amplitudes 45
2.4.1 Renormalisation of UV Divergences 45
2.4.2 Factorisation of IR Divergences 47

In chapter 1 we reviewed how scattering amplitudes can be obtained from Green's functions via the LSZ reduction formula. The QCD lagrangian (1.13) provides Feynman rules with which one can build all Feynman diagrams necessary for the perturbative computation of any amplitude in the theory.

Though in principle a straightforward task, the computation of S-matrix elements quickly becomes very complex even for relatively simple processes. As the number of external states n and loops L grows, the number of Feynman diagrams does

too. The complexity of each Feynman diagram also grows quickly: the spin and colour tensors generated by the Feynman rules become more complicated and the kinematic complexity of the loop integrals increases. For large enough values of n and L the issues above become serious computational bottlenecks. However the simplicity of the results which have already been obtained is often in direct contrast with the complexity of the intermediate stages of computations. This seems to indicate that a better understanding of the structure of scattering amplitudes can dramatically simplify their computation.

A motivating example is that of $\mathcal{N} = 4$ super Yang–Mills (sYM) theory. There, conformal symmetry and the absence of UV divergences constrain the structure of the scattering amplitudes. As a result, one can often avoid direct Feynman-diagrammatic computations and instead "guess" amplitudes based on their analytic structure. Even more striking is the example of $\mathcal{N} = 4$ sYM in the large-N_c limit, whose scattering amplitudes enjoy dual super-conformal symmetry and where all-loop expressions have been found using similar methods (see for instance ref. [18] for a review on the topic of integrability).

It is important to stress that if one were to try and replicate these results by simply using Feynman diagrams, one would discover that the simplicity of these theories would be completely hidden, only manifesting itself at the end of the computation.

In QCD, many fewer symmetries are present and many of the striking simplifications of $\mathcal{N} = 4$ sYM are absent. Still, the hope is that the understanding gained in super-symmetric theories, and the computational methods derived from them, can inspire similar treatments of QCD amplitudes. Though this goal has not yet been achieved in general, some inspiring results have been obtained. At tree-level the Britto-Cachazo-Feng-Witten (BCFW) [19] and the Berends-Giele [20] recursion relations allow one to recursively build higher-point amplitudes in terms of lower-point ones exploiting the factorisation properties of scattering amplitudes and Feynman diagrams. One-loop amplitudes can instead be obtained via the generalised

unitarity method [21–24]. Within this framework an ansatz is made for the final amplitude in terms of scalar Feynman integrals and unfixed coefficients. One can then determine these coefficients by performing (generalised) unitarity cuts [25] on the ansatz and matching them to fused tree-level amplitudes. This allows one to obtain compact results for general amplitudes by exploiting their analytic structure and without ever encountering the complexity of naive Feynman-diagrammatic calculations. Beyond one loop, results have been obtained via generalisations of the unitarity method (see for instance refs. [26] and [27]). Still, unitarity methods at two loops and beyond are much more intricate that their one loop counterpart do not seem to provide a clear computational or conceptual advantage.

In this thesis, we take a different, perhaps more standard approach. We use Feynman diagrams as the main tool for the computation of amplitudes, but supplement them with a variety of techniques to tame the complexity of the calculations. It turns out that, regardless of the method used, a deep understanding of the mathematical structure of (QCD) scattering amplitudes can drastically reduce the amount of work required to compute them.

Our approach in what follows can be summarised by *divide et impera*. The main idea is to break down each amplitude into simple(r) pieces and only at the end assemble the final result by exploiting all available symmetries. This has the two-fold benefit of simplifying intermediate stages of calculations and highlighting the fundamental building blocks of the theory. Let us start with some general definitions.

The bare QCD scattering amplitude for a process involving n quarks and gluons, defined in eq. (1.39), can be written as

$$\mathcal{M}^{c_1\dots c_n}_{\lambda_1\dots\lambda_n}(p_1,\dots,p_n) = (4\pi\alpha_{s,0})^{\frac{n}{2}-1}\mathcal{A}^{c_1\dots c_n}_{\lambda_1\dots\lambda_n}(p_1,\dots,p_n)\,, \tag{2.1}$$

where the c_i and λ_i stand for colour and helicity indices respectively and the tree-level power of the coupling is factored out. Colour indices are in the (anti-)fundamental representation of $SU(N_c)$ for (anti-)quarks and in the adjoint representation for

gluons, while helicity indices can take values $\pm 1/2$ for (anti-)quarks and ± 1 for gluons.[1] We will simply use $\pm$ for both quarks and gluons to refer to their positive or negative helicity states. The p_i are momenta of the external particles in the all-outgoing convention (see eq. (1.32)) so that momentum conservation reads $\sum_{i=1}^{n} p_i^\mu = 0$.

The linearly independent degrees of freedom describing the process can be counted to be $3n - 10$: we start with $4n$ four-momenta components from which we subtract n on-shellness constraints $p_i^2 = 0$ as well as the 10 degrees of freedom of the Poincaré group. In general, due to the fact that there can only be as many independent external momenta as the number of space-time dimensions, non-linear constraints can arise among the $3n - 10$ degrees of freedom mentioned above. We will not consider these extra relations in this thesis. A common set of variables used to describe the kinematics of a scattering amplitude are the Mandelstam invariants

$$s_{ij\ldots k} = (p_i + p_j + \cdots + p_k)^2 \tag{2.2}$$

of which only $3n - 10$ are linearly independent due to momentum conservation.

2.1 Helicity Amplitudes

Ultimately, we are interested in computing scattering amplitudes for specific (four dimensional) helicity configurations of the external quarks and gluons, *i.e.* helicity amplitudes. In chapter 1 we introduced dimensional regularisation, which we will be using throughout this thesis. However d-dimensional external states have extra polarisation states which we are not interested in. A simple way of projecting them out is to simply fix the external polarisation vectors and momenta to their four-dimensional value. This slight modification of conventional dimensional regularisation (CDR) is referred to as 't Hooft–Veltman (tHV) scheme. We will adopt the tHV scheme for all the calculations presented in this thesis.

[1] This is true in four space-time dimensions, see the beginning of section 2.1 for further details on helicity states in dimensional regularisation.

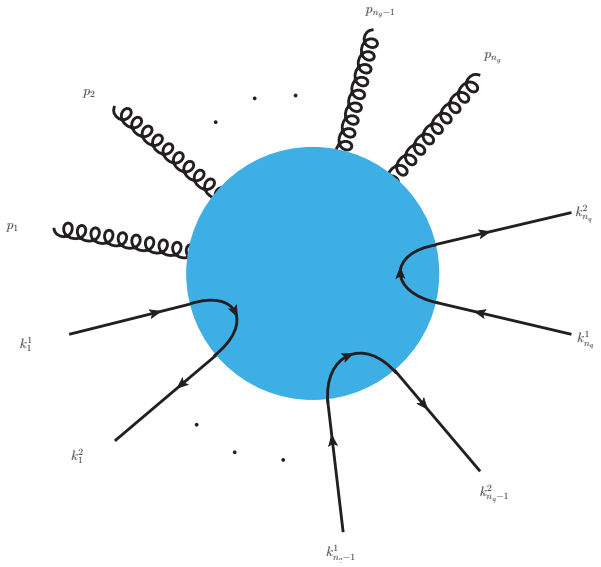

Figure 2.1: General form of a QCD scattering amplitude involving different quark flavours.

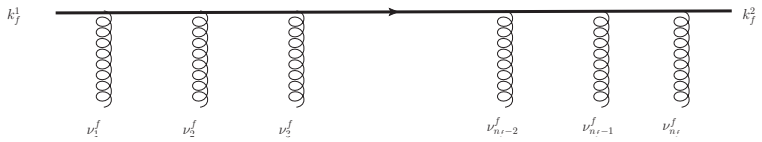

Figure 2.2: Quark-gluon interactions inside the amplitude. The indices in the figure correspond to those of the fermion line $\Gamma^f_{\nu_1^f \dots \nu_{n_f}^f}$ in eq. (2.3).

Let us start by considering a scattering amplitude for n_g gluons with momenta $p_{i=1,\dots,n_g}$ and n_q quark–anti-quark pairs of different flavours with momenta $k^{i=1,2}_{f=1,\dots,n_q}$ as in fig. 2.1. After the Dirac spinor algebra has been performed for internal quark loops, each term contributing to such an amplitude is of the form

$$\left(\prod_{i=1}^{n_g} \epsilon_{\mu_i}(p_i)\right) \left(\prod_{f=1}^{n_q} \overline{u}(k_f^2)\Gamma^f_{\nu_1^f \dots \nu_{n_f}^f} u(k_f^1)\right) T^{\mu_1 \dots \mu_{n_g} \nu_1^1 \dots \nu_{n_{n_q}}^{n_q}} , \tag{2.3}$$

where $\epsilon_{\mu_i}(p_i)$ and $\overline{u}(k_f^2)$ are the gluon and quark polarisation vectors, Γ^f are products of Dirac gamma matrices ($\Gamma \sim \gamma\gamma\dots\gamma$) and T is a Lorentz tensor containing the loop integrals. After the loop integration has been performed, the tensor T can only depend on the external momenta p_i, k_f^j, the metric $g_{\mu\nu}$ as well as the Levi-Civita tensor $\epsilon_{\mu\nu\rho\sigma}$. It follows that the full amplitude can be decomposed on the space of helicity tensors[2] obtained by contracting the first two terms of eq. (2.3) for any

[2]By *helicity tensor* we mean a tensor whose indices are fully contracted with polarisation

possible Γ^f with any tensor in T after loop integration. Imposing the Dirac equation for the external (anti-)quarks, requiring transversality of the gluon polarisation vectors and fixing the gluon reference vectors q_i so that $\epsilon(p_i)\cdot q_i = 0$, greatly reduces the number of tensors contributing to the amplitude. However, when external quarks are involved, the size of the helicity tensor space can grows with the perturbative order since higher-loop diagrams can contain longer strings of gamma matrices.

This is where working in the tHV scheme comes in handy: we use the fact that external states are kept in four dimensions to further restrict the space of tensors needed.

Following refs. [28, 29], we consider a fermion line $\overline{u}(p_2)\gamma^{\mu_1}\gamma^{\mu_2}\dots\gamma^{\mu_n}u(p_1)$. We can split each gamma matrix as a sum of its four dimensional components and its (-2ϵ)-dimensional ones

$$\gamma^\mu = \gamma_4^\mu + \gamma_{-2\epsilon}^\mu\,, \tag{2.4}$$

and use $\{\gamma_4^\mu, \gamma_{-2\epsilon}^\nu\} = 0$ to anti-commute all four-dimensional components to the right. This allows us to write the original string as a sum of terms of the type $\overline{u}(p)\gamma_{-2\epsilon}^{\mu_1}\dots\gamma_{-2\epsilon}^{\mu_m}\gamma_4^{\mu_{m+1}}\dots\gamma_4^{\mu_n}u(q)$. It is then possible to prove by induction [30] the factorisation formula

$$\overline{u}(p)\gamma_{-2\epsilon}^{\mu_1}\dots\gamma_{-2\epsilon}^{\mu_m}\gamma_4^{\mu_{m+1}}\dots\gamma_4^{\mu_n}u(q) = \mathrm{Tr}(\gamma_{-2\epsilon}^{\mu_1}\dots\gamma_{-2\epsilon}^{\mu_m})\;\overline{u}(p)\gamma_4^{\mu_{m+1}}\dots\gamma_4^{\mu_n}u(q)\,, \tag{2.5}$$

which in turn implies that (in the tHV scheme) spinor chains are linearly independent if and only if they are linearly independent in four dimensions.

For instance for the process *i.e.* $0 \to q(p_1) + \bar{q}(p_2) + Q(p_3) + \bar{Q}(p_4)$ at L loops the size of the basis reduces from $2L$ to just 2, which can be chosen as

$$\overline{u}(p_2)\gamma^\mu u(p_1)\;\overline{u}(p_4)\gamma^\mu u(p_3) \quad\text{and}\quad \overline{u}(p_2)\not{p}_3 u(p_1)\;\overline{u}(p_4)\not{p}_1 u(p_3)\,. \tag{2.6}$$

Once a basis of n_T tensors has been identified, we can work with the assumption that the amplitude can be decomposed as

$$\mathcal{A} = \sum_{i=1}^{n_T} \mathcal{F}_i\, T_i\,, \tag{2.7}$$

vectors.

where the T_i are the tensors in the basis and the $\mathcal{F}_i$ are Lorentz scalar *form factors* which are independent of the choice of external helicities. Because all the loop-momentum dependence is now contained in helicity-independent scalar form factors, we are free to fix the polarisation vectors for specific values of the external (four-dimensional) helicity states. This can be achieved very efficiently via the spinor helicity formalism.

2.1.1 Spinor Helicity Formalism

Let us start by recalling that a fermion field Ψ satisfying the Dirac equation can be written as

$$\Psi(x) = \sum_{s=\pm} \int \frac{d^3p}{(2\pi)^3 2E_p} \left[b_s(p) u_s(p) e^{ipx} + d_s^\dagger(p) v_s(p) e^{-ipx} \right] , \tag{2.8}$$

where $s = \pm$ stands for spin, $b_s(p)$ and $d_s^\dagger(p)$ are respectively the annihilation operator of a positive energy state and the creation operator of a negative energy state with momentum p, while $u_s(p)$ and $v_s(p)$ are their corresponding Dirac-spinor wave functions. In the massless case however these states are degenerate and $u_\pm = v_\mp$. The helicity projection operators are represented by

$$P_- = \frac{1}{2}(1 - \gamma_5), \quad P_+ = \frac{1}{2}(1 + \gamma_5) \tag{2.9}$$

and in the all-outgoing convention we define the helicity states to be the eigenstates $P_\pm u_\pm = u_\pm$ which implies

$$u_- = \begin{pmatrix} |p\rangle_\alpha \\ 0 \end{pmatrix} , \qquad u_+ = \begin{pmatrix} 0 \\ |p]^{\dot\alpha} \end{pmatrix} . \tag{2.10}$$

The Weyl spinors $|p\rangle_\alpha$ and $|p]^{\dot\alpha}$ are then solutions to respectively the left- and right-handed Weyl equation

$$p_\mu \sigma^\mu_{\alpha\dot\alpha} |p]^{\dot\alpha} = 0 , \quad p^\mu \overline{\sigma}_\mu^{\dot\alpha\alpha} |p\rangle_\alpha = 0 , \tag{2.11}$$

where undotted spinor indices correspond to the right-handed representation of $SU(2)$, while dotted indices correspond to the left-handed one. Above we used the sets of matrices

$$\sigma^\mu_{\alpha\dot\alpha} = (\mathbb{I}, \sigma^i)_{\alpha\dot\alpha} \quad \text{and} \quad \overline{\sigma}^{\mu,\dot\alpha\alpha} = (\mathbb{I}, -\sigma^i)^{\dot\alpha\alpha} , \tag{2.12}$$

with σ^i the Pauli matrices

$$\sigma^1 = \begin{pmatrix} 0 & 1 \\ 1 & 0 \end{pmatrix}, \quad \sigma^2 = \begin{pmatrix} 0 & -i \\ i & 0 \end{pmatrix}, \quad \sigma^3 = \begin{pmatrix} 1 & 0 \\ 0 & -1 \end{pmatrix}. \tag{2.13}$$

The on-shell condition $p^2 = 0$ can then be rewritten as

$$\det(p_\mu \sigma^\mu_{\alpha\dot{\alpha}}) = 0 \quad \Longrightarrow \quad p_{\alpha\dot{\alpha}} \equiv p_\mu \sigma^\mu_{\alpha\dot{\alpha}} = \lambda_\alpha \overline{\lambda}_{\dot{\alpha}}\,, \tag{2.14}$$

where in the last equality we used the fact that a two-by-two rank-1 matrix can always be decomposed as the direct product of two two-dimensional vectors. Requiring that the momentum p^μ should be real fixes $\overline{\lambda}_{\dot{\alpha}} = (\lambda_\alpha)^*$. Therefore to each massless four-momentum p^μ we can associate a spinor λ_α which is however determined up to an overall phase. In fact, the transformation $\lambda \to e^{i\phi}\lambda$ leaves eq. (2.14) as well as the reality condition unchanged and this $U(1) \in SU(2)$ symmetry corresponds to the little-group invariance of helicity states in the Lorentz picture.

Plugging eq. (2.14) into eq. (2.11) we find

$$\overline{\lambda}_{\dot{\alpha}} |p]^{\dot{\alpha}} = 0\,, \quad \lambda^\alpha |p\rangle_\alpha = 0 \implies \overline{\lambda}_{\dot{\alpha}} = |p]_{\dot{\alpha}}\,, \quad \lambda_\alpha = |p\rangle_\alpha\,. \tag{2.15}$$

$SU(2)$ indices are raised and lowered by the two dimensional Levi-Civita tensor and we define the notation

$$\langle p|^\alpha = \epsilon^{\alpha\beta}|p\rangle_\beta, \quad |p]^{\dot{\alpha}} = \epsilon^{\dot{\alpha}\dot{\beta}}[p|_{\dot{\beta}}\,. \tag{2.16}$$

Conventions for $\epsilon^{\alpha\beta}$ and other details and useful formulas within the spinor-helicity formalism can be found in appendix B Finally, we define the anti-symmetric spinor (and Lorentz) invariants

$$[pq] = [p|_{\dot{\alpha}}|q]^{\dot{\alpha}} = -[qp] \quad \text{and} \quad \langle pq\rangle = \langle p|^\alpha |q\rangle_\alpha = -\langle qp\rangle\,. \tag{2.17}$$

in terms of which scalar products of massless four momenta read

$$p \cdot q = \frac{1}{2}[pq]\langle qp\rangle\,. \tag{2.18}$$

Finally, the spinor helicity variables allow us to write the gluon polarisation vectors for negative and positive helicity states for the i-th gluon as

$$\epsilon^\mu_{i,-} = \frac{\langle i|^\alpha \sigma^\mu_{\alpha\dot{\alpha}} |q_i]^{\dot{\alpha}}}{\sqrt{2}[i\ q_i]} = \frac{\langle i\ \mu\ q_i]}{\sqrt{2}[i\ q_i]}, \qquad \epsilon^\mu_{i,+} = \frac{[i|_{\dot{\alpha}}\ \overline{\sigma}^{\mu,\dot{\alpha}\alpha}\ |q_i\rangle_\alpha}{\sqrt{2}\langle q_i\ i\rangle} = \frac{[i\ \mu\ q_i\rangle}{\sqrt{2}\langle q_i\ i\rangle}, \tag{2.19}$$

where q_i is a massless reference momentum satisfying $q_i \cdot p_i = 0$ and we defined the notation

$$\begin{cases} \langle i|^{\alpha}\sigma^{\mu}_{\alpha\dot{\alpha}}|j]^{\dot{\alpha}} \equiv \langle i\,\mu\,j] \\ [j|_{\dot{\alpha}}\,\overline{\sigma}^{\mu,\dot{\alpha}\alpha}\,|i\rangle_{\alpha} \equiv [j\,\mu\,i\rangle \end{cases} \quad \Longrightarrow \; \langle i\,\mu\,j] = [j\,\mu\,i\rangle\,. \tag{2.20}$$

From the definitions above one can check that the polarisation vectors satisfy the requirements

$$\epsilon_{i,-}\cdot\epsilon_{i,+} = 0\,, \qquad \epsilon_{i,\pm}\cdot(\epsilon_{i,\pm})^* = -1\,. \tag{2.21}$$

2.1.2 Tensor Projection

Having introduced the spinor-helicity formalism, we can use eqs. (2.10) and (2.19) to explicitly fix helicities of external states. For each configuration $\boldsymbol{\lambda} = (\lambda_1 \ldots \lambda_n)$ we can factorise an overall *spinor factor* $s_{\boldsymbol{\lambda}}$ to account for the scaling of the tensors (and of the helicity amplitudes) under little group transformations:

$$T_i|_{\boldsymbol{\lambda}} = R_{i,\boldsymbol{\lambda}}\, s_{\boldsymbol{\lambda}} \tag{2.22}$$

where T_i are the tensors defined at the beginning of section 2.1 evaluated at fixed values of the external helicity states and $R_{j,\boldsymbol{\lambda}}$ are defined to be invariant under the full Lorentz group. Plugging eq. (2.22) into eq. (2.7) we obtain the explicit expression for the helicity amplitudes

$$\mathcal{A}|_{\boldsymbol{\lambda}} = \left(\sum_j R_{j,\boldsymbol{\lambda}}\,\mathcal{F}^j\right)\, s_{\boldsymbol{\lambda}} \equiv \mathcal{H}_{\boldsymbol{\lambda}}\, s_{\boldsymbol{\lambda}}, \tag{2.23}$$

where $\mathcal{H}_{\boldsymbol{\lambda}}$ are spinor-stripped helicity amplitudes. As a final ingredient we need to know how to compute the form factors. This can be done by defining corresponding projectors P_i and a product $\circ$ so that

$$P_i \circ T_j = \delta_{ij}\,. \tag{2.24}$$

The T_j can be interpreted as the basis of a vector space and the projectors can be concretely defined as elements in the dual space, *i.e.*

$$P_i = \sum_{j=1}^{n_T} c_{ij} T_j^{\dagger}\,, \tag{2.25}$$

where the coefficients c_{ij} are to be determined, and the product $\circ$ is defined as a sum over the helicities of the external states, so that

$$\begin{aligned} \epsilon^{*\mu}(p,q) \circ \epsilon^{\nu}(p,q) &= -g^{\mu\nu} + \frac{p^\mu q^\nu + p^\nu q^\mu}{p\cdot q}\,, \\ u(p) \circ \overline{u}(p) &= \not{p}\,. \end{aligned} \tag{2.26}$$

One can then find the explicit form of the projectors by plugging eq. (2.25) into eq. (2.24) and solving for the c_{ij}. Once the expression for the coefficients is known, the form factors can be obtained by direct projection of the amplitude:

$$P_i \circ \mathcal{A} = \mathcal{F}_i. \tag{2.27}$$

2.2 Colour Decomposition

Looking at the Feynman rules eqs. (1.16) to (1.18), we immediately notice that the colour structures never mix with the kinematics, a property which can be expressed via the amplitude decomposition

$$\mathcal{A}^{c_1\ldots c_n}_{\lambda_1\ldots\lambda_n}(p_1,\ldots,p_n) = \sum_i \mathcal{C}^{c_1\ldots c_n}_{[i]} \mathcal{A}^{[i]}_{\lambda_1\ldots\lambda_n}(p_1,\ldots,p_n) \equiv \boldsymbol{\mathcal{C}}\cdot\boldsymbol{\mathcal{A}}_{\lambda_1\ldots\lambda_n}(p_1,\ldots,p_n) \tag{2.28}$$

where the $\mathcal{C}$ are tensors in colour space carrying all colour indices and the $\mathcal{A}^{[i]}$ are colour-independent *partial amplitudes*. In the second equality we introduced the colour-vector notation [31–33]

$$(\boldsymbol{\mathcal{C}})_i = \mathcal{C}^{c_1\ldots c_n}_{[i]}\,, \quad (\boldsymbol{\mathcal{A}})_i = \mathcal{A}^{[i]}\,. \tag{2.29}$$

The *colour decomposition* of eq. (2.28) is not unique, however one way to determine a sufficient set of tensors $\mathcal{C}_i$ and the corresponding partial amplitudes is as follows. We first rewrite all structure constants due to pure gluon vertices in terms of generators of the fundamental representation via

$$f^{abc} = -2i\mathrm{Tr}\{T^a[T^b,T^c]\}\,, \tag{2.30}$$

and then replace every pair of contracted generators via the *Fiertz identity*

$$(T^a)_i{}^j (T^a)_k{}^h = \frac{1}{2}\left(\delta_i{}^h\delta_k{}^j - \frac{1}{N_c}\delta_i{}^j\delta_k{}^h\right)\,. \tag{2.31}$$

The only objects that can be left at this point are strings of generators, traces of generators and Kronecker deltas of fundamental indices:

$$(T^{a_1}\dots T^{a_r})_i{}^j, \quad \mathrm{Tr}[T^{a_1}\dots T^{a_r}], \quad \delta_i{}^j. \tag{2.32}$$

In particular, gluon amplitudes have no (anti-)fundamental indices and therefore are entirely written in terms of traces of generators. Defining the shorthand $\mathrm{Tr}^\sigma[1\dots n] \equiv \mathrm{Tr}[T^{a_{\sigma(1)}}\dots T^{a_{\sigma(n)}}]$ for a permutation $\sigma \in S_n$, they can be written in the compact form

$$\mathcal{A}_{\boldsymbol{\lambda}}^{a_1\dots a_n} = \sum_{t=1}^{n} \sum_{\substack{1<i_1<\dots<i_t=n \\ \delta_k\geq\delta_{k+1}}} \sum_{\sigma\in S_n(i_1,\dots,i_t)} \mathcal{A}_{\sigma,\boldsymbol{\lambda}}^{(\delta_1+1,\dots,\delta_t+1)} \prod_{j=1}^{t} \mathrm{Tr}^\sigma[i_{j-1}\dots i_j] \tag{2.33}$$

where $\delta_k = i_k - i_{k-1}$, $i_0 = 1$ and we defined the sub-set of permutations $S_n(i_1,\dots,i_t) \equiv S_n/I_n(i_1,\dots,i_t)$ with $I_n(i_1,\dots,i_t)$ the sub-group of permutations defined by

$$\sigma \in I_n(i_1,\dots,i_t) \iff \prod_{j=1}^{t+1} \mathrm{Tr}^\sigma[i_{j-1}\dots i_j] = \prod_{j=1}^{t+1} \mathrm{Tr}^{id}[i_{j-1}\dots i_j]\,. \tag{2.34}$$

Note that any term of eq. (2.33) containing at least one trace of a single generator vanishes since $\mathrm{Tr}(T^a) = 0$ in $SU(N_c)$. To make eq. (2.33) more concrete let us give an example. The amplitude for four-gluon scattering, at any loop order, can be written as

$$\begin{aligned}
\mathcal{A}_{\boldsymbol{\lambda}}^{a_1\dots a_4} &= \sum_{\sigma\in S_4(1)} \mathcal{A}_{\sigma,\boldsymbol{\lambda}}^{(1)} \mathrm{Tr}^\sigma[1234] + \sum_{\sigma\in S_4(1,1)} \mathcal{A}_{\sigma,\boldsymbol{\lambda}}^{(1,1)} \mathrm{Tr}^\sigma[12]\mathrm{Tr}^\sigma[34] \\
&= \mathcal{A}_{1234,\boldsymbol{\lambda}}^{(4)} \mathrm{Tr}[1234] + \mathcal{A}_{1243,\boldsymbol{\lambda}}^{(4)} \mathrm{Tr}[1243] + \mathcal{A}_{1324,\boldsymbol{\lambda}}^{(4)} \mathrm{Tr}[1324] \\
&+ \mathcal{A}_{1342,\boldsymbol{\lambda}}^{(4)} \mathrm{Tr}[1342] + \mathcal{A}_{1423,\boldsymbol{\lambda}}^{(4)} \mathrm{Tr}[1423] + \mathcal{A}_{1432,\boldsymbol{\lambda}}^{(4)} \mathrm{Tr}[1432] \\
&+ \mathcal{A}_{1234,\boldsymbol{\lambda}}^{(2,2)} \mathrm{Tr}[12]\mathrm{Tr}[34] + \mathcal{A}_{1324,\boldsymbol{\lambda}}^{(2,2)} \mathrm{Tr}[13]\mathrm{Tr}[24] + \mathcal{A}_{1423,\boldsymbol{\lambda}}^{(2,2)} \mathrm{Tr}[14]\mathrm{Tr}[23]\,.
\end{aligned} \tag{2.35}$$

When external quark and anti-quark states are involved eq. (2.33) has to be modified in order to account for the external (anti-)fundamental indices and the colour tensors appearing in the amplitude can in general be written as products of the objects like those in eq. (2.32). This is best shown via examples, which can be found in chapter 3.

The coefficients $\mathcal{A}_{\sigma,\boldsymbol{\lambda}}^{(i_1,\dots,i_t)}$ are usually referred to as colour-ordered *partial amplitudes* and since they multiply a basis of colour-tensor space they are individually gauge invariant. This makes them ideal building blocks for scattering amplitudes.

Nevertheless not all partial amplitudes are independent: there exists a minimal set of so-called *primitive amplitudes* which encode the full information about the amplitude. In order to identify the primitive amplitudes one needs to first understand the different types of relations which exist among partial amplitudes. We briefly review them below.

Cyclic Invariance Because the full amplitude is invariant under permutations of the external gluons $(p_i, \lambda_i) \to (p_{\sigma(i)}, \lambda_{\sigma(i)})$, the partial amplitudes enjoy the same permutation symmetries of the colour tensors they multiply.

For example, the single-trace gluon partial amplitudes $A^{(1)}_{12\ldots n,\boldsymbol{\lambda}}$ are invariant under cyclic permutations of all indices, while the double-trace gluon partial amplitudes $\mathcal{A}^{(m,n-m)}_{12\ldots n,\boldsymbol{\lambda}}$ are invariant under cyclic permutations of both the first m and the last $n-m$ indices. In the case of amplitudes involving quarks we have for instance that the $q(p_1)\bar{q}(p_2) \to q(p_3)\bar{q}(p_4)$ partial amplitude multiplying the colour structure $\delta^{j_2}_{i_1}\delta^{j_4}_{i_3}$ is symmetric under the exchange $(1,2) \leftrightarrow (3,4)$.

Reflection The colour structure of amplitudes involving n gluons in the external states is real valued. For pure Yang–Mills amplitudes this is a direct consequence of the fact that the structure constants f^{acb} are real and the statement holds diagram by diagram. In QCD amplitudes the statement holds only after summing diagrams over quark and anti-quark internal loops. Taking the complex conjugate in colour space of the l.h.s. of eq. (2.28) and using

$$(\mathrm{Tr}[T^{a_1}\ldots T^{a_n}])^* = (-1)^n \mathrm{Tr}[T^{a_n}\ldots T^{a_1}] \tag{2.36}$$

one finds the reflection identity

$$A^{(m_1,m_2,\ldots,m_t)}_{id,\boldsymbol{\lambda}} = (-1)^n A^{(m_1,m_2,\ldots,m_t)}_{\sigma^r,\boldsymbol{\lambda}} \tag{2.37}$$

where the permutation σ^r reflects the order of all indices in the corresponding traces. Going back to the four-gluon example this implies

$$\mathcal{A}^{(4)}_{1234,\boldsymbol{\lambda}} = \mathcal{A}^{(4)}_{4321,\boldsymbol{\lambda}}\,, \qquad \mathcal{A}^{(2,2)}_{1234,\boldsymbol{\lambda}} = \mathcal{A}^{(2,2)}_{2143,\boldsymbol{\lambda}}\,, \tag{2.38}$$

whereas in a five-gluon amplitude we would find (see chapter 4)

$$\mathcal{A}^{(5)}_{12345,\boldsymbol{\lambda}} = -\mathcal{A}^{(5)}_{54321,\boldsymbol{\lambda}}\,, \qquad \mathcal{A}^{(3,2)}_{12345,\boldsymbol{\lambda}} = -\mathcal{A}^{(3,2)}_{32154,\boldsymbol{\lambda}} \tag{2.39}$$

and permutations thereof.

$U(1)$ decoupling relations Pure $U(N_c)$ Yang–Mills partial amplitudes are identical to $SU(N_c)$ ones. This is because one can split $U(N_c) = U(1) \times SU(N_c)$, which means $U(N_c)$ Yang–Mills theory describes standard $SU(N_c)$ Yang–Mills plus a free $U(1)$ gauge boson[3]. In particular $U(N_c)$ scattering amplitudes involving at least one photon in the external states vanish. This information can be used to impose relations among different $SU(N_c)$ Yang–Mills partial amplitudes. These relations can be obtained by setting one or more generators T^a to the identity matrix in eq. (2.33) and by requiring that the coefficients of the different resulting colour structures in the r.h.s. vanish independently. For instance at tree-level, where only single traces are present, one can set all generators to the identity to find the relation

$$A^{(n)}_{123\ldots n} + A^{(n)}_{213\ldots n} A_1(213\ldots n) + \cdots + A^{(n)}_{23\ldots 1n} = 0 \tag{2.40}$$

At one-loop, taking as an example eq. (2.35) where single and double traces are present, we can set T^{a_1} and T^{a_2} to the identity to find the relation

$$N_c A^{(2,2)}_{1234} = -\left(\mathcal{A}^{(4)}_{1234,\boldsymbol{\lambda}} + \mathcal{A}^{(4)}_{1243,\boldsymbol{\lambda}} + \mathcal{A}^{(4)}_{1324,\boldsymbol{\lambda}} + \mathcal{A}^{(4)}_{1342,\boldsymbol{\lambda}} + \mathcal{A}^{(4)}_{1423,\boldsymbol{\lambda}} + \mathcal{A}^{(4)}_{1432,\boldsymbol{\lambda}}\right) \tag{2.41}$$

and similarly at five points we can set $T^{a_4} = T^{a_5} = I$ to get

$$\begin{aligned} &N_c A^{(3,2)}_{12345} = \\ &\quad -\left[\left(\mathcal{A}^{(5)}_{12345,\boldsymbol{\lambda}} + \mathcal{A}^{(5)}_{12435,\boldsymbol{\lambda}} + \mathcal{A}^{(5)}_{14235,\boldsymbol{\lambda}} + \mathcal{A}^{(5)}_{12453,\boldsymbol{\lambda}} + \mathcal{A}^{(5)}_{14253,\boldsymbol{\lambda}} + \mathcal{A}^{(5)}_{14523,\boldsymbol{\lambda}}\right) + (4 \leftrightarrow 5)\right]. \end{aligned} \tag{2.42}$$

Note that whenever quarks enter the scattering process, both as external or internal states, these identities fail since the $U(1)$ photon stops being free and amplitudes involving external photons do not vanish in general. In Yang-Mills but beyond one loop, $U(1)$ decoupling relations hold but involve partial amplitudes which are outside of pure $SU(N_c)$.

[3]Sometimes referred to as photon.

Over-completeness Pure Yang–Mills scattering amplitudes, whose Feynman diagrams are entirely written in terms of adjoint generators f^{abc}, span a subspace of colour space, as explained in [34]. This implies that extra relations due to the over-completness of the colour basis of eq. (2.28). The resulting identities are sometimes referred to as generalised photon-decoupling identities.

The relations among partial amplitude we just described, together with CPT invariance of S-matrix elements in QCD, allow us to identify a minimal set of primitive amplitudes from which the full result can be obtained. Explicit examples will be given in chapters 3 and 4.

2.3 Feynman Integrals

When analytically computing scattering amplitudes, independently of the method followed, one eventually encounters Feynman integrals, *i.e.* integrals over the unconstrained internal momenta. In our case, after helicity projection and colour decomposition of scattering amplitudes, one is left with a list of scalar form factors which contain all dependence on the loop integrals. The purpose of this section is to set the notation for Feynman integrals and describe some of the techniques involved in their computation.

2.3.1 Representations

We write an L-loop scalar Feynman integral in dimensional regularisation as,

$$I_{\vec{\nu}}[\mathcal{N}] = e^{L\epsilon\gamma_E}(\mu^2)^{L\epsilon}\int\prod_{i=1}^{L}\frac{\mathrm{d}^d\ell_i}{i\pi^{d/2}}\frac{\mathcal{N}(\ell_i)}{\mathcal{D}_1^{\nu_1}\cdots\mathcal{D}_E^{\nu_E}} \equiv \int\mathfrak{D}^L\ell\frac{\mathcal{N}(\ell_i)}{\mathcal{D}_1^{\nu_1}\cdots\mathcal{D}_E^{\nu_E}}\,, \tag{2.43}$$

where $\mathcal{D}_e = q_e^2 - m_e^2 + i\varepsilon$ are the E propagator denominators of the corresponding graph, $\mathcal{N}$ is a Lorentz-invariant numerator and we defined the L-loop integration measure

$$\int\mathfrak{D}^L\ell \to e^{L\epsilon\gamma_E}(\mu^2)^{L\epsilon}\int\prod_{i=1}^{L}\frac{\mathrm{d}^d\ell_i}{i\pi^{d/2}}\,. \tag{2.44}$$

More precisely, with form factors in mind, we require $\mathcal{N}$ to be a polynomial in the scalar products of loop and external momenta of uniform mass dimension. The ν_e are positive integers accounting for doubled propagators and we defined the vector $\vec{\nu} = (\nu_1, \ldots, \nu_E)$. The edge momenta q_e are linear combinations of the loop momenta ℓ_i and the external momenta with coefficients ± 1 or 0. The overall factor $e^{L\epsilon\gamma_E}$ is a conventional normalisation taylored to $\overline{\text{MS}}$ renormalisation.

A simple example is the one-loop massles box integral with no numerator, which in the all-outgoing convention reads

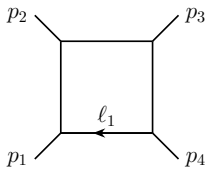

$$= \int \mathfrak{D}\ell \frac{1}{\mathcal{D}_1\mathcal{D}_2\mathcal{D}_3\mathcal{D}_4}\,, \quad \begin{cases} \mathcal{D}_1 = (\ell_1)^2 \\ \mathcal{D}_2 = (\ell_1 - p_1)^2 \\ \mathcal{D}_3 = (\ell_1 - p_1 - p_2)^2 \\ \mathcal{D}_4 = (\ell_1 - p_1 - p_2 - p_3)^2 \end{cases} . \tag{2.45}$$

When working with Feynman diagrams, one finds loop integrals of the form in eq. (2.43), but various other representations exist. Each representation may render some properties of the integrals manifest while obscuring others, so it is usually appropriate to change representation depending on the task at hand.

A very useful modification of the representation in eq. (2.43) is the propagator denominator (PD) representation. Starting from the set of E denominators for a Feynman integral, one can write the $\mathcal{D}_i$ as linear combinations of scalar products by explicitly writing the q_e as linear combinations of external and loop momenta and expanding the squares:

$$\begin{aligned} \mathcal{D}_e = &\sum_{\substack{i=1,\ldots,L \\ j=1,\ldots,L}} M^{(2)}_{e,(ij)} \ell_i \cdot \ell_j \; + \sum_{\substack{i=1,\ldots,L \\ j=1,\ldots,n-1}} M^{(1)}_{e,(ij)} \ell_i \cdot p_j \\ &+ \sum_{\substack{i=1,\ldots,n-1 \\ j=1,\ldots,n-1}} M^{(0)}_{e,(ij)} p_i \cdot p_j \; - m_e^2 \,. \end{aligned} \tag{2.46}$$

We can then invert eq. (2.46), solving as many scalar products $\ell_i \cdot \ell_j$ and $\ell_i \cdot p_j$ in terms of propagator denominators. Plugging the result back into eq. (2.43) allows us to "partial fraction" the integrand, cancelling powers of the $\mathcal{D}_i$ between numerator and denominator. However, usually, not all scalar products can be expressed in terms of inverse propagators and the remaining scalar products which

can not be expressed in terms of $\mathcal{D}_e$ are called irreducible scalar products (ISPs). In order to obtain a uniform notation for Feynman integrals, which is particularly useful for their systematic characterisation, we can upgrade the set of original denominators by adding extra spurious ones

$$\{\mathcal{D}_1, \ldots, \mathcal{D}_E\} \to \{\mathcal{D}_1, \ldots, \mathcal{D}_E, \mathcal{D}_{E+1}, \ldots, \mathcal{D}_{E'}\} \tag{2.47}$$

so that all scalar products can be expressed in terms of the larger set of denominators. The total number E' has to match the number of independent scalar products involving at least one loop momentum, which at L loops and n points corresponds to $E' = L(L+1)/2 + L(n-1)$. At one loop $E' = E$ and no extra denominators are needed, while at higher loops usually $E' > E$. For the box integral in eq. (2.45) we find

$$\ell_1^2 = \mathcal{D}_1\,, \quad \ell_1 \cdot p_1 = \frac{1}{2}(\mathcal{D}_2 - \mathcal{D}_1)\,,$$
$$\ell_1 \cdot p_2 = \frac{1}{2}(\mathcal{D}_3 - \mathcal{D}_2 - s_{12})\,, \quad \ell_1 \cdot p_3 = \frac{1}{2}(\mathcal{D}_4 - \mathcal{D}_3 + s_{12})\,.$$

In the PD representation, integrals are simply determined by the list of propagator denominators, which defines an *integral family*, and a vector of integers specifying the power of each denominator, which can now be negative to account for numerators. We can therefore define a new class of integrals as

$$\mathcal{J}^{\mathfrak{f}}_{\vec{\rho}} = \int \mathfrak{D}^L \ell \prod_{e=1}^{E(\mathfrak{f})} \frac{1}{\mathcal{D}_e^{\rho_e}}\,, \quad \rho_e \in \mathbb{Z}\,, \tag{2.48}$$

where $\mathfrak{f}$ labels the integral family, *i.e.* it defines the list of inverse propagators $\mathcal{D}_e$. Within an integral family $\mathfrak{f}$ we call a sector $\mathfrak{s}$, the set of integrals which share the same list of positive denominator powers. In the box example, the integrals $\mathcal{J}^{Box}_{1,1,1,0}$, $\mathcal{J}^{Box}_{1,1,1,-1}$ and $\mathcal{J}^{Box}_{1,1,2,0}$ would all belong to the sector $\mathfrak{s} = \{1,1,1,0\}$. After one has enlarged the set of denominators $\mathcal{D}_e$ to obtain eq. (2.48), it is possible that the denominator list of some sectors will not correspond to the propagators of any Feynman integral. Since these do not naturally arise from Feynman diagrams we will mostly focus our attention on sectors which can be associated to a Feynman graph and we will refer to them as *topologies*.

Another representation[4] which will be useful later in this thesis is the Feynman-parameter representation, which we report for the integrals with unit numerators

$$I_{\vec{\nu}}[1] = (\mu^2)^{2L-\nu} \frac{e^{L\epsilon\gamma_E}\Gamma(\nu - Ld/2)}{\prod_{i=e'}^{E}\Gamma(\nu_{e'})} \int_0^\infty \frac{\prod_{e=1}^{E} \mathrm{d}\alpha_e}{\mathrm{GL}(1)} \frac{\mathcal{U}(\alpha)^{\nu-(L+1)d/2}}{\mathcal{F}(\alpha)^{\nu-Ld/2}}\,, \tag{2.49}$$

where the GL(1) denominator accounts for the projective invariance of the integration over the Feynman parameters α_e and we defined the total propagator power $\nu = \sum_e \nu_e$. It is equivalent to the usual notation $\delta(1 - \sum_{e\in A}\alpha_e)$ with A a subset of $\{1,\dots,E\}$.

The quantities $\mathcal{U}$ and $\mathcal{F}$ are the Symanzik polynomials of the Feynman graph and are defined as

$$\mathcal{U}(\alpha) = \sum_{T\in\mathcal{T}_1}\prod_{e\notin T}\alpha_e\,, \tag{2.50a}$$

$$\mathcal{F}(\alpha) = -\sum_{T\in\mathcal{T}_2} p(T)^2 \prod_{e\notin T}\alpha_e - \mathcal{U}(\alpha)\sum_{e=1}^{E} m_e^2\alpha_e\,, \tag{2.50b}$$

where $\mathcal{T}_n$ is the set of spanning n-forests of the graph, and $p^\mu(T)$ is the total momentum flowing across the 2-forest $T \in \mathcal{T}_2$. Defining the quantities A and B as

$$\sum_{e=1}^{E}\alpha_e\mathcal{D}_e = \sum_{i,j=1}^{L} A_{ij}\ell_i\cdot\ell_j - 2\sum_{i=1}^{L}\ell_i\cdot B_i + C\,, \tag{2.51}$$

one can compute the Symanzik polynomials via the equations

$$\mathcal{U} = \det A, \tag{2.52a}$$

$$\mathcal{F} = \det A\left(-B^T A^{-1} B + C\right). \tag{2.52b}$$

In general, scattering amplitudes depends on a multitude of different Feynman integrals. These will appear with different sets of propagators (denominators $\mathcal{D}_i$) as well as numerators $\mathcal{N}$.

However it turns out that a large number of linear relations exist between Feynman integrals. In practice this allows to identify a minimal set of linearly independent *master integrals* and write all other integrals as linear combination of this basis.

The task of computing scalar form factors then splits in two:

[4]Among other representations are the Baikov representation, the Schwinger representation, the Lee-Pomeransky representation and the Feynman-parameter representation. See [35] for a pedagogical presentation.

- finding all relations among Feynman integrals and solving them in terms of master integrals,
- computing the (comparatively) small set of master integrals.

Let us start with the first.

2.3.2 Integration-by-parts Relations

In order to derive relations among Feynman integrals, we can exploit their translation invariance, a defining property of dimensional regularisation as described in and around eq. (1.22). We start by taking a generic integral $\int \mathrm{d}^d x f(x)$ and performing an infinitesimal shift of the integration variable

$$\int \mathrm{d}^d x\, f(x) = \int \mathrm{d}^d (x + \alpha v(x))\, f(x + \alpha v(x))\,, \tag{2.53}$$

with $\alpha \ll 1$ and $v(x)$ an x-dependent vector. We can then Taylor-expand the integrand and the measure of integration in α to obtain

$$\int \mathrm{d}^d x\, f(x) = \int \mathrm{d}^d x\, \left(f(x) + \alpha\, f(x) \frac{d}{dx^\mu} v^\mu(x) + \alpha\, v^\mu(x) \frac{d}{dx^\mu} f(x) + \mathcal{O}(\alpha^2) \right), \tag{2.54}$$

and requiring the equation to hold order-by-order in α we find

$$\int \mathrm{d}^d x\, \frac{d}{dx^\mu} \left[v^\mu(x)\, f(x) \right] = 0 \tag{2.55}$$

which is referred to as *integration-by-parts* (IBP) relation. In other words, the divergence of a vector field in dimensional regularisation always yields zero, independently of the convergence properties of the field at infinity, giving a generalisation of Gauss's theorem. Were we not working in dimensional regularisation, we should worry about the presence of a boundary term at infinity which might spoil eq. (2.55).

Applying eq. (2.55) to the case of Feynman integrals we get

$$\int \mathfrak{D}^L \ell \frac{\partial}{\partial \ell_j^\mu} \left[v^\mu(\ell)\, \frac{\mathcal{N}(\ell)}{\mathcal{D}_1^{\nu_1} \cdots \mathcal{D}_E^{\nu_E}} \right] = 0 \tag{2.56}$$

where we can identify x with ℓ_j. We can then distribute the ℓ_j derivative (using the notation $\partial_{\ell^\mu} \equiv \frac{\partial}{\partial \ell^\mu}$) and obtain

$$\int \mathfrak{D}^L \ell \left[\frac{(\partial_{\ell_j^\mu} v^\mu)\, \mathcal{N}}{\mathcal{D}_1^{\nu_1} \cdots \mathcal{D}_E^{\nu_E}} + \frac{v^\mu \partial_{\ell_j^\mu} \mathcal{N}}{\mathcal{D}_1^{\nu_1} \cdots \mathcal{D}_E^{\nu_E}} - \sum_e \frac{\nu_e v^\mu \partial_{\ell_j^\mu} \mathcal{D}_e}{\mathcal{D}_e} \frac{\mathcal{N}}{\mathcal{D}_1^{\nu_1} \cdots \mathcal{D}_E^{\nu_E}} \right] = 0\,, \tag{2.57}$$

where all terms in the sum correspond to individual Feynman integrals (modulo the irrelevant overall normalisation factor). Eq. (2.57) is therefore a linear relation among Feynman integrals. Writing down all relations for the different choices of v^μ, ℓ_j and $\mathcal{N}$, one finds a system of linear equations.

Though in principle a simple operation, writing down and solving such systems of IBPs turns out to be one of the main bottlenecks of state-of-the-art scattering amplitude calculations, for which one might have to solve systems of millions or even billions[5] of equations.

2.3.3 Other Integral Relations

In addition to IBPs it is possible to find extra relations among Feynman integrals. Here we will review Lorentz invariance identities, loop-momentum shift identities and sector relations.

Lorentz Invariance Identities

A scalar Feynman integral $\mathcal{I}$ is invariant under a Lorentz transformation of the external momenta: $\mathcal{I}(p) = \mathcal{I}(\Lambda p)$. The generator of such a transformation is

$$\omega^{\mu\nu} = \sum_{i=1}^{n} \left(p_i^\mu \frac{\partial}{\partial p_i^\nu} - p_i^\nu \frac{\partial}{\partial p_i^\mu} \right)\,, \tag{2.58}$$

and it annihilates any scalar Feynman integral

$$\omega^{\mu\nu}\, \mathcal{I} = 0\,. \tag{2.59}$$

In order to obtain scalar relations among integrals, one can contract eq. (2.59) with any antisymmetric combination of external momenta:

$$(p_i^\mu p_j^\nu - p_i^\nu p_j^\mu)\, \omega_{\mu\nu}\, \mathcal{I} = 0\,. \tag{2.60}$$

[5] though many of the equations produced by eq. (2.56) are actually linearly dependent.

These are the Lorentz invariance (LI) relations. Counting all possible antisymmetric combinations of n external momenta, of which only $n-1$ are independent due to momentum conservation, one finds $(n-1)(n-2)/2$ LI relations, irrespective of the loop order. It should be noted that the Lorentz invariance identities of eq. (2.60) are not independent from IBP relations, in the sense that they can be written as linear combinations of IBPs. However, from a practical viewpoint, it turns out that including LI relations in the system and solving them immediately can simplify the task of IBP reduction.

Shift relations

Shift invariance is one of the defining axioms of dimensionally regularised Feynman integrals, as discussed in section 1.4. Above we saw how invariance under infinitesimal shifts can be used to derive IBP relations. Here we focus on finite shifts, which can also provide useful identities among integrals. More precisely, when a loop-momentum shift

$$\ell_i \to S(\ell_i) = L_{ij}\ell_j + E_{ij}p_j \tag{2.61}$$

is such that the set of propagators of a given sector is shifted to itself (possibly after a permutation of the propagators), it can be used to find a relation among integrals within that sector by explicitly performing the shift and requiring equivalence of the integrals:

$$\int \mathfrak{D}^L \ell \frac{\mathcal{N}(\ell_i)}{\mathcal{D}_1^{\nu_1}\cdots\mathcal{D}_E^{\nu_E}} = \int \mathfrak{D}^L \ell \frac{\mathcal{N}(S(\ell_i))}{\mathcal{D}_1^{\nu_1}\cdots\mathcal{D}_E^{\nu_E}}\,. \tag{2.62}$$

By definitions, the denominators in the r.h.s. and l.h.s. of the equations above are going to be identical, but the numerators might differ. This is known as a *sector symmetry*. Whenever one is working with multiple sectors (within one or more integral families) it is also possible to find loop-momentum shifts that map one sector onto another. The corresponding integral identities are known as *sector relations* [36].

2.3.4 The Laporta Algorithm

It is well known that the choice of master integrals and the order in which the relations are solved can have a great impact on the complexity of the expressions appearing in intermediate stages of IBP reduction. This becomes more and more relevant when the number of scales increases.

The Laporta algorithm [37] provides a choice of master integrals by defining an ordering among integrals, and it can be defined in a process-independent way. Loosely following the algorithm, one starts by defining an ordering among all Feynman integrals by associating a weight to each integral. The highest weight integral is eliminated from the system by solving one of the equations which contains it and plugging the solution into all remaining IBPs. This procedure is then repeated until no equations are left. The algorithm does not identify the list of master integrals a priori: they are instead automatically determined as the set of integrals which remain unconstrained after the algorithm terminates. It is worth pointing out that it is not obvious that as the rank of the integrals considered grows the Laporta algorithm should always terminate with the same set of master integrals. Altough this turns out to be true, it would be interesting to investigate which and many relations are crucial for this to happen.

The Laporta algorithm is simple to automate on a computer and it benefits from a high degree of parallelisation, making it the most popular choice as the backbone of IBP reduction codes. However it is generally understood that the master integrals obtained via the Laporta algorithm do not usually yield compact representations of scattering amplitudes and, after the system of equations has been solved, a change of basis is normally performed.

The question of how to choose a "good" basis of master integrals is in most cases an ill-posed one, since different bases might be suitable for different purposes. For example in section 2.3.5 we will see that choosing a so-called *canonical* basis makes the solution of Feynman integrals particularly simple. However, though better than "randomly selected" Laporta bases, canonical bases are not necessarily the best option when it comes to the representations of scattering amplitudes. Indeed, in some

cases, more compact representations of scattering amplitudes can be achieved via over-complete, process dependent bases. We will come back to this topic in chapter 5.

2.3.5 Differential Equations and Iterated Integrals

The integral relations we just discussed, together with an algorithm to express them in terms of a set of master integrals, solve the first of the two points presented at the end of section 2.3.1. We now turn to the second: computing the master integrals.

A large class of Feynman integrals, characterised by the property of *linear reducibility* [38–40], can be integrated directly, for instance via the Feynman-parameter representation (2.49). In this thesis we will focus on an alternative approach: the method of differential equations [41]. Rather than focusing on individual integrals and studying them on a case-by-case basis, this method leverages IBP relations to find (coupled) linear differential equations satisfied by the whole set of master integrals. Upon solving these equations one finds analytic expressions for all integrals involved simultaneously[6]. Let us now review how the method works.

As mentioned before, after integration, scalar Feynman integrals must be functions of the space-time dimensions and the external invariants only. For concreteness we choose to parametrise the kinematics via the Mandelstam variables of eq. (2.2). We label the set of all independent Mandelstam variables by $\vec{s}$ and the individual ones by s_I, where I corresponds to some set of external momenta $I = (ij\dots k)$.

Let us see then how differentiation with respect to s_I acts on the space of master integrals, which we denote by $\mathcal{M}_i$. When using parametric representations, the dependence on the independent s_I is explicit and one can simply differentiate the integrand. For consistency, here we stick to the representation given in eq. (2.48) and

[6]In practice, since the system of equations is usually block triangular, it is convenient to solve the system starting from lower-sector integrals and progressively increasing the propagator count.

we need to understand how ∂_{s_I} acts on the integrand of loop-momentum Feynman integrals. This can be done starting from the ansatz

$$\partial_{s_I} = \sum_{k,h=1}^{n-1} C^I_{hk}\, p_h \cdot \frac{\partial}{\partial p_k}\,, \tag{2.63}$$

where we expressed the derivative with respect to s_I in terms of derivatives with respect to the independent external momenta. The coefficients C^I_{hk} are rational functions of the Mandelstam invariants and need to be fixed. To do so we can use the Lorentz invariance identities of eq. (2.60) together with the consistency conditions

$$\begin{cases} \partial_{s_I} s_J = \delta_{IJ}\,, \\ \partial_{s_I} p_j^2 = m_j^2 \partial_{s_I}\,, \end{cases} \tag{2.64}$$

for s_I and s_J independent Mandelstam variables and j all external particles. Once the C^I_{hk} have been determined, using the PD representation (2.48) we find

$$\partial_{s_I} \mathcal{M}_i = \sum_{k,h=1}^{n-1} C^I_{hk} \int \mathfrak{D}^L \ell \left(p_h \cdot \frac{\partial}{\partial p_k} \right) \left(\prod_{e=1}^{E)} \frac{1}{\mathcal{D}_e^{\rho_e}} \right)\,. \tag{2.65}$$

Working out the derivatives on the r.h.s. and expressing the resulting integrals as a linear combinations of master integrals via IBPs, we find the relations

$$\partial_{s_I} \mathcal{M}_k = \sum_h \bar{c}^{s_I}_{kh}(\epsilon, \vec{s})\, \mathcal{M}_h\,. \tag{2.66}$$

Moving to a more compact notation, we indicate the vector of master integrals with $\vec{\mathcal{M}}$ and by d the full differential with respect to the kinematic invariants

$$\mathrm{d}g = \sum_I \partial_{s_I} g\, \mathrm{d}s_I\,. \tag{2.67}$$

Eq. (2.66) then implies

$$\mathrm{d}\vec{\mathcal{M}} = \boldsymbol{A}(\epsilon, \vec{s}) \cdot \vec{\mathcal{M}}\,, \tag{2.68}$$

with $\boldsymbol{A}$ a 1-form valued matrix. At this point we can define a particularly nice set of master integrals, the *canonical* basis $\vec{\mathcal{M}}^{can}$ [42–44], by requiring that they satisfy the differential equation

$$\mathrm{d}\vec{\mathcal{M}}^{can} = \epsilon\, \boldsymbol{A}^{can}(\vec{s}) \cdot \vec{\mathcal{M}}^{can}\,, \tag{2.69}$$

where the ϵ-dependence has factorised in front. We also require the matrix $\boldsymbol{A}^{can}$ to be in d log-form:

$$\boldsymbol{A}^{can}(\vec{s}) = \sum_k \boldsymbol{A}_k \, \mathrm{d}\log \alpha_k(\vec{s}) \,, \tag{2.70}$$

where the $\boldsymbol{A}_k$ are matrices of rational numbers and α_k are functions of the invariants, known as *letters*. The full set of letters is usually called *alphabet*.

It is not at all guaranteed that such a basis exists for any given integral family, but in every case treated in this thesis it is possible to find one. The problem of determining canonical bases of master integrals is currently an active area of research.

Once a canonical basis has been found, one can write the analytic solution for the master integrals as a Laurent series in ϵ by expanding the formal solution of eq. (2.69):

$$\vec{\mathcal{M}}^{can}(\vec{s}) = \mathbb{P}\exp\left(\int_{\gamma(\vec{s},\vec{s}_0)} \epsilon \, \boldsymbol{A}(\vec{s})\right) \vec{\mathcal{M}}^{can}(\vec{s}_0) \,. \tag{2.71}$$

Here $\gamma(\vec{s},\vec{s}_0)$ stands for a continuous path connecting $\vec{s}_0$ to $\vec{s}$ and $\mathbb{P}$ enforces path-ordering of the matrices along $\gamma(\vec{s},\vec{s}_0)$. The boundary value $\vec{\mathcal{M}}^{can}(\vec{s}_0)$ can usually be determined by a combination of regularity conditions in certain kinematic limits and direct evaluation.

The functions arising from eq. (2.71) can in general be written as

$$g^{(w)}_{\vec{l}}(\vec{s}) = \int_{\gamma(\vec{s},\vec{s}_{w-1})} \mathrm{d}\log(\alpha_{\ell_w}(\vec{s}_{w-1})) \cdots \int_{\gamma(\vec{s}_2,\vec{s}_1)} \mathrm{d}\log(\alpha_{\ell_2}(\vec{s}_1)) \int_{\gamma(\vec{s}_1,\vec{s}_0)} \mathrm{d}\log(\alpha_{\ell_1}) \tag{2.72}$$

where $\gamma(\vec{s}_i,\vec{s}_j)$ are ordered "segments" of the path $\gamma(\vec{s},\vec{s}_0)$ defined in eq. (2.71). The choice of path γ determines the set of functions and can significantly impact the simplicity of final representation of the integrals. Above, we used w to indicate the length of the vector $\vec{l}$, which in turn determines the list of letters entering the definition above. The integer w counts the number of iterated integrations and is referred to as *transcendental weight*. The $g^{(w)}_{\vec{l}}$ belong to a class of functions commonly called Chen iterated integrals [45]. A canonical master integral m can always[7] be written as

$$m(\vec{s}) = \sum_{w=0} \epsilon^w \sum_{w'=0}^{w} \sum_{\vec{l}\in\mathbb{N}^{w'}} t^{(w-w')}_{\vec{l}} g^{(w')}_{\vec{l}}(\vec{s}) \,, \tag{2.73}$$

[7] provided that we chose an overall normalisation so that the integral starts at $\mathcal{O}(\epsilon^0)$.

where we defined $g_{\vec{l}}^{(0)} = 1$. Above, the $t_{\vec{l}}^{(w)}$ are constants which are given by the value of canonical integral at some reference point $\vec{s}_0$, used as a boundary condition for eq. (2.69). They are also associated a transcendental weight w and by convention ϵ is assigned transcendental weight -1, so that the integrals of the form in eq. (2.73) have overall transcendental weight $w = 0$.

Multiple Polylogarithms In addition to the general discussion above, here we also define the special class of iterated integrals referred to as *multiple polylogarithms* (MPLs) [46, 47]:

$$\begin{aligned} G_l(x) &= \int_0^x \frac{dx'}{x'-l} \quad \text{for } l \neq 0\,, \\ G_{l_1,l_2,\ldots,l_n}(x) &= \int_0^x \frac{dx'}{x'-l_1} G_{l_2,\ldots,l_n}(x') \quad \text{if at least one } l_i \neq 0\,, \\ G_{\underbrace{0,\ldots,0}_{n}}(x) &= \frac{1}{n!}\log^n(x)\,. \end{aligned} \tag{2.74}$$

MPLs turn out to cover the functional space needed for the representation of a large number of scattering amplitudes. Their recursive definition simplifies the study of their analytic structure as well as their analytic continuation across branch-cuts.

2.3.6 Divergences of Feynman Integrals

In previous sections we have established a method to express Feynman integrals as a Laurent expansion in ϵ. In practice one observes that the vast majority of integrals which appear in scattering amplitudes have poles in the dimensional regulator and therefore are divergent as one takes the limit $\epsilon \to 0$. So far we have not been too concerned with the origin of such divergences, but understanding them at the level of Feynman integrals and eventually for whole scattering amplitudes can teach us a lot about the structure of gauge theories. In this section we focus on the singularities of Feynman integrals as standalone mathematical objects. In the section 2.4 we describe how they come together and can be accounted for within full scattering amplitudes.

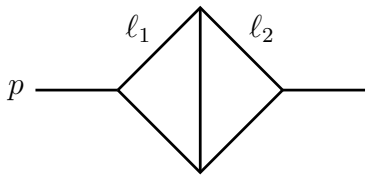

Figure 2.3: A simple two-loop two-point integral.

UV Divergences and Weinberg's Theorem

UV divergences arise in Feynman integrals due to regions where loop momenta become large. Let us make this more precise. We define a sub-integration by identifying a sub-graph and integrating over loop-momentum configurations which keep all its propagators fixed. For any given sub-integration, we can always perform a linear transformation of the loop-momentum variables so that the new loop momenta correspond to integration over a subset S of the loop momenta ℓ_i holding the remaining ones fixed. Rescaling the unfixed loop momenta in S as $\ell^\mu \to \rho\, \ell^\mu$ with $\rho \gg 1$, we find that the product of integrand and measure scales as ρ^ω, where ω defines the superficial degree of divergence of the sub-integration. In particular, the superficial degree of divergence of the whole integral is defined choosing S as the whole set of loop momenta.

Weinberg's power-counting theorem[8] states that a Feynman integral is UV-finite if the integral as well as all its sub-integrations have negative superficial degree of divergence.

For instance, for the *kite* integral of fig. 2.3, we can list all distinct linear combinations $c_i^{(v)}\ell_i$ of loop momenta entering the denominators for a fixed loop-momentum routing: $\{\ell_1, \ell_2, \ell_1 + \ell_2\}$. Next, to identify all allowed sub-integrations, we build all possible subsets of these linear combinations $\{c_i^{(v)}\ell_i \in V\}$, and fix each element in the subset to a different constant,

$$\begin{gathered}\{\ell_1 = d_1,\ \ell_2 = d_2\}\ , \quad \{\ell_1 = d_1,\ \ell_1 + \ell_2 = d_2\}\ , \quad \{\ell_2 = d_1,\ \ell_1 + \ell_2 = d_2\}\ , \\ \{\ell_1 = d\}\ , \quad \{\ell_2 = d\}\ , \quad \{\ell_1 + \ell_2 = d\}\ .\end{gathered} \tag{2.75}$$

[8]The convergence criterion known today as Weinberg's theorem was introduced by Dyson [48] and proven rigorously by Weinberg [49] in the case of Euclidean metric. A simpler proof and an extension to the Minkowski case was presented by Hahn and Zimmermann [50, 51], while Nakanishi gave a proof based on the parametric representation [52, 53].

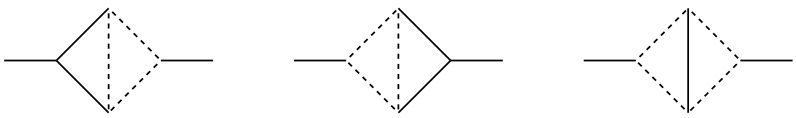

Figure 2.4: Graphical depiction of sub-integrations for the integral in fig. 2.3. The active sub-integrations are indicated by dashed lines, while the momenta corresponding to solid lines are kept fixed.

Finally, for each subset, we solve the corresponding system of equations for the loop momenta and retain only subsets which leave at least one ℓ_i unconstrained.

The subsets in the top row leave no loop momentum unconstrained and can therefore be ignored. Conversely, each of the subsets in the bottom row leaves one degree of freedom unfixed and therefore corresponds to a sub-integration. Graphically, these three subsets can be associated to the diagrams shown in fig. 2.4. Performing the power counting relative to the various (sub-)integrations we find that the integral is UV finite. However, one can check that if one were to add a scalar numerator of the type discussed in section 2.3, its most general form compatible with UV-finiteness would be

$$\mathcal{N} = a + b\, \ell_1 \cdot p + c\, \ell_2 \cdot p\,, \tag{2.76}$$

where a, b and c do not depend on the loop momenta. Higher-degree polynomials in the loop momenta would immediately result in sub-divergences due to the triangle sub-integrations (left and middle of fig. 2.4).

IR Divergences and Landau Equations

IR divergences are instead associated to finite configurations of the loop momenta, in which a subset of the propagators vanish. In general, the domain of integration of a Feynman integral contains IR-divergent surfaces of various dimensions. These correspond to solutions of the Landau equations [54–56] (see also ref. [57] for an up-to-date literature review). In presenting the Landau equations, it is convenient to rewrite the integral of eq. (2.43) in the mixed representation:

$$I[\mathcal{N}(\ell_i)] = \Gamma(E) \int \mathfrak{D}^L \ell \int_0^\infty \frac{\prod_{e=1}^E \mathrm{d}\alpha_e}{\mathrm{GL}(1)} \frac{\mathcal{N}(\ell_i)}{[\alpha_1 \mathcal{D}_1 + \cdots + \alpha_E \mathcal{D}_E]^E}\,, \tag{2.77}$$

All non-UV singularities of the integral correspond to configurations of the integration variables which satisfy,

$$\forall i = 1, \ldots, L: \quad \sum_{e=1}^{E} \alpha_e \frac{\partial}{\partial \ell_i} \mathcal{D}_e = 0\,, \tag{2.78a}$$

$$\forall e = 1, \ldots, E: \quad \alpha_e \mathcal{D}_e = 0\,. \tag{2.78b}$$

These are the Landau equations, which are necessary but not sufficient conditions for the appearance of singularities. They should be viewed as a system of equations for the loop momenta and the kinematic invariants for some values of $\alpha_e \geq 0$ where at least one α_e is strictly positive. Solutions to the Landau equations are called *Landau singularities*. Landau singularities which are present independently of the values of the external kinematic invariants correspond to potential IR divergences, which manifest themselves as poles in the dimensional regulator ϵ. In order to determine whether a Feynman integral actually develops an IR divergence due to a Landau singularity one can often resort to power-counting arguments. This will be discussed more in detail in section 5.3.2. Let us for now focus on the solution of the Landau equations.

The set of equations (2.78a) are linear in the loop momenta, while (2.78b) are quadratic. We proceed by first solving the linear system (2.78a) for the loop momenta, expressing them in terms of the external momenta and the α parameters. We then substitute the solution into the remaining equations (2.78b), and obtain a system of polynomial equations for the α parameters. In many cases the latter system can be solved easily, as we will see below.

An immediate consequence of eqs. (2.51) and (2.52a) is that the linear system (2.78a) is non-degenerate if and only if $\mathcal{U} \neq 0$. Let us consider this non-degenerate case first. As the square matrix A is of full rank, the linear system (2.78a) admits a unique solution,

$$\ell_i^\mu = \left(A^{-1}\right)_{ij} B_j^\mu\,. \tag{2.79}$$

(A parametrisation-independent form of the solution in terms of the graph spanning trees can be found in ref. [57]). We now substitute this solution into the quadratic

equations (2.78b), which become simply

$$\forall e = 1, \ldots, E\colon \quad \alpha_e \frac{\partial}{\partial \alpha_e} \mathcal{F} = 0\,. \tag{2.80}$$

These equations are *also* sometimes referred to as "the Landau equations"; they describe singularities of the integrand in the Feynman-parameter representation[9] when $\mathcal{U} \neq 0$.[10]

To solve eq. (2.80), observe that, due to Euler's homogeneous function theorem, eq. (2.80) implies $\mathcal{F} = 0$. In many cases, $\mathcal{F}$ can be brought into a *subtraction-free* form, meaning that each monomial in $\mathcal{F}$ has the same sign in a certain region of the kinematic space (equivalently, there exists a Euclidean region[11] of the integral). In particular, this holds for planar Feynman graphs. In these cases the $k(T)^2$ in eq. (2.50b) are Mandelstam invariants of consecutive external momenta (with respect to the planar ordering), which can be made negative simultaneously.

For $\alpha_e \geq 0$, a subtraction-free polynomial $\mathcal{F}$ can only vanish if each monomial in $\mathcal{F}$ vanishes independently, which in turn implies eq. (2.80). Therefore, for a subtraction-free $\mathcal{F}$, solving eq. (2.80) is equivalent to setting all monomials in $\mathcal{F}$ to zero independently. The solutions have the form,

$$\alpha_{e_1} = 0, \quad \ldots, \quad \alpha_{e_m} = 0\,, \tag{2.81}$$

where $e_1, \ldots, e_m$ is a proper subset of edge labels $\{1, \ldots, E\}$.

When $\mathcal{F}$ does not admit a subtraction-free form, we must solve eq. (2.80) explicitly. It is believed that the general form of the solution in such cases is nonetheless also given by eq. (2.81). That is, IR divergences cannot arise due to cancellation between terms in $\mathcal{F}$.

One possible strategy to prove this for a given diagram is as follows. Instead of summing eq. (2.80) to get $\mathcal{F} = 0$, which is not subtraction-free, consider the

[9] The "third representation" of ref. [58].

[10] A version of eq. (2.80) which captures also the singularities with $\mathcal{U} = 0$ is obtained by replacing $\mathcal{F}$ with the *world-line action* $\mathcal{F}/\mathcal{U}$ [53].

[11] The same term is sometimes used to refer to a region where *all* Mandelstam variables are positive. This is not possible in general for non planar Feynman integrals when all external states are massless.

most general linear combination of eq. (2.80):

$$\sum_{e=1}^{E} w_e \alpha_e \frac{\partial}{\partial \alpha_e} \mathcal{F} = 0 \,. \tag{2.82}$$

The left-hand side of eq. (2.82) contains the same monomials as $\mathcal{F}$, but the coefficients of these monomials are now linear functions of w_e. Demanding that all coefficients are non-zero and have the same sign in some region of the kinematic space, one obtains a system of linear inequalities on w_e. If one can find a solution of this system (e.g. using numerical linear optimisation routines), then solving eq. (2.80) is equivalent to setting each monomial in $\mathcal{F}$ to zero independently as in the subtraction-free case, therefore no cancellations can occur. We illustrate this procedure in section 5.4.3 when we discuss the massless non-planar double box integral.

Having solved the parameter-space Landau equations (2.80), it remains to check that the solution is consistent with the condition $\mathcal{U} \neq 0$, and compute the corresponding loop momenta using eq. (2.79).

We turn next to the degenerate case, $\mathcal{U} = 0$. As we can see from eq. (2.50a), $\mathcal{U}$ is always subtraction-free, so this condition implies that a subset of α_e vanishes, and all such subsets are identified by setting all monomials in $\mathcal{U}$ to zero. Each solution of $\mathcal{U} = 0$ corresponds to the situation where a sub-diagram γ of the original graph G (formed by the edges for which $\alpha_e = 0$) does not contribute to the Landau equations; effectively, they turn into analogous equations for the *reduced diagram* G/γ obtained by contracting the sub-diagram γ to a point. This means that solutions of the Landau equations in the degenerate case can be found by recursively solving the non-degenerate equations for the reduced diagrams.

A convenient way to implement this in a computer code is by using the following factorisation formulae for the Symanzik polynomials (for example, see ref. [59, Proposition 4.1] and references therein):

$$\mathcal{U}_G|_{\alpha_\gamma \to \lambda \alpha_\gamma} = \lambda^{L_\gamma} \mathcal{U}_\gamma \, \mathcal{U}_{G/\gamma} + \mathcal{O}\left(\lambda^{L_\gamma + 1}\right), \tag{2.83a}$$

$$\mathcal{F}_G|_{\alpha_\gamma \to \lambda \alpha_\gamma} = \lambda^{L_\gamma} \mathcal{U}_\gamma \, \mathcal{F}_{G/\gamma} + \mathcal{O}\left(\lambda^{L_\gamma + 1}\right), \tag{2.83b}$$

where $\lambda \ll 1$ and $\alpha_\gamma \to \lambda\alpha_\gamma$ means that α_e are replaced by $\lambda\alpha_e$ for all edges in γ, while L_γ is the number of loops in the sub-diagram γ. Equation (2.83a) also shows that $\mathcal{U}$ vanishes only when γ contains at least one loop, so the degenerate case $\mathcal{U} = 0$ actually corresponds to IR sub-divergences with one or more loop momenta unconstrained.

2.4 Divergences of Scattering Amplitudes

In section 2.3 we reviewed how Feynman integrals develop singularities for generic values of the external kinematics. The same divergences are inherited by scattering amplitudes, where they combine to reproduce factorised and universal structures. UV divergences are entirely reproduced by a redefinition of the quantities in the lagrangian and are cancelled when renormalising the theory, while IR divergences can be re-summed into exponentials which only depend on the charge and momenta of the external states.

Because both UV and IR divergences do not mix amplitudes for different helicity configurations or particle types, in the following we will simply refer to the spinor-stripped helicity amplitudes of eq. (2.23) via the symbol $\mathcal{H}$.

2.4.1 Renormalisation of UV Divergences

In chapter 1 we claimed that performing calculations with the renormalised lagrangian yields UV-finite results. Let us then see how one can obtain a renormalised amplitude starting from a bare amplitude in the case of massless QCD.

Making reference to eqs. (1.31), (1.36) and (2.1), suppose we want to compute a renormalised scattering amplitude $\mathcal{T}$. Applying the LSZ reduction formula in the massless case we find

$$\mathcal{T}(p_1, \dots, p_n) = \lim_{p_i^2 \to 0} \left(\prod_{i=1}^{n} \int \mathrm{d}^d x_i \, e^{ip_i \cdot x_i} \frac{\xi_i^{A_i} \left(\Box_i\right)_{A_i B_i}}{i\sqrt{\mathcal{Z}_i}} \right) G^{B_1 \dots B_n} \left[\boldsymbol{\Phi}(\boldsymbol{x})\right] \quad . \tag{2.84}$$

where the one-particle pole residues $\mathcal{Z}_i$ are computed using the renormalised lagrangian and we used the shorthand

$$G^{B_1 \dots B_n} \left[\boldsymbol{\Phi}(\boldsymbol{x})\right] = \left\langle \Omega \mid T \left\{ \Phi_1^{B_1}(x_1) \dots \Phi_n^{B_n}(x_n) \right\} \mid \Omega \right\rangle \, . \tag{2.85}$$

Now, because of the structure of the renormalised lagrangian (1.20), we can swap the renormalised Green's function G for the bare one G_0 dividing by the appropriate field renormalisation factors:

$$G^{B_1\dots B_n}\left[\mathbf{\Phi}(\boldsymbol{x})\right](\alpha_s) = \left(\prod_{i=1}^{n}\frac{1}{\sqrt{Z_i}}\right) G_0^{B_1\dots B_n}\left[\mathbf{\Phi}(\boldsymbol{x})\right](\alpha_{s,0})\,. \tag{2.86}$$

Crucially, in dimensional regularisation massless on-shell bare perturbative two-point correlation functions vanish except at tree-level. This is because all Feynman integrals appearing in its loop corrections are scaleless. We can use this to write

$$\begin{aligned}\frac{i\Delta_i^{AB}(p)}{p^2+i\varepsilon} \simeq \int \mathrm{d}^d x\, e^{ip\cdot x}\, G_0^{B_1B_2}\left[\mathbf{\Phi}(\boldsymbol{x})\right](\alpha_{s,0}) = \\ Z_i \int \mathrm{d}^d x\, e^{ip\cdot x}\, G^{B_1B_2}\left[\mathbf{\Phi}(\boldsymbol{x})\right](\alpha_s) \simeq \frac{iZ_i\mathcal{Z}_i\Delta_i^{AB}(p)}{p^2+i\varepsilon} \implies Z_i\mathcal{Z}_i = 1\,,\end{aligned} \tag{2.87}$$

were we recall that $\Delta_i^{AB}(p)$ is the kinetic operator of the free theory. At this point we can plug eqs. (2.86) and (2.87) into eq. (2.84) to obtain

$$\mathcal{T}(p_1,\dots,p_n) = \lim_{p_i^2\to 0}\left(\prod_{i=1}^{n}\int \mathrm{d}^d x_i\, e^{ip_i\cdot x_i}\frac{\xi_i^{A_i}\left(\Box_i\right)_{A_iB_i}}{i}\right) G_0^{B_1\dots B_n}\left[\mathbf{\Phi}(\boldsymbol{x})\right]\ . \tag{2.88}$$

Let us briefly review what we obtained: the renormalised scattering amplitude in QCD (as well as other massless renormalisable gauge theories) can be obtained by applying the LSZ formula to bare Green's functions and then simply renormalising the coupling, no wave-function renormalisation needed! This is due to the fact that the bare residues $\mathcal{Z}_{i,0}$ are exactly equal to unity in perturbation theory due to an exact cancellation of UV and IR divergences (as well as of the finite parts) of the two point function. For the same reason, all non-amputated Green's functions are identically zero and we can directly restrict our calculation to amputated Feynman diagrams.

Applying this to eq. (2.1), reorganising the expansion of the full amplitude in powers of $\alpha_s/4\pi$, and collecting an overall power of the renormalised coupling,

allows us to define the UV-renormalied spinor-stripped helicity amplitudes

$$\begin{aligned}
\boldsymbol{\mathcal{R}}^{(0)} &= \boldsymbol{\mathcal{H}}^{(0)}\,,\\
\boldsymbol{\mathcal{R}}^{(1)} &= \boldsymbol{\mathcal{H}}^{(1)} - \frac{n-2}{2}\frac{\beta_0}{\epsilon}\boldsymbol{\mathcal{H}}^{(0)}\,,\\
\boldsymbol{\mathcal{R}}^{(2)} &= \boldsymbol{\mathcal{H}}^{(2)} - \frac{n}{2}\frac{\beta_0}{\epsilon}\boldsymbol{\mathcal{H}}^{(1)} + \left(\frac{n(n-2)}{8}\frac{\beta_0^2}{\epsilon^2} - \frac{n-2}{4}\frac{\beta_1}{\epsilon}\right)\boldsymbol{\mathcal{H}}^{(0)}\,,\\
\boldsymbol{\mathcal{R}}^{(3)} &= \boldsymbol{\mathcal{H}}^{(3)} - \frac{n+2}{2}\frac{\beta_0}{\epsilon}\boldsymbol{\mathcal{H}}^{(2)} + \left(\frac{n(n+2)}{8}\frac{\beta_0^2}{\epsilon^2} - \frac{n}{4}\frac{\beta_1}{\epsilon}\right)\boldsymbol{\mathcal{H}}^{(1)}\\
&\quad + \left(-\frac{n(n^2-4)}{48}\frac{\beta_0^3}{\epsilon^3} + \frac{(3n+2)(n-2)}{24}\frac{\beta_1\beta_0}{\epsilon^2} - \frac{n-2}{6}\frac{\beta_2}{\epsilon}\right)\boldsymbol{\mathcal{H}}^{(0)}\,,
\end{aligned} \tag{2.89}$$

where we used the colour-vector notation introduced in eqs. (2.28) and (2.29). The renormalised amplitudes $\boldsymbol{\mathcal{R}}^{(\ell)}$ are thus free of UV divergences and all poles in ϵ can be attributed to IR divergences.

2.4.2 Factorisation of IR Divergences

In sections 1.4 and 2.4.1 we saw that UV divergences are fully accounted for by renormalisation of the fields and the strong coupling. Though the first result describing the universal structure of QCD infrared singularities was presented by Catani in ref. [33], we will now see that IR can also be treated within the language of renormalisation.

The concepts reviewed below were first presented in refs. [60–63] and rely on the one-to-one correspondence of the IR divergences of gauge-theory amplitudes with the UV divergences of the effective field theory (EFT) describing the soft and collinear degrees of freedom. A concrete realisation of such an EFT is soft-collinear effective-theory (SCET) [64–67]. In ref. [60, 61] it has been shown that IR singularities of QCD exactly match the UV poles of S-matrix elements in SCET.

As a result, QCD scattering amplitudes can be written in terms of a multiplicative colour-space operator $\boldsymbol{\mathcal{Z}}$ as

$$\boldsymbol{\mathcal{R}}(\epsilon,\{p\},\mu) = \boldsymbol{\mathcal{Z}}(\epsilon,\{p\},\mu_{IR},\mu)\,\boldsymbol{\mathcal{F}}(\epsilon,\{p\},\mu_{IR},\mu), \tag{2.90}$$

Figure 2.5: Schematic representation of the correspondence between the IR divergences of QCD and the UV divergences of the corresponding low-energy EFT. The cut-off scale μ_{IR} acts both as an IR regulator of QCD and a UV regulator of the EFT. Matching of the two theories requires that observables should agree when the typical energies are approximately μ_{IR}. Therefore the existence of and EFT for the soft/collinear degrees of freedom of QCD implies the renormalisability of its IR divergences.

where $\{p\}$ stands for the list of external momenta, μ is the UV renormalisation scale and $\boldsymbol{\mathcal{F}}$ is an IR finite *hard* amplitude which can be expanded perturbatively as

$$\boldsymbol{\mathcal{F}} = \sum_{\ell=0} \left(\frac{\alpha_s}{4\pi}\right)^{\ell} \boldsymbol{\mathcal{F}}^{(\ell)} \,. \tag{2.91}$$

Above, μ_{IR} is the IR factorisation scale, defined to separate the high-energy/large-angle degrees of freedom from the soft/collinear ones. Because the UV renormalised amplitude $\boldsymbol{\mathcal{R}}$ does not depend on our choice of μ_{IR}, one can write the renormalisation group equation

$$\frac{\mathrm{d}}{\mathrm{d}\log\mu_{IR}}\boldsymbol{\mathcal{F}} = -\left[\boldsymbol{\mathcal{Z}}^{-1}\,\frac{\mathrm{d}}{\mathrm{d}\log\mu_{IR}}\boldsymbol{\mathcal{Z}}\right]\,\boldsymbol{\mathcal{F}}\,. \tag{2.92}$$

This in turn defines the *soft/collinear anomalous dimension*

$$\boldsymbol{\Gamma}(\epsilon,\{p\},\mu_{IR},\mu) = \left[\boldsymbol{\mathcal{Z}}^{-1}(\epsilon,\{p\},\mu_{IR},\mu)\,\frac{\mathrm{d}}{\mathrm{d}\log\mu_{IR}}\boldsymbol{\mathcal{Z}}(\epsilon,\{p\},\mu_{IR},\mu)\right]\,, \tag{2.93}$$

which governs the evolution in μ_{IR} of the hard function $\boldsymbol{\mathcal{F}}$. Fixing $\mu_{IR} = \mu$ one can formally solve eq. (2.93) to find

$$\boldsymbol{\mathcal{Z}}(\epsilon,\{p\},\mu) = \mathbb{P}\exp\left[-\int_0^{\mu}\frac{\mathrm{d}\mu'}{\mu'}\boldsymbol{\Gamma}(\{p\},\mu')\right] = \sum_{n=0}^{\infty}\left(\frac{\alpha_s}{4\pi}\right)^n \boldsymbol{\mathcal{Z}}_n\,, \tag{2.94}$$

with $\mathbb{P}$ the *path-ordering* symbol, *i.e.* colour operators are ordered from left to right with decreasing values of μ'. The soft-collinear anomalous dimension $\boldsymbol{\Gamma}$ receives perturbative corrections (see [68] for a recent review on the topic). In particular, up to three loops, following the notation of [69] where $\boldsymbol{\Gamma}$ was first

computed to this perturbative order, the anomalous dimension operator for n coloured external particles is written as

$$\mathbf{\Gamma}(\{p\},\mu) = \mathbf{\Gamma}_{\text{dipole}}(\{p\},\mu) + \mathbf{\Delta}_4(\{p\}) \,, \tag{2.95}$$

where dipole and quadrupole contributions appear. The dipole IR anomalous dimension $\mathbf{\Gamma}_{\text{dipole}}$ is a sum of terms, each depending on the momenta of a pair of external particles, and collects all pair-wise colour correlations of the external states as well a colour-diagonal collinear contribution. Explicitly, it takes the standard form

$$\mathbf{\Gamma}_{\text{dipole}}(\{p\},\mu) = \sum_{1\leq i<j\leq n} \mathbf{T}_i^a \, \mathbf{T}_j^a \, \gamma^{\text{K}}(\alpha_s) \, \log\left(\frac{\mu^2}{-s_{ij}-i\delta}\right) + \sum_{i=1}^{n} \gamma^i(\alpha_s) \,, \tag{2.96}$$

with $\mathbf{T}_i^a$ the $SU(N_c)$ generators in the representation of the i-th external particle which act on the amplitude by contraction with the colour index the i-th parton. The quantity γ^{K} is the QCD cusp anomalous dimension [70–76] and $\gamma^{i=q,g}$ are the quark and gluon collinear anomalous dimensions [68, 77–79]. They are given explicitly in appendix A.1 up to the third perturbative order.

When performing the integral in eq. (2.94), and only considering corrections up to three loops, the path-ordering operator can be ignored since $\mathbf{\Gamma}$ does not depend on the scale μ and therefore

$$[\mathbf{\Gamma}(\{p\},\mu_1), \mathbf{\Gamma}(\{p\},\mu_2)] = 0 \,. \tag{2.97}$$

Furthermore it is also useful to define the expansions

$$\mathbf{\Gamma}_{\text{dipole}} = \sum_{n=0}^{\infty} \mathbf{\Gamma}_n \left(\frac{\alpha_s}{4\pi}\right)^{n+1} , \qquad \Gamma' = \frac{\partial \mathbf{\Gamma}_{\text{dipole}}}{\partial \log \mu} = \sum_{n=0}^{\infty} \Gamma'_n \left(\frac{\alpha_s}{4\pi}\right)^{n+1} . \tag{2.98}$$

The operator $\mathbf{\Delta}_4$ appears instead for the first time at three loops and contains colour correlations among up to four external legs. It can be expanded in α_s as

$$\mathbf{\Delta}_4(\{p\}) = \mathbf{\Delta}_4(\{\rho\}) = \sum_{L=3}^{\infty} \left(\frac{\alpha_s}{4\pi}\right)^L \mathbf{\Delta}_4^{(L)}(\{\rho\}) \,. \tag{2.99}$$

The leading order contribution $\mathbf{\Delta}_4^{(3)}(\{\rho\})$ was computed in ref. [69] and more details on its structure will be given in chapter 3.

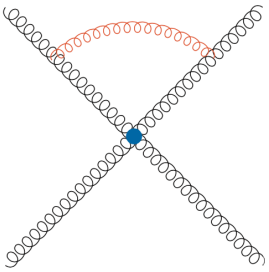

Figure 2.6: Sample Feynman diagram contributing to the dipole IR anomalous dimension $\mathbf{\Gamma}_{\text{dipole}}$. Dipole soft divergences arise from the region of loop-momentum space where all components of the red gluon are small compared to the other scale in the process. Collinear divergences arise when the momentum associated with the red gluon becomes proportional to the momentum of one the external emitting gluons.

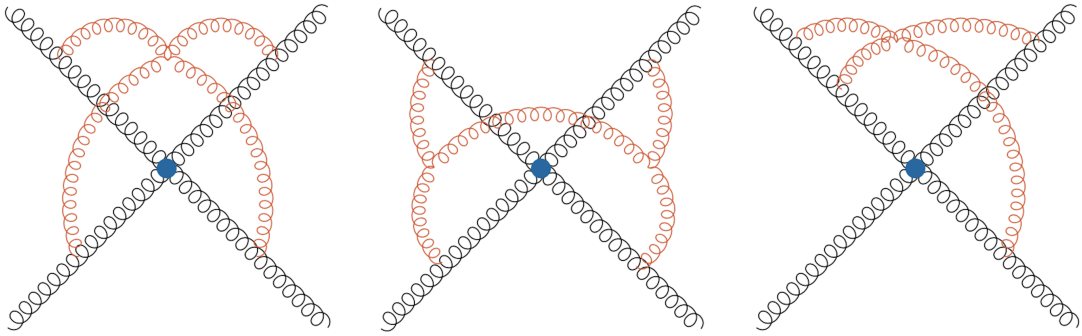

Figure 2.7: Sample Feynman diagrams contributing to the three-loop quadrupole correction $\mathbf{\Delta}_4^{(3)}(\{\rho\})$ in four-point gluon scattering. Quadrupole divergences arise from the region of loop-momentum space where all components of the red gluons are much smaller than the other scales in the amplitude. The central dot represents any possible tree-level sub-diagram.

In terms of the quantities defined above, one can write the perturbative coefficients of the IR operator $\boldsymbol{\mathcal{Z}}$ as

$$
\begin{aligned}
\boldsymbol{\mathcal{Z}}_1 &= \frac{\Gamma_0'}{4\epsilon^2} + \frac{\mathbf{\Gamma}_0}{2\epsilon}\,, \\
\boldsymbol{\mathcal{Z}}_2 &= \frac{{\Gamma_0'}^2}{32\epsilon^4} + \frac{\Gamma_0'}{8\epsilon^3}\left(\mathbf{\Gamma}_0 - \frac{3}{2}\beta_0\right) + \frac{\mathbf{\Gamma}_0}{8\epsilon^2}(\mathbf{\Gamma}_0 - 2\beta_0) + \frac{\Gamma_1'}{16\epsilon^2} + \frac{\mathbf{\Gamma}_1}{4\epsilon}\,, \\
\boldsymbol{\mathcal{Z}}_3 &= \frac{{\Gamma_0'}^3}{384\epsilon^6} + \frac{{\Gamma_0'}^2}{64\epsilon^5}(\mathbf{\Gamma}_0 - 3\beta_0) + \frac{\Gamma_0'}{32\epsilon^4}\left(\mathbf{\Gamma}_0 - \frac{4}{3}\beta_0\right)\left(\mathbf{\Gamma}_0 - \frac{11}{3}\beta_0\right) + \frac{\Gamma_0'\Gamma_1'}{64\epsilon^4} \\
&\quad + \frac{\mathbf{\Gamma}_0}{48\epsilon^3}(\mathbf{\Gamma}_0 - 2\beta_0)(\mathbf{\Gamma}_0 - 4\beta_0) + \frac{\Gamma_0'}{16\epsilon^3}\left(\mathbf{\Gamma}_1 - \frac{16}{9}\beta_1\right) + \frac{\Gamma_1'}{32\epsilon^3}\left(\mathbf{\Gamma}_0 - \frac{20}{9}\beta_0\right) \\
&\quad + \frac{\mathbf{\Gamma}_0\mathbf{\Gamma}_1}{8\epsilon^2} - \frac{\beta_0\mathbf{\Gamma}_1 + \beta_1\mathbf{\Gamma}_0}{6\epsilon^2} + \frac{\Gamma_2'}{36\epsilon^2} + \frac{\mathbf{\Gamma}_2 + \mathbf{\Delta}_4^{(3)}}{6\epsilon}\,.
\end{aligned}
\tag{2.100}
$$

Plugging these into eq. (2.90) and solving for the perturbative coefficients of

the hard function we find

$$\begin{aligned}
\boldsymbol{\mathcal{F}}^{(0)} &= \boldsymbol{\mathcal{R}}^{(0)} \,, \\
\boldsymbol{\mathcal{F}}^{(1)} &= \boldsymbol{\mathcal{R}}^{(1)} - \boldsymbol{\mathcal{I}}_1 \, \boldsymbol{\mathcal{R}}^{(0)} \,, \\
\boldsymbol{\mathcal{F}}^{(2)} &= \boldsymbol{\mathcal{R}}^{(2)} - \boldsymbol{\mathcal{I}}_2 \, \boldsymbol{\mathcal{R}}^{(0)} - \boldsymbol{\mathcal{I}}_1 \, \boldsymbol{\mathcal{R}}^{(1)} \,, \\
\boldsymbol{\mathcal{F}}^{(3)} &= \boldsymbol{\mathcal{R}}^{(3)} - \boldsymbol{\mathcal{I}}_3 \, \boldsymbol{\mathcal{R}}^{(0)} - \boldsymbol{\mathcal{I}}_2 \, \boldsymbol{\mathcal{R}}^{(1)} - \boldsymbol{\mathcal{I}}_1 \, \boldsymbol{\mathcal{R}}^{(2)} \,,
\end{aligned} \tag{2.101}$$

where the IR subtraction operators read

$$\begin{aligned}
\boldsymbol{\mathcal{I}}_1 &= \boldsymbol{\mathcal{Z}}_1 \,, \\
\boldsymbol{\mathcal{I}}_2 &= \boldsymbol{\mathcal{Z}}_2 - \boldsymbol{\mathcal{Z}}_1^2 \,, \\
\boldsymbol{\mathcal{I}}_3 &= \boldsymbol{\mathcal{Z}}_3 - 2\boldsymbol{\mathcal{Z}}_1\boldsymbol{\mathcal{Z}}_2 + \boldsymbol{\mathcal{Z}}_1^3 + \boldsymbol{\Delta}_4^{(3)} \,.
\end{aligned} \tag{2.102}$$

This concludes the discussion on the structure of IR divergences of QCD scattering amplitudes up to three loops.

At higher loops the soft-collinear anomalous dimension $\boldsymbol{\Gamma}$ is expected to receive corrections which involve colour correlations of more than four external states. At four loops, their structure was constrained for instance in the Regge limit [80], but exact calculations have yet to be performed beyond the three-loop order.

3

Three-Loop Four-Point Scattering

Contents

3.1 Introduction 52
3.2 Colour and Helicity Decomposition 53
3.3 Loop Integrals 59
3.4 Analytic Continuation 62
3.5 Crossed Channels and Equal Flavour Amplitudes . . . 66
3.6 Infrared Structure and Quadrupole Radiation 67
3.7 Analytic Results and Numerical Evaluation 69
3.8 The Gluon Regge Trajectory 72

3.1 Introduction

In this chapter we focus on the computation of all three-loop scattering amplitudes of four particles in QCD. Crossing symmetry, charge and parity conjugation allow

Loops	0	1	2	3
$0 \to q\bar{q}Q\bar{Q}$	1	9	158	3584
$0 \to q\bar{q}gg$	3	30	595	14971
$0 \to gggg$	4	81	1771	48723

Table 3.1: Number of amputated QCD Feynman diagrams contributing to the processes in eq. (3.1) at different loop orders.

us to reproduce all possible channels starting from the set of processes

$$\begin{aligned} 0 &\to q(p_1) + \bar{q}(p_2) + Q(p_3) + \bar{Q}(p_4), \\ 0 &\to q(p_1) + \bar{q}(p_2) + g(p_3) + g(p_4), \\ 0 &\to g(p_1) + g(p_2) + g(p_3) + g(p_4), \end{aligned} \tag{3.1}$$

where q and Q stand for two different flavours of quark. All external momenta are taken to be outgoing and massless:

$$p_1^\mu + p_2^\mu + p_3^\mu + p_4^\mu = 0, \quad p_i^2 = 0. \tag{3.2}$$

Because we work in the tHV scheme they can also taken to be strictly four-dimensional. The scattering processes above can then be parametrised in terms of the usual set of Mandelstam invariants

$$s_{12} = (p_1 + p_2)^2, \; s_{13} = (p_1 + p_3)^2, \; s_{23} = (p_2 + p_3)^2, \tag{3.3}$$

which satisfy the relation $s_{13} = -s_{12} - s_{23}$. The physical scattering process $1 + 2 \to 3 + 4$ can be obtained by changing sign to the momenta of incoming particles: $p_{1,2} \to -p_{1,2}$ and by imposing

$$s_{12} > 0, \; s_{13} < 0, \; s_{23} < 0\,, \tag{3.4}$$

which corresponds to the s-channel region of fig. 3.1.

3.2 Colour and Helicity Decomposition

For any of the processes in eq. (3.1)

$$X = \{q\bar{q}Q\bar{Q}\,, q\bar{q}gg\,, gggg\}\,, \tag{3.5}$$

we write the scattering amplitude as

$$\mathcal{A}_X = 4\pi\alpha_{s,0}\, \boldsymbol{\mathcal{A}}_X \cdot \boldsymbol{\mathcal{C}}^X\,, \tag{3.6}$$

where $\alpha_{s,0}$ is the bare strong coupling, $\mathcal{A}^{[i]}$ are colour-ordered *partial amplitudes*. The bold quantities $\boldsymbol{\mathcal{A}}_X$ and $\boldsymbol{\mathcal{C}}^X$ are the colour vectors defined by eq. (2.29). The colour tensors for $0 \to q\bar{q}Q\bar{Q}$ read

$$\mathcal{C}_1^{q\bar{q}Q\bar{Q}} = \delta_{i_1}^{i_4}\delta_{i_3}^{i_2}\,, \qquad \mathcal{C}_2^{q\bar{q}Q\bar{Q}} = \delta_{i_1}^{i_2}\delta_{i_3}^{i_4}\,, \tag{3.7}$$

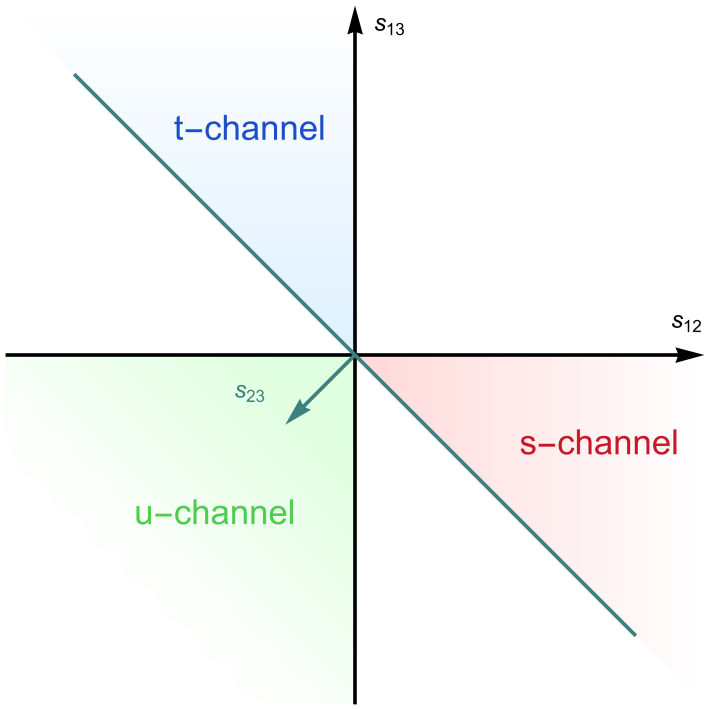

Figure 3.1: Mandelstam plane describing the physical scattering regions, commonly known as s, t and u channels. White regions are unphysical, in the sense that they do not correspond to any choice of real four-momenta.

for $0 \to q\bar{q}gg$ they are

$$\mathcal{C}_1^{q\bar{q}gg} = (T^{a_3}T^{a_4})_{i_1}^{i_2}\,, \qquad \mathcal{C}_2^{q\bar{q}gg} = (T^{a_4}T^{a_3})_{i_1}^{i_2}\,, \qquad \mathcal{C}_3^{q\bar{q}gg} = \mathrm{Tr}[T^{a_3}T^{a_4}]\,\delta_{i_1}^{i_2}\,, \tag{3.8}$$

and the ones for $0 \to gggg$ are defined as

$$\begin{aligned}
\mathcal{C}_1^{gggg} &= \mathrm{Tr}[T^{a_1}T^{a_2}T^{a_3}T^{a_4}] + \mathrm{Tr}[T^{a_1}T^{a_4}T^{a_3}T^{a_2}]\,,\\
\mathcal{C}_2^{gggg} &= \mathrm{Tr}[T^{a_1}T^{a_2}T^{a_4}T^{a_3}] + \mathrm{Tr}[T^{a_1}T^{a_3}T^{a_4}T^{a_2}]\,,\\
\mathcal{C}_3^{gggg} &= \mathrm{Tr}[T^{a_1}T^{a_3}T^{a_2}T^{a_4}] + \mathrm{Tr}[T^{a_1}T^{a_4}T^{a_2}T^{a_3}]\,,\\
\mathcal{C}_4^{gggg} &= \mathrm{Tr}[T^{a_1}T^{a_2}]\mathrm{Tr}[T^{a_3}T^{a_4}]\,,\\
\mathcal{C}_5^{gggg} &= \mathrm{Tr}[T^{a_1}T^{a_3}]\mathrm{Tr}[T^{a_2}T^{a_4}]\,,\\
\mathcal{C}_6^{gggg} &= \mathrm{Tr}[T^{a_1}T^{a_4}]\mathrm{Tr}[T^{a_2}T^{a_3}]\,.
\end{aligned} \tag{3.9}$$

In order to compute the partial amplitudes for definite helicity configurations we can use the tensor projection method in the tHV scheme in conjunction with the spinor helicity formalism. Following the steps described in section 2.1.2, we decompose

the partial amplitudes on a tensor basis as

$$\boldsymbol{\mathcal{A}}_X = \sum_{j=1} \boldsymbol{\mathcal{F}}_X^j \, T_j^X, \tag{3.10}$$

where the Lorentz tensors T_j^X can be chosen as (see ref. [29])

$$\begin{aligned} T_1^{q\bar{q}Q\bar{Q}} &= \bar{u}(p_2)\,\gamma_\alpha\,u(p_1)\;\bar{u}(p_4)\,\gamma^\alpha\,u(p_3)\;, \\ T_2^{q\bar{q}Q\bar{Q}} &= \bar{u}(p_2)\,\not{p}_3\,u(p_1)\;\bar{u}(p_4)\,\not{p}_2\,u(p_3) \end{aligned} \tag{3.11}$$

for quark scattering,

$$\begin{aligned} T_1^{q\bar{q}gg} &= \bar{u}(p_2)\not{\epsilon}_3 u(p_1)\,\epsilon_4\cdot p_2\,, \qquad T_2^{q\bar{q}gg} = \bar{u}(p_2)\not{\epsilon}_4 u(p_1)\,\epsilon_3\cdot p_1\,, \\ T_3^{q\bar{q}gg} &= \bar{u}(p_2)\not{p}_3 u(p_1)\,\epsilon_3\cdot p_1\,\epsilon_4\cdot p_2\,, \qquad T_4^{q\bar{q}gg} = \bar{u}(p_2)\not{p}_3 u(p_1)\,\epsilon_3\cdot\epsilon_4\,, \end{aligned} \tag{3.12}$$

for quark-gluon scattering and

$$\begin{aligned} T_1^{gggg} &= \epsilon_1{\cdot}p_3\;\epsilon_2{\cdot}p_1\;\epsilon_3{\cdot}p_1\;\epsilon_4{\cdot}p_2\;, \\ T_2^{gggg} &= \epsilon_1{\cdot}p_3\;\epsilon_2{\cdot}p_1\;\epsilon_3{\cdot}\epsilon_4, \quad T_3^{gggg} = \epsilon_1{\cdot}p_3\;\epsilon_3{\cdot}p_1\;\epsilon_2{\cdot}\epsilon_4, \\ T_4^{gggg} &= \epsilon_1{\cdot}p_3\;\epsilon_4{\cdot}p_2\;\epsilon_2{\cdot}\epsilon_3, \quad T_5^{gggg} = \epsilon_2{\cdot}p_1\;\epsilon_3{\cdot}p_1\;\epsilon_1{\cdot}\epsilon_4, \\ T_6^{gggg} &= \epsilon_2{\cdot}p_1\;\epsilon_4{\cdot}p_2\;\epsilon_1{\cdot}\epsilon_3, \quad T_7^{gggg} = \epsilon_3{\cdot}p_1\;\epsilon_4{\cdot}p_2\;\epsilon_1{\cdot}\epsilon_2, \\ T_8^{gggg} &= \epsilon_1{\cdot}\epsilon_2\;\epsilon_3{\cdot}\epsilon_4 + \epsilon_1{\cdot}\epsilon_4\;\epsilon_2{\cdot}\epsilon_3 + \epsilon_1{\cdot}\epsilon_3\;\epsilon_2{\cdot}\epsilon_4\;, \end{aligned} \tag{3.13}$$

for gluon scattering.

In order to obtain the above set of tensors, the reference vectors q_i of the external gluons have been fixed as follows:

$$\begin{cases} q_3 = p_4,\; q_4 = p_3 & \text{for } q\bar{q}gg \to 0, \\ q_1 = p_2,\; q_2 = p_3,\; q_3 = p_4,\; q_4 = p_1 & \text{for } gggg \to 0. \end{cases} \tag{3.14}$$

The form factors can then be obtained via tensor-projection of the amplitudes as described in section 2.1.2. In particular, we define process-dependent projectors

$$P_i^X = \sum_{j=1} c_{ij}^X (T_j^X)^\dagger\,, \qquad \text{with} \quad P_i^X \circ T_j^X = \delta_{ij} \tag{3.15}$$

where the product $\circ$ was defined in eq. (2.26) and the coefficient matrices c_{ij}^X are given by

$$
\begin{aligned}
c^{q\bar{q}Q\bar{Q}} &= \frac{1}{(d-3)s_{12}^2 s_{13}^2 s_{23}^2}\begin{pmatrix} \frac{1}{4}s_{13}^2 s_{23}^2 & s_{13}s_{23}(s_{13}-s_{23}) \\ s_{13}s_{23}(s_{13}-s_{23}) & \frac{1}{2}(s_{13}^2+s_{23}^2)+\frac{1}{4}(d-4)s_{12}^2 \end{pmatrix}, \\
c^{q\bar{q}gg} &= \frac{1}{2(d-3)s_{12}^2 s_{13}^3 s_{23}}\begin{pmatrix} s_{13}^2 s_{23}^2 & 0 & -s_{13}s_{23}^2 & 0 \\ 0 & s_{13}^2 s_{23}^2 & s_{13}s_{23}^2 & 0 \\ -s_{13}s_{23}^2 & s_{13}s_{23}^2 & (ds_{23}^2-4s_{12}s_{13}) & (s_{12}-s_{13})s_{12}s_{13} \\ 0 & 0 & (s_{12}-s_{13})s_{12}s_{13} & s_{12}^2 s_{13}^2 \end{pmatrix}, \\
c^{gggg} &= \frac{s_{12}^2 s_{23}^2}{s_{13}}\left[\frac{s_{13}}{3}c_4^{gggg}+(d-4)c_\epsilon^{gggg}\right],
\end{aligned}
\tag{3.16}
$$

where we defined the symmetric matrices

$$
c_4^{gggg} = \begin{pmatrix}
8Q & X & Z_{12} & -X & X & -Z_{23} & -X & -\frac{s_{13}Y}{2} \\
X & 10 & R_2 & -1 & 1 & -R_1 & -1 & -s_{13} \\
Z_{12} & R_2 & W_{12} & -R_2 & R_2 & -R_1R_2 & -R_2 & -R_2s_{13} \\
-X & -1 & -R_2 & 10 & -1 & R_1 & 1 & s_{13} \\
X & 1 & R_2 & -1 & 10 & -R_1 & -1 & -s_{13} \\
-Z_{23} & -R_1 & -R_1R_2 & R_1 & -R_1 & W_{23} & R_1 & R_1s_{13} \\
-X & -1 & -R_2 & 1 & -1 & R_1 & 10 & s_{13} \\
-\frac{s_{13}Y}{2} & -s_{13} & -R_2s_{13} & s_{13} & -s_{13} & R_1s_{13} & s_{13} & s_{13}^2
\end{pmatrix},
\tag{3.17}
$$

$$
c_\epsilon^{gggg} = \begin{pmatrix}
Ps_{13}^3 & 1 & \frac{R_1s_{12}^2}{s_{23}^2} & -1 & 1 & -\frac{R_2s_{23}^2}{s_{12}^2} & -1 & 0 \\
1 & s_{13} & 0 & 0 & 0 & 0 & 0 & 0 \\
\frac{R_1s_{12}^2}{s_{23}^2} & 0 & \frac{s_{12}^2s_{13}}{s_{23}^2} & 0 & 0 & 0 & 0 & 0 \\
-1 & 0 & 0 & s_{13} & 0 & 0 & 0 & 0 \\
1 & 0 & 0 & 0 & s_{13} & 0 & 0 & 0 \\
-\frac{R_2s_{23}^2}{s_{12}^2} & 0 & 0 & 0 & 0 & \frac{s_{13}s_{23}^2}{s_{12}^2} & 0 & 0 \\
-1 & 0 & 0 & 0 & 0 & 0 & s_{13} & 0 \\
0 & 0 & 0 & 0 & 0 & 0 & 0 & 0
\end{pmatrix}
\tag{3.18}
$$

and used the shorthands

$$
\begin{aligned}
Q &= \frac{2s_{13}^4+3\left(s_{12}^4+s_{23}^2s_{12}^2+s_{23}^4\right)}{s_{12}^2s_{13}^2s_{23}^2}, \quad P = \frac{d-\frac{12s_{13}^2}{s_{12}s_{23}}+6}{s_{13}^4}+\frac{4}{s_{12}^2s_{23}^2}, \\
Z_{12} &= \frac{4\left(3s_{12}^3+s_{13}^2s_{12}-s_{13}^3\right)}{s_{12}s_{13}s_{23}^2}, \quad Z_{23} = -\frac{4\left(s_{13}^3-s_{23}s_{13}^2-3s_{23}^3\right)}{s_{12}^2s_{13}s_{23}}, \\
W_{12} &= \frac{2\left(4s_{12}^2+s_{13}^2\right)}{s_{23}^2}+2, \quad W_{23} = \frac{2\left(s_{12}^2+s_{13}^2+4s_{23}^2\right)}{s_{12}^2}, \\
X &= \frac{2s_{13}}{s_{12}s_{23}}+\frac{12}{s_{13}}, \quad Y = \frac{4s_{13}}{s_{12}s_{23}}+\frac{6}{s_{13}}, \\
R_1 &= \frac{s_{23}}{s_{12}}+2, \quad R_2 = \frac{s_{12}}{s_{23}}+2.
\end{aligned}
\tag{3.19}
$$

With this we can determine the scalar form factors as $\boldsymbol{\mathcal{F}}_X^j = P_j^X \circ \boldsymbol{\mathcal{A}}_X$. In order to build helicity amplitudes we can now proceed as described in section 2.1.2, evaluating the tensors T_i^X for specific helicity configurations by plugging in eqs. (3.2), (3.2) and (3.2) the explicit form of the polarisation vectors in the spinor helicity formalism (see eqs. (2.10) and (2.19)).

There are two parity-independent helicity configurations for the quark process, four for the mixed process and eight for the gluon one. Denoting by $\boldsymbol{\lambda} = (\lambda_1, \lambda_2, \lambda_3, \lambda_4)$ the list of signs of the helicities of the four incoming external states, they are

$$\begin{aligned}
\boldsymbol{\lambda}_{q\bar{q}Q\bar{Q}} &\in \{(-,+,-,+),\ (-,+,+,-)\},\\
\boldsymbol{\lambda}_{q\bar{q}gg} &\in \{(-,+,-,-),\ (-,+,-,+),\ (-,+,+,-),\ (-,+,+,+)\},\\
\boldsymbol{\lambda}_{gggg} &\in \{(+,+,+,+),\ (-,+,+,+),\ (+,-,+,+),\ (+,+,-,+),\\
&\qquad (+,+,+,-),\ (+,+,-,-),\ (+,-,+,-),\ (+,-,-,+)\}.
\end{aligned} \tag{3.20}$$

The corresponding spinor factors, defined as in eq. (2.23), can be chosen as

$$\begin{aligned}
&\left\{s^{q\bar{q}Q\bar{Q}}_{+-+-}, s^{q\bar{q}Q\bar{Q}}_{+--+}\right\} = \left\{\frac{[13]}{[24]}, \frac{[14]}{[23]}\right\},\\
&\left\{s^{q\bar{q}gg}_{-+--}, s^{q\bar{q}gg}_{-+-+}, s^{q\bar{q}gg}_{-++-}, s^{q\bar{q}gg}_{-+++}\right\} = \left\{\frac{2\langle 34\rangle^2}{[13]\langle 23\rangle}, \frac{2[24]\langle 13\rangle}{[23]\langle 24\rangle}, \frac{2[23]\langle 41\rangle}{[24]\langle 32\rangle}, \frac{2[34]^2}{[31]\langle 23\rangle}\right\},\\
&\{s^{gggg}_{++++}, s^{gggg}_{-+++}, s^{gggg}_{+-++}, s^{gggg}_{++-+}, s^{gggg}_{+++-}, s^{gggg}_{++--}, s^{gggg}_{+-+-}, s^{gggg}_{+--+}\} =\\
&\qquad \left\{\frac{[12][34]}{\langle 12\rangle\langle 34\rangle}, \frac{[34][23][24]}{[12][14]\langle 24\rangle}, \frac{[34][13][14]}{[21][24]\langle 14\rangle}, \frac{[14][21][24]}{[32][34]\langle 24\rangle},\right.\\
&\qquad\qquad \left.\frac{[13][23][12]}{[42][14]\langle 12\rangle}, \frac{[12]\langle 34\rangle}{\langle 12\rangle[34]}, \frac{[13]\langle 24\rangle}{\langle 13\rangle[24]}, \frac{[14]\langle 23\rangle}{\langle 14\rangle[23]}\right\}.
\end{aligned} \tag{3.21}$$

This allows us to write an explicit expression for the helicity amplitudes

$$\boldsymbol{\mathcal{A}}_X|_{\boldsymbol{\lambda}} = \left(\sum_j R^X_{j,\boldsymbol{\lambda}}\, \boldsymbol{\mathcal{F}}^j_X\right)\ s^X_{\boldsymbol{\lambda}} \equiv \boldsymbol{\mathcal{H}}_{X,\boldsymbol{\lambda}}\, s^X_{\boldsymbol{\lambda}}, \tag{3.22}$$

and define the spinor-stripped partial amplitudes $\boldsymbol{\mathcal{H}}_{X,\boldsymbol{\lambda}}$.

The formal colour and helicity decomposition of amplitudes holds at all orders in perturbation theory, however in order to explicitly compute the $\boldsymbol{\mathcal{H}}_{X,\boldsymbol{\lambda}}$ we need to perform a perturbative expansion in the coupling α_s:

$$\boldsymbol{\mathcal{H}}_{X,\boldsymbol{\lambda}} = \sum_{\ell=0} \left(\frac{\alpha_s}{4\pi}\right)^\ell \boldsymbol{\mathcal{H}}^{(\ell)}_{X,\boldsymbol{\lambda}}\,. \tag{3.23}$$

At each loop order ℓ we can compute $\boldsymbol{\mathcal{H}}^{(\ell)}_{X,\boldsymbol{\lambda}}$ starting from the sum of ℓ-loop Feynman diagrams contributing to the process.

In section 2.2 we saw that only a subset of partial (helicity) amplitudes need to be computed directly and the remaining ones can be obtained via symmetry relations. Part of this information was already used in eq. (3.20), where only parity-independent helicity configurations were listed. For $0 \to q\bar{q}Q\bar{Q}$ no further relations exist between the partial amplitudes, so the colour structures and helicity configurations corresponding to primitive amplitudes are

$$\mathcal{H}^{[1],(\ell)}_{q\bar{q}Q\bar{Q},\boldsymbol{\lambda}},\ \mathcal{H}^{[2],(\ell)}_{q\bar{q}Q\bar{Q},\boldsymbol{\lambda}} \quad \text{for} \quad \boldsymbol{\lambda} = \begin{cases} (+,-,+,-) \\ (+,-,-,+) \end{cases} . \tag{3.24}$$

For the processes involving gluons we can instead exploit Bose symmetry to restrict the set of independent amplitudes. Starting from $0 \to q\bar{q}gg$, the partial amplitudes associated to $\mathcal{C}_2^{q\bar{q}gg}$ can be obtained from those of $\mathcal{C}_1^{q\bar{q}gg}$ by exchanging particles 3 and 4 (the two gluons), and the partial amplitudes of $\mathcal{C}_3^{q\bar{q}gg}$ are symmetric under the same exchange. As a result a set of primitive amplitudes can be chosen as

$$\mathcal{H}^{[1],(\ell)}_{q\bar{q}gg,\boldsymbol{\lambda}} \quad \text{for} \quad \boldsymbol{\lambda} = \begin{cases} (-,+,-,-) \\ (-,+,-,+) \\ (-,+,+,-) \\ (-,+,+,+) \end{cases} \qquad \text{and} \quad \mathcal{H}^{[3],(\ell)}_{q\bar{q}gg,\boldsymbol{\lambda}} \quad \text{for} \quad \boldsymbol{\lambda} = \begin{cases} (-,+,-,-) \\ (-,+,-,+) \\ (-,+,+,+) \end{cases} . \tag{3.25}$$

Moving to four-gluon scattering, we find that the symmetry of the amplitude under the exchange of any two gluons implies that at all loop orders a set of primitive amplitudes[1] can be chosen as

$$\mathcal{H}^{[1],(\ell)}_{gggg,\boldsymbol{\lambda}},\ \mathcal{H}^{[4],(\ell)}_{gggg,\boldsymbol{\lambda}} \quad \text{for} \quad \boldsymbol{\lambda} = \begin{cases} (+,+,+,+) \\ (-,+,+,+) \\ (-,-,+,+) \\ (-,+,-,+) \end{cases} . \tag{3.26}$$

Though this information would in principle allow one to avoid the computation of all other partial amplitudes, in refs. [81–83] the full list of colour factors of eqs. (3.7)

[1] at one loop the set is even smaller due to photon-decoupling identities.

to (3.9) and helicity configurations of eq. (3.20) was computed up to three loops. The relations among partial amplitudes then served as a strong check of our results.

As a final remark, we point out that once the loop order has been fixed one can further decompose the partial amplitudes in powers of N_c and n_f, as described in section 2.2. In particular we can define the expansion[2]

$$\mathcal{H}^{[i],(\ell)} = N_c^{\ell-H} \sum_{h=0}^{\lfloor(\ell-H)/2\rfloor} \sum_{k=0}^{\ell} \frac{1}{N_c^{2h}} \left(\frac{n_f}{N_c}\right)^k \mathcal{H}_{h,k}^{[i],(\ell)}\,, \tag{3.27}$$

where the helicity ($\boldsymbol{\lambda}$) and process (X) dependence has been dropped for readability and H determines the leading power of N_c. Specifically, for the primitive amplitudes defined above, we find

$$\begin{cases} H = 0 \quad \text{for} \quad \mathcal{H}^{[1],(\ell)}_{q\bar{q}Q\bar{Q},\boldsymbol{\lambda}}, \mathcal{H}^{[1],(\ell)}_{q\bar{q}gg,\boldsymbol{\lambda}}, \mathcal{H}^{[1],(\ell)}_{gggg,\boldsymbol{\lambda}}\,, \\ H = 1 \quad \text{for} \quad \mathcal{H}^{[2],(\ell)}_{q\bar{q}Q\bar{Q},\boldsymbol{\lambda}}, \mathcal{H}^{[3],(\ell)}_{q\bar{q}gg,\boldsymbol{\lambda}}, \mathcal{H}^{[4],(\ell)}_{gggg,\boldsymbol{\lambda}}\,. \end{cases} \tag{3.28}$$

Because the partial amplitudes $\mathcal{H}^{[i],(\ell)}$ are gauge invariant and a gauge transformation cannot mix powers of N_c and n_f, the coefficients $\mathcal{H}^{[i],(\ell)}_{h,k}$ are also independently gauge invariant, offering a further opportunity for the decomposition of these amplitudes into smaller building blocks. Equation (3.27) allows us to directly extract pure Yang–Mills amplitudes[3] by retaining only terms for which $k = 0$, or equivalently setting $n_f = 0$. Furthermore, the planar-limit of these amplitudes, which corresponds to taking the limits $N_c \to \infty$ and $n_f \to \infty$ while keeping the quantities $\alpha_s N_c$ and n_f/N_c fixed, is equivalent to only retaining terms for which which $H = 0$ and $h = 0$.

3.3 Loop Integrals

All Feynman integrals appearing at one loop belong to the box family of fig. 3.2 and to the ones obtained from it by crossing the external legs. At two loops three topologies appear: double box, non-planar double box and beetle (see fig. 3.3). However, the beetle, in fig. 3.3(c), is entirely reducible in terms of sub-sectors of the double-box. At three loops nine irreducible integral topologies appear. Using

[2]We recall that $[i]$ indicates the colour-vector component as defined in eq. (2.29).

[3]The four-gluon amplitude at $n_f = 0$ would then correspond to the one in Yang–Mills theory, but the amplitudes involving external quarks but with no quark loops have no analogue in Yang–Mills.

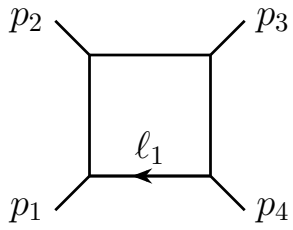

Figure 3.2: Massless Box

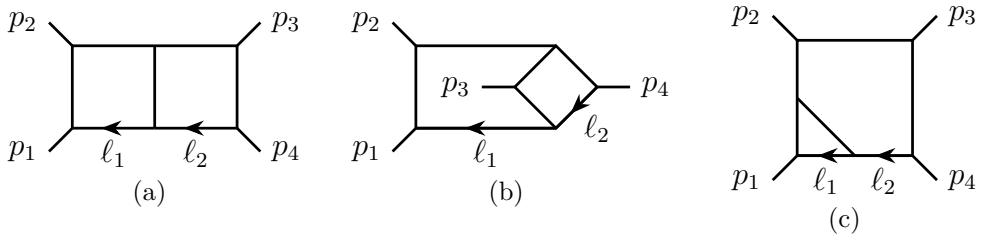

Figure 3.3: Two-loop topologies: (a) double box, (b) non-planar double box, (c) beetle.

the PD representation for Feynman integrals (see eq. (2.48) for details), all needed integrals can be grouped into six integral families: one at one loop, two at two loops and three a three loops. Table 3.2 contains the definition of the propagator denominators that were employed in this calculation.

We now turn our focus the three-loop computation, which poses the main challenge. After summing all Feynman diagrams, performing the colour and spinor algebra, and rewriting scalar products in terms of propagator denominators, we find that $\mathcal{O}(10^7)$ integrals belonging to the integral families PL, NPL1, NPL2 and their crossings appear. As a first simplification, one can leverage sector symmetries and sector relations, described in section 2.3.3. These can be obtained in an automated fashion via `Reduze 2` [36, 84], which in this case requires a high level of parallelisation because of the sheer number of integrals to be parsed. After plugging the resulting identities back into the amplitude and performing all possible algebraic simplifications, one is left with scattering amplitudes whose analytic expressions are about one order of magnitude smaller. This is also reflected by the number of Feynman integrals which drops to $\mathcal{O}(10^6)$. At this point one can proceed with IBP reduction to master integrals. At one and two loops this is a

Family	Box	Double-Box	Non-Planar Double-Box
$\mathcal{D}_1$	ℓ_1^2	ℓ_1^2	ℓ_1^2
$\mathcal{D}_2$	$(\ell_1+p_1)^2$	$(\ell_1+p_1)^2$	$(\ell_1+p_1)^2$
$\mathcal{D}_3$	$(\ell_1+p_1+p_2)^2$	$(\ell_1+p_1+p_2)^2$	$(\ell_1+p_1+p_2)^2$
$\mathcal{D}_4$	$(\ell_1+p_1+p_2+p_3)^2$	$(\ell_1+p_1+p_2+p_3)^2$	$(\ell_1+p_1+p_2+p_3)^2$
$\mathcal{D}_5$	–	ℓ_2^2	ℓ_2^2
$\mathcal{D}_6$	–	$(\ell_2+p_1)^2$	$(\ell_2+p_1)^2$
$\mathcal{D}_7$	–	$(\ell_2+p_1+p_2)^2$	$(\ell_2+p_1+p_2)^2$
$\mathcal{D}_8$	–	$(\ell_2+p_1+p_2+p_3)^2$	$(\ell_2+p_1+p_2+p_3)^2$
$\mathcal{D}_9$	–	$(\ell_1-\ell_2)^2$	$(\ell_1-\ell_2)^2$
Family	PL	NPL1	NPL2
$\mathcal{D}_1$	ℓ_1^2	ℓ_1^2	ℓ_1^2
$\mathcal{D}_2$	$(\ell_1+p_1)^2$	$(\ell_1+p_1)^2$	$(\ell_1+p_1)^2$
$\mathcal{D}_3$	$(\ell_1+p_1+p_2)^2$	$(\ell_1+p_1+p_2)^2$	$(\ell_1+p_1+p_2)^2$
$\mathcal{D}_4$	$(\ell_1+p_1+p_2+p_3)^2$	$(\ell_1+p_1+p_2+p_3)^2$	$(\ell_1-\ell_2+p_3)^2$
$\mathcal{D}_5$	ℓ_2^2	ℓ_2^2	ℓ_2^2
$\mathcal{D}_6$	$(\ell_2+p_1)^2$	$(\ell_2+p_1)^2$	$(\ell_2+p_1)^2$
$\mathcal{D}_7$	$(\ell_2+p_1+p_2)^2$	$(\ell_2+p_1+p_2)^2$	$(\ell_2+p_1+p_2)^2$
$\mathcal{D}_8$	$(\ell_2+p_1+p_2+p_3)^2$	$(\ell_2+p_1+p_2+p_3)^2$	$(\ell_2-p_3)^2$
$\mathcal{D}_9$	ℓ_3^2	ℓ_3^2	ℓ_3^2
$\mathcal{D}_{10}$	$(\ell_3+p_1)^2$	$(\ell_3+p_1)^2$	$(\ell_3+p_1)^2$
$\mathcal{D}_{11}$	$(\ell_3+p_1+p_2)^2$	$(\ell_3+p_1+p_2)^2$	$(\ell_3+p_1+p_2)^2$
$\mathcal{D}_{12}$	$(\ell_3+p_1+p_2+p_3)^2$	$(\ell_3+p_1+p_2+p_3)^2$	$(\ell_2-\ell_3-p_1-p_2-p_3)^2$
$\mathcal{D}_{13}$	$(\ell_1-\ell_2)^2$	$(\ell_1-\ell_2)^2$	$(\ell_1-\ell_2)^2$
$\mathcal{D}_{14}$	$(\ell_2-\ell_3)^2$	$(\ell_2-\ell_3)^2$	$(\ell_2-\ell_3)^2$
$\mathcal{D}_{15}$	$(\ell_3-\ell_1)^2$	$(\ell_1-\ell_2+\ell_3)^2$	$(\ell_3-\ell_1)^2$

Table 3.2: Integral families for two-to-two massless scattering up to three loops.

simple task, which was again solved using `Reduze 2`. Reduction to master integrals at three loops was performed using `Finred`, an implementation of the Laporta algorithm [85] developed by Andreas von Manteuffel which makes use of finite field arithmetic [86–89] and syzygy algorithms [90–95].

Taking into account the integral families of table 3.2 and their crossings, there are 6 master integrals at one loop, 39 at two loops and 486 at three loops. A canonical basis for the three-loop master integrals was provided in ref. [96], where the integrals were also computed up to transcendental weight 6 using the method of differential equations described in section 2.3.5. Using the same basis, an independent calculation was also performed in ref. [97] and agreement was found.[4]

[4]Up to a change in the conventional sign of the $i\varepsilon$ prescription.

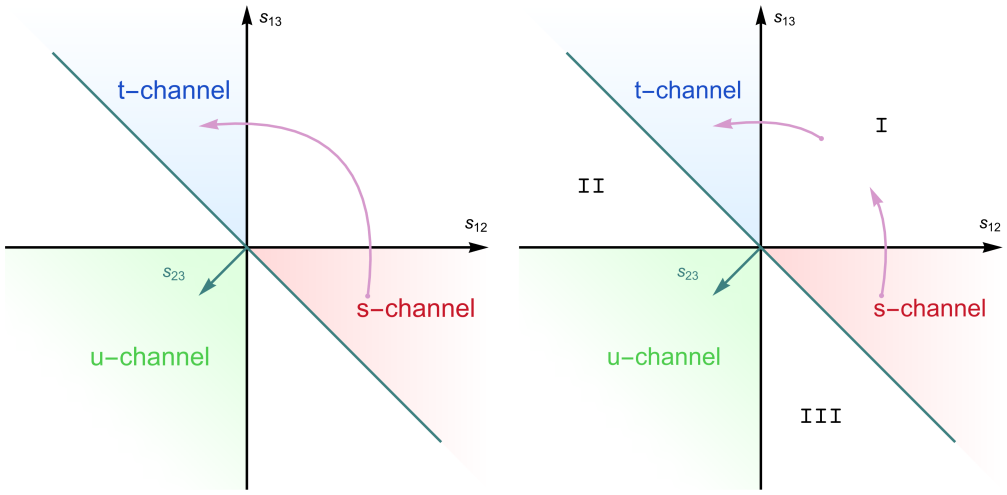

Figure 3.4: Path for the analytic continuation from s to t channel. Along the path in (a) one encounter two branch cuts, the first at $s_{13} = 0$ and the second at $s_{12} = 0$. The analytic continuation is therefore split in two parts, one for each branch cut (b).

The analytic expression for the master integrals up to three loops can be written in terms of harmonic polylogarithms (HPLs). They correspond to the subset of MPLs in eq. (2.74) obtained by restricting $l_i = 0, \pm 1$. More specifically, using the dimensionless variable

$$x = -s_{13}/s_{12}\,, \tag{3.29}$$

the only letters needed for the Feynman integrals in question are 0 and 1.

3.4 Analytic Continuation

The set of HPLs described above is real-valued and well defined in the physical region of eq. (3.4), which corresponds to $0 < x < 1$. However, in order to compute amplitudes in crossed channels, we might be interested in moving to different regions of the diagram in fig. 3.1, where $x < 0$ or $x > 1$. For instance the t-channel region corresponds to $x > 1$, while the u-channel region corresponds to $x < 0$. To reach these regions one has to cross multiple branch cuts of the HPLs and therefore analytic continuation is required.

Branch cut	$s \to I$	$I \to t$	$t \to II$	$II \to u$	$u \to III$	$III \to s$
y	$-s_{13}/s_{12}$	s_{12}/s_{13}	$-s_{23}/s_{13}$	s_{13}/s_{23}	$-s_{12}/s_{23}$	s_{23}/s_{12}

Table 3.3: Variables associated to all possible branch cuts in fig. 3.4(b). It is understood that if the branch cut is crossed in the opposite direction, the variable should be chosen with the opposite sign $y \to -y$.

In general, the analytic continuation of scattering amplitudes is conceptually well understood. However, in practice, the complexity of moving from one region to another depends on the class of functions arising from the Feynman integrals involved in the process. In particular, one usually aims to represent amplitudes in terms of functions which are manifestly real in the channel considered. This is usually a very difficult problem.

In the case of four-point massless scattering, it turns out to be achievable (as described in ref. [98]) thanks to fact that HPLs are a particularly simple set of univariate functions. In particular, the ones appearing in the scattering amplitudes of this chapter only have branch cuts in correspondence of the lines in fig. 3.1 where either s_{12}, s_{13} or s_{23} vanish and the HPLs develop logarithmic singularities. Importantly, one can move between any two scattering regions by analytically continuing across one branch cut at a time. This is illustrated by fig. 3.4 for the path from s- to t-channel. In order to cross any given branch cut, it is convenient to define a dimensionless variable

$$y = \pm s_{cut}/s_{+}\,, \tag{3.30}$$

where s_{cut} and s_{+} are Mandelstam variables, the first defining the branch cut, the second being the positive one among the remaining two. The sign is determined by requiring that $y > 0$ before the branch cut has been crossed. For instance, in fig. 3.4(b) the variable associated with the first continuation is $y = -s_{13}/s_{12}$, while for the second $y = s_{12}/s_{13}$. See table 3.3 for all possible choices of y.

With this change of variables, the cut is always at $y = 0$ and it is crossed going from $y > 0$ to $y < 0$. At weight-1 one can find by hand the transformation

from HPLs of argument z to HPLs of argument y. For higher weights one can then recursively apply the identity

$$G_{l_1,\ldots,l_n}(z) = \int \mathrm{d}y \frac{\mathrm{d}z/\mathrm{d}y}{z(y)-l_1} G_{l_2,\ldots,l_n}(z) + c_{l_1,\ldots,l_n}\,, \tag{3.31}$$

with $c_{l_1,\ldots,l_n}$ a constant of integration. For all possible changes of variables $z = z(y)$ one can verify that the kernel of integration can be written as a the linear combination

$$\frac{\mathrm{d}z/\mathrm{d}y}{z(y)-l_1} = \frac{C_1}{y-1} + \frac{C_0}{y} + \frac{C_{-1}}{y+1} \tag{3.32}$$

with C_l rational coefficients.

Assuming that the lower-weight function $G_{l_2,\ldots,l_n}(z(y))$ can be expressed in terms of HPLs with argument y, one can simply integrate the r.h.s. to find the transformation for $G_{l_1,\ldots,l_n}(z(y))$. The integration constants $c_{l_1,\ldots,l_n}$ can then be fixed by evaluating both sides near $y = 0$.

Let us now turn to the issue of continuing from $y < 0$ to $y > 0$. As mentioned above, the HPLs develop logarithmic singularities as $y \to 0$. In particular, $G_{\vec{l}}(y)$ is divergent in this limit only when the vector of letters has at least one zero. For instance $\vec{l} = (0,0,1,0,1)$ leads to a divergence, but $\vec{l} = (1,0,1,0,1)$ does not.

We can make all divergences explicit using the shuffle identity which all MPLs satisfy:

$$G_{l_1,\ldots,l_n}(x)\, G_{r_1,\ldots,r_m}(x) = \sum_{\vec{q}\in\vec{l}\sqcup\!\sqcup\vec{r}} G_{\vec{q}}(x)\,, \tag{3.33}$$

where $\vec{l}\sqcup\!\sqcup\vec{r}$ is the set of permutations of the vector $(\vec{l},\vec{r})$ which preserve the relative ordering of elements in $\vec{l}$ and in $\vec{r}$. The set of equations in (3.33) can be used to express all divergent weight-w HPLs in the following form[5]:

$$G_{\underbrace{0,\ldots,0}_{n},\underbrace{1,\ldots}_{w-n}}(y) = \sum_{k=0}^{n} \log(y)^k H_k(y)\,, \tag{3.34}$$

with $H_k(y)$ a linear combination of weight-$(w-k)$ HPLs with no trailing 0's. In the equation above, the powers of $\log(y)$ make the logarithmic singularities of the

[5]Note that in the l.h.s. of the equation above, the ellipses following the letter 1 can represent any combination of 0's and 1's.

branch cut manifest and they can be continued to $y < 0$ by assigning a small positive imaginary part to $s_{cut} \to s_{cut} + i\delta$, so that crossing the branch cut amounts to

$$\log(y) = \log\left(\frac{\pm s_{cut}}{s_+}\right) \to \log(y \pm i\delta) \to \log(-y) \pm i\pi\,. \tag{3.35}$$

To find the expression for the $H_k(y)$ in the new region we proceed recursively. Assuming that the analytic continuation up to weight $w-1$ is known, we only need to continue $H_0(y)$ in eq. (3.34), which is equivalent to computing the continuation of all required regular HPLs of the type $G_{\pm 1,\ldots}(y)$ for $y < 0$. This can be done by changing variables form y to $y' = -y$ using eq. (3.31) and plugging into its r.h.s. the already known continuation of lower-weight HPLs.

Let us now apply this up to weight 2 to the first branch cut of fig. 3.4(b) at $s_{13} = 0$. We use the variable $y = -s_{13}/s_{12} = x$, which for the purpose of analytic continuation receives a small negative imaginary part: $y \to y - i\delta$. An immediate consequence is that the singular logarithm develops a negative imaginary part

$$\begin{aligned} G_0(y) &\to \log(y - i\delta) \to \log(y') - i\pi = G_0(y') - i\pi\,, \\ G_1(y) &\to \log(1 - y + i\delta) \to \log(1 + y') = G_{-1}(y')\,. \end{aligned} \tag{3.36}$$

With the continuation at weight 1 in hand we move to weight 2, where we find two functions: $G_{0,1}(y)$ and $G_{1,0}(y)$. Using the shuffle identities eq. (3.33) we get

$$\begin{aligned} G_{0,1}(y) &= -G_{1,0}(y) + G_0(y)G_1(y)\,, \\ G_{1,0}(y) &= G_{1,0}(y)\,, \end{aligned} \tag{3.37}$$

where only one weight-2 function is left ($G_{1,0}$). We proceed using eqs. (3.31) and (3.32):

$$\frac{\mathrm{d}}{\mathrm{d}y'} G_{1,0}(y - i\delta) = \frac{1}{y'+1} G_0(y - i\delta) = \frac{1}{y'+1}\left(G_0(y') - i\pi\right)\,, \tag{3.38}$$

where in the last equality we used eq. (3.36). We then integrate back to weight 2 and find

$$G_{1,0}(y - i\delta) = G_{-1,0}(y') - i\pi G_{-1}(y') + c\,, \tag{3.39}$$

with c a constant of integration which can be fixed by evaluating both sides at $y = 0$. Because all HPLs in the equation above are regular at that point, and in

particular they vanish, we find $c = 0$. Overall, plugging eqs. (3.36) and (3.39) into eq. (3.37) we find

$$\begin{aligned} G_{0,1}(y) &\to -G_{0,-1}(y')\,, \\ G_{1,0}(y) &\to G_{-1,0}(y') - i\pi G_{-1}(y')\,. \end{aligned} \tag{3.40}$$

We could now continue iteratively up to any desired weight. In the case of the three loop calculations described in this chapter the maximum transcendental weight needed to describe the finite remainders is 6.

3.5 Crossed Channels and Equal Flavour Amplitudes

In section 3.1 we anticipated that the explicit results for the scattering amplitudes of the processes eq. (3.1) in the s-channel region (3.4) can be used to derive those for all other processes via a combination of crossings of the external legs and parity transformations.

In the interest of clarity we rewrite eq. (3.1) as a list of $2 \to 2$ scattering processes

$$\bar{q}(-p_1) + q(-p_2) \to Q(p_3) + \bar{Q}(p_4)\,, \tag{3.41}$$

$$\bar{q}(-p_1) + q(-p_2) \to g(p_3) + g(p_4)\,, \tag{3.42}$$

$$g(-p_1) + g(-p_2) \to g(p_3) + g(p_4)\,, \tag{3.43}$$

and in the same notation we list the additional processes we are interested in:

$$\bar{q}(-p_1) + Q(-p_2) \to Q(p_3) + \bar{q}(p_4)\,, \tag{3.44}$$

$$q(-p_1) + Q(-p_2) \to Q(p_3) + q(p_4)\,, \tag{3.45}$$

$$\bar{q}(-p_1) + \bar{Q}(-p_2) \to \bar{Q}(p_3) + \bar{q}(p_4)\,, \tag{3.46}$$

$$\bar{q}(-p_1) + g(-p_2) \to \bar{q}(p_3) + g(p_4)\,, \tag{3.47}$$

$$q(-p_1) + g(-p_2) \to q(p_3) + g(p_4)\,, \tag{3.48}$$

$$g(-p_1) + g(-p_2) \to \bar{q}(p_3) + q(p_4)\,. \tag{3.49}$$

In table 3.4 we give the list of transformations required to obtain these additional processes. Working at the level of helicity amplitudes, it is understood that starting

Target	Original	Analytic Region	Crossing
(3.44)	(3.41)	u channel	$p_2 \leftrightarrow p_4$
(3.45)	(3.41)	t channel	$p_4 \to p_2 \to p_1 \to p_4$
(3.46)	(3.41)	t channel	$p_3 \to p_2 \to p_4 \to p_3$
(3.47)	(3.42)	t channel	$p_2 \leftrightarrow p_3$
(3.48)	(3.42)	t channel	$p_3 \to p_2 \to p_1 \to p_3$
(3.49)	(3.42)	s channel	$p_{1,2} \leftrightarrow p_{4,3}$

Table 3.4: Transformations required to obtain the additional processes of eqs. (3.44) to (3.49). Processes in the "Target" column can be obtained starting from the corresponding ones in the "Original" column, analytically continuing them to the region indicated according to section 3.4 and changing names to the momenta according to the "Crossing" column.

from a particular helicity configuration of one of the original processes and then following table 3.4, one will obtain an helicity configuration for the final process dictated by the crossing of external momenta performed. Helicity configurations related by a parity transformation ($+ \leftrightarrow -$) can be obtained by acting the external spinors with the exchange $\langle ij\rangle \leftrightarrow [ji]$.

In addition to the processes of eqs. (3.44) to (3.49), it is also possible to derive amplitudes for the scattering of four identical quarks:

$$\bar{q}(-p_1) + q(-p_2) \to q(p_3) + \bar{q}(p_4)\,, \tag{3.50}$$

$$q(-p_1) + q(-p_2) \to q(p_3) + q(p_4)\,, \tag{3.51}$$

$$\bar{q}(-p_1) + \bar{q}(-p_2) \to \bar{q}(p_3) + \bar{q}(p_4)\,. \tag{3.52}$$

Starting from (3.50), we notice that the Feynman diagrams contributing to this processes are the sum of the ones of processes (3.41) and (3.44):

$$\mathcal{A}_{\boldsymbol{\lambda}}^{q\bar{q}\to\bar{q}q} = \mathcal{A}_{\boldsymbol{\lambda}}^{q\bar{q}\to\bar{Q}Q} + \mathcal{A}_{\boldsymbol{\lambda}}^{q\bar{Q}\to\bar{Q}q}\,. \tag{3.53}$$

Finally processes (3.51) and (3.52) can be obtained from (3.50) as described in table 3.5.

3.6 Infrared Structure and Quadrupole Radiation

Once the bare spinor-stripped helicity amplitudes $\boldsymbol{\mathcal{H}}_{X,\boldsymbol{\lambda}}^{(\ell)}$ have been computed as a Laurent expansion in ϵ and the Feynman integrals expressed in terms of HPLs, the

Target	Original	Analytic Region	Crossing
(3.51)	(3.50)	t channel	$p_1 \leftrightarrow p_4$
(3.52)	(3.50)	t channel	$p_2 \leftrightarrow p_3$

Table 3.5: Transformations required to obtain the equal quark processes of eqs. (3.51) and (3.52) from the one of eq. (3.50).

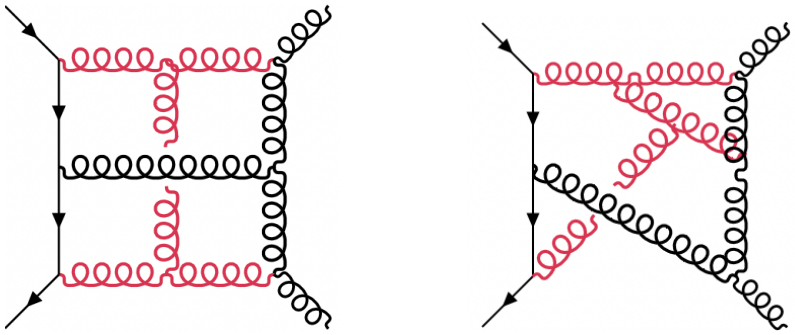

(a) (b)

Figure 3.5: Sample diagrams with quadrupole soft divergences, reinterpreted as tree-level diagrams (black lines) plus virtual soft gluons (red lines). Diagrams (a) and (b) involve colour correlations between four and three external partons and contribute to the first and second line of eq. (3.54), respectively.

structure of these amplitudes becomes manifest. In particular all poles in ϵ should be predicted by UV renormalisation and IR factorisation as described in section 2.3.6.

We can verify this by first computing UV-renormalised amplitudes via eq. (2.89) and then subtracting IR divergences as in eq. (2.101). The new ingredient in these three-loop computations is $\mathbf{\Delta}_4^{(3)}$, the three-loop quadrupole contribution to the soft anomalous dimension. It was first computed via Wilson line matrix elements in ref. [69] and because at three loops it can only receive contributions from soft gluon webs (as for example in ref. fig. 3.5) it is expected to be universal across all Yang–Mills theories. Its first direct confirmation was achieved in ref. [99], where it correctly predicted the IR divergences of $\mathcal{N} = 4$ four-point three-loop scattering amplitudes.

The three-loop QCD scattering amplitude for the processes of eq. (3.1) allow to explicitly confirm the universality of quadrupole radiation using the expression

$$\mathbf{\Delta}_4^{(3)} = f_{abe} f_{cde} \Bigg[-16\, C \sum_{i=1}^{4} \sum_{\substack{1 \le j < k \le 4 \\ j,k \neq i}} \left\{ \mathbf{T}_i^a, \mathbf{T}_i^d \right\} \mathbf{T}_j^b \mathbf{T}_k^c + 128 \left[\mathbf{T}_1^a \mathbf{T}_2^c \mathbf{T}_3^b \mathbf{T}_4^d D_1(x) - \mathbf{T}_4^a \mathbf{T}_1^b \mathbf{T}_2^c \mathbf{T}_3^d D_2(x) \right] \Bigg], \tag{3.54}$$

where we recalled the definition of the dimensionless ratio $x = -s_{13}/s_{12}$. We also used the pure transcendental weight 5 quantities

$$C = \zeta_5 + 2\zeta_2\zeta_3\,, \tag{3.55}$$

$$\begin{aligned} D_1(x) = &-2\bar{G}_{1,4} - \bar{G}_{2,3} - \bar{G}_{3,2} + 2\bar{G}_{1,1,3} + 2\bar{G}_{1,2,2} - 2\bar{G}_{1,3,0} - \bar{G}_{2,2,0} - \bar{G}_{3,1,0} \\ &+ 2\bar{G}_{1,1,2,0} - 2\bar{G}_{1,2,0,0} + 2\bar{G}_{1,2,1,0} + 4\bar{G}_{1,0,0,0,0} - 2\bar{G}_{1,1,0,0,0} + \frac{1}{2}\zeta_5 - 5\zeta_2\zeta_3 \\ &+ \zeta_2[5\bar{G}_3 + 5\bar{G}_{2,0} + 2\bar{G}_{1,0,0} - 6(\bar{G}_{1,2} + \bar{G}_{1,1,0})] + \zeta_3(\bar{G}_2 + 2\bar{G}_{1,0} - 2\bar{G}_{1,1}) \\ &- i\pi[-\zeta_3\bar{G}_0 + \bar{G}_{2,2} + \bar{G}_{3,0} + \bar{G}_{3,1} + \bar{G}_{2,0,0} + 2(\bar{G}_{1,3} - \bar{G}_{1,1,2} - \bar{G}_{1,2,1} - \bar{G}_{1,0,0,0})] \\ &+ i\pi\zeta_2(-\bar{G}_2 + 2(\bar{G}_{1,1} + \bar{G}_{1,0})) - 11i\pi\zeta_4\,, \end{aligned} \tag{3.56}$$

$$\begin{aligned} D_2(x) = &\,2\bar{G}_{2,3} + 2\bar{G}_{3,2} - \bar{G}_{1,1,3} - \bar{G}_{1,2,2} - 2\bar{G}_{2,1,2} + 2\bar{G}_{2,2,0} - 2\bar{G}_{2,2,1} \\ &+ 2\bar{G}_{3,1,0} - 2\bar{G}_{3,1,1} - \bar{G}_{1,1,2,0} - \bar{G}_{1,2,1,0} - 2\bar{G}_{2,1,1,0} + 4\bar{G}_{2,1,1,1} - \zeta_5 + 4\zeta_2\zeta_3 \\ &+ \zeta_3\bar{G}_{1,1} + \zeta_2[-6\bar{G}_3 - 6\bar{G}_{2,0} + 2\bar{G}_{2,1} + 5(\bar{G}_{1,2} + \bar{G}_{1,1,0})] \\ &+ i\pi(\zeta_3\bar{G}_1 + 2\bar{G}_{3,0} - \bar{G}_{1,1,2} - \bar{G}_{1,2,0} - \bar{G}_{1,2,1} + 2\bar{G}_{2,0,0} - 2\bar{G}_{2,1,0} \\ &+ 2\bar{G}_{2,1,1} - \bar{G}_{1,1,0,0}) + i\pi\zeta_2(4\bar{G}_2 - \bar{G}_{1,1})\,. \end{aligned} \tag{3.57}$$

where we introduced the compact notation for the HPLs similar to that in refs. [100, 101],

$$\bar{G}_{a_1,\ldots,a_n,\underbrace{0,\ldots,0}_{n_0}} = G_{\underbrace{0,\ldots,0}_{|a_1|-1},\mathrm{sgn}(a_1),\ldots,\underbrace{0,\ldots,0}_{|a_n|-1},\mathrm{sgn}(a_n),\underbrace{0,\ldots,0}_{n_0}}(x).$$

The expression in eq. (3.54) was obtained by analytic continuation to the physical scattering region of eq. (4.6) of the result in ref. [69] which were given in terms of single-valued transcendental functions.

3.7 Analytic Results and Numerical Evaluation

As a result of the computations described in previous sections, any of the UV-renormalised scattering amplitudes discussed in this chapter can be explicitly written

as

$$\begin{aligned}\boldsymbol{\mathcal{A}} &= 4\pi\alpha_s \sum_{\ell=0}^{2} \left(\frac{\alpha_s}{4\pi}\right)^{\ell} \boldsymbol{\mathcal{R}}^{(\ell)} \\ &= 4\pi\alpha_s \sum_{i,\ell} \sum_{k=-2\ell}^{6-2\ell} \sum_{\vec{l}}^{\dim(\vec{l})\leq k} \left(\frac{\alpha_s}{4\pi}\right)^{\ell} \mathcal{C}_{[i]} \frac{1}{\epsilon^k} R^{[i],(\ell)}_{k,\vec{l}} G_{\vec{l}}(x)\end{aligned} \tag{3.58}$$

where $R^{[i],(\ell)}_{k,\vec{l}}$ are rational functions of the invariant $x = -s_{13}/s_{12}$. The $6 - 2\ell$ upper bound represents a truncation of higher powers of ϵ which still allows one to perform infrared subtraction of the three-loop amplitudes. Explicit `Mathematica`-readable expressions for the finite remainders defined by eq. (2.101) were published as ancillary files to the `arXiv` submissions of refs. [81–83].

Let us now comment on the validation of our results. First, we have checked that our results for the lower loop amplitudes are consistent with the literature. In particular, we have compared our tree-level, one-loop and two-loop results for the bare helicity amplitudes for $q\bar{q} \to Q\bar{Q}$, $q\bar{q} \to q\bar{q}$, $q\bar{q} \to gg$ and $gg \to gg$ in the helicity configurations listed above against the results provided in refs. [98] and found analytical agreement through to weight six.[6]

We have also checked that our one-loop expressions match results obtained with the automated one-loop generator `OpenLoops` [102, 103]. At the three-loop level, we have verified that the IR singularities of our results for the renormalized helicity amplitudes of eq. (3.58) match the pattern described in sections 2.4.2 and 3.6, which provides a highly non-trivial check. From the high-energy limit ($|s_{12}| \gg |s_{13}|$) of our amplitudes, which will be discussed more in detail in section 3.8, we determined that our amplitude exhibit the correct Regge behaviour at NNLL accuracy up to two loops and at NLL accuracy at three loops.

In figure 3.6, we show the contributions to the squared amplitude at different orders in α_s, normalized by the respective tree-level squared amplitude. We average (sum) over polarization and colour in the initial (final) states. Below we define more in detail the quantities we present in the plots. We define the contraction

[6] Upon complex conjugation due to a mismatch of sign in the $i\varepsilon$ prescription for the analytic continuation

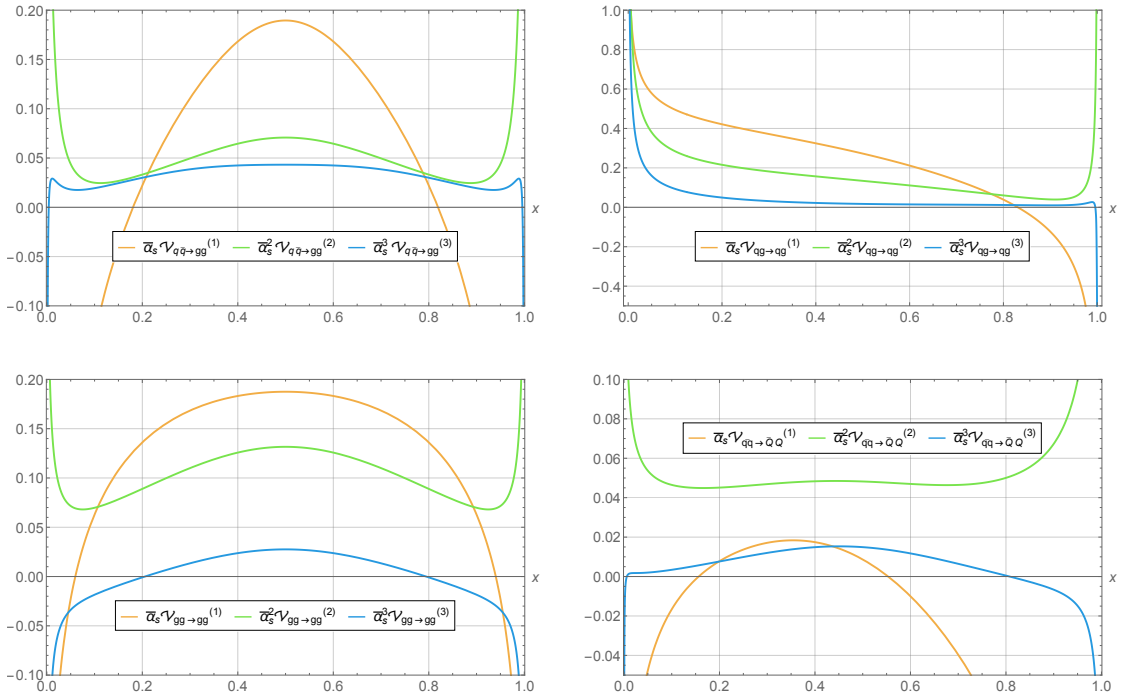

Figure 3.6: Perturbative expansion of the amplitude squared for the processes $q\bar{q} \to gg$, $qg \to qg$, $gg \to gg$ and $q\bar{q} \to \bar{Q}Q$ as functions of $x = -s_{13}/s_{12}$. Values are normalized by the tree-level amplitude squared. Plotted quantities are defined in eq. (3.61) and we fixed $\mu^2 = s_{12} = m_Z^2$, $\alpha_s(m_Z) = 0.118$, $n_f = 5$ and $N_c = 3$.

between different loop amplitudes in colour space as

$$\langle \mathcal{A}^{(\ell)} | \mathcal{A}^{(\ell')} \rangle \equiv \mathcal{N} \sum_{i,j,\boldsymbol{\lambda}} \mathrm{Tr}\left[C_{[i]}^{\dagger} \mathcal{C}_{[j]} \right] |s_{\boldsymbol{\lambda}}|^2 \mathcal{F}_{\boldsymbol{\lambda}}^{[i],(\ell)*} \mathcal{F}_{\boldsymbol{\lambda}}^{[j],(\ell')}, \tag{3.59}$$

where $\mathcal{F}$ are defined in eq. (2.101) as colour vectors, $\mathcal{C}_{[i]}$ are the colour tensors of eqs. (3.7) to (3.9), $s_{\boldsymbol{\lambda}}$ are the spinor factors of eq. (3.21) and $\mathcal{N}$ is the initial-state colour and polarization averaging factor, which and takes the following values:

$$\mathcal{N} = \begin{cases} \frac{1}{4N_c^2} & \text{for } q\bar{q} \to gg, \\ \frac{1}{4N_c(N_c^2-1)} & \text{for } qg \to qg, \\ \frac{1}{4(N_c^2-1)^2} & \text{for } gg \to gg, \\ \frac{1}{4N_c^2} & \text{for } q\bar{q} \to \bar{Q}Q. \end{cases} \tag{3.60}$$

Process dependence of all quantities appearing in eq. (3.59) is left implicit and the initial and final state polarization sum runs over all helicity configurations.

The quantities plotted in fig. 3.6 are defined as

$$\begin{aligned}
&\mathcal{V}^{(0)} = 1, && \mathcal{V}^{(1)} = 2\frac{\mathbb{R}\langle\mathcal{A}^{(0)}|\mathcal{A}^{(1)}\rangle}{\langle\mathcal{A}^{(0)}|\mathcal{A}^{(0)}\rangle}, \\
&\mathcal{V}^{(2)} = \frac{\langle\mathcal{A}^{(1)}|\mathcal{A}^{(1)}\rangle}{\langle\mathcal{A}^{(0)}|\mathcal{A}^{(0)}\rangle} + 2\frac{\mathbb{R}\langle\mathcal{A}^{(0)}|\mathcal{A}^{(2)}\rangle}{\langle\mathcal{A}^{(0)}|\mathcal{A}^{(0)}\rangle}, && \mathcal{V}^{(3)} = 2\frac{\mathbb{R}\langle\mathcal{A}^{(1)}|\mathcal{A}^{(2)}\rangle}{\langle\mathcal{A}^{(0)}|\mathcal{A}^{(0)}\rangle} + 2\frac{\mathbb{R}\langle\mathcal{A}^{(0)}|\mathcal{A}^{(3)}\rangle}{\langle\mathcal{A}^{(0)}|\mathcal{A}^{(0)}\rangle}.
\end{aligned} \tag{3.61}$$

and for the numerical evaluation we have set $\mu^2 = s_{12} = m_Z^2$, $\alpha_s(m_Z) = 0.118$, $n_f = 5$ and $N_c = 3$.

3.8 The Gluon Regge Trajectory

In the high-energy or *Regge limit*, scattering amplitudes become particularly simple and are known to exhibit universal factorization properties. In the following, we consider the processes

$$A(-p_1) \;+\; B(-p_2) \;\to\; A(p_3) \;+\; B(p_4), \tag{3.62}$$

where A and B are either q, $\bar{q}$ or g. The Regge limit is defined as $s \to \infty$ for fixed scattering angle, that is

$$|s_{12}| \approx |s_{23}| \gg |s_{13}| \tag{3.63}$$

In the variable $x = -s_{13}/s_{12}$ used in previous sections, the Regge limit corresponds to $x \to 0$ and scattering amplitudes develop logarithmic singularities which appear as powers of $\log(x)$. Following the investigation in refs. [104–106], we split the renormalised amplitude into the definite $s_{12} \leftrightarrow s_{23}$ signature amplitudes

$$\boldsymbol{\mathcal{R}}_{\pm}^{AB} = \lim_{x\to 0} \frac{1}{2} \left[\boldsymbol{\mathcal{R}}_{\mathrm{AB}\to\mathrm{AB}} \pm \boldsymbol{\mathcal{R}}_{\mathrm{AB}\to\mathrm{AB}}|_{p_1\leftrightarrow p_3}\right] . \tag{3.64}$$

which are often referred to as the even (+) and odd (−) amplitudes. We also introduce the signature-symmetric logarithm

$$L = \frac{1}{2}\left[\ln\left(\frac{-s_{12}-i\delta}{-s_{13}}\right) + \ln\left(\frac{-s_{23}-i\delta}{-s_{13}}\right)\right] \sim -\ln(x) + \frac{i\pi}{2}\,, \tag{3.65}$$

where by $\sim$ we mean that the two expressions coincide in the small-x limit.

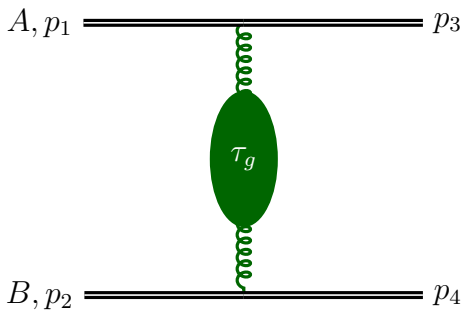

Figure 3.7: Schematic representation of Regge factorisation in the LL approximation.

Because in the Regge limit $|L| \to \infty$, it is convenient to reorganise the amplitude as

$$\boldsymbol{\mathcal{R}}^{AB}_{\pm} = \sum_{h=0} \left(\frac{\alpha_s}{4\pi}\right)^h \sum_{k=0} \left(\frac{\alpha_s L}{4\pi}\right)^k \boldsymbol{\mathcal{R}}^{AB}_{\pm,(k,h)} \tag{3.66}$$

where the coefficients do not contain any power of α_s or L and, as done in ref. [104], one can show that $\boldsymbol{\mathcal{R}}^{AB}_{+,(k,h)}$ are purely imaginary, while $\boldsymbol{\mathcal{R}}^{AB}_{-,(k,h)}$ are purely real. The inner series in eq. (3.66) involves the effective coupling $\alpha_s L$, which grows large as $L \to \infty$. As soon as $\alpha_s L \approx 4\pi$, the sum can no longer be truncated at any finite order since all its terms give comparable contributions. One must therefore re-sum the series. A perturbative expansion can nevertheless still be performed by truncating the outer series at some finite value of h. The leading contribution, for $h = 0$ corresponds to what is usually called leading-logarithmic (LL) accuracy. It is equivalent to keeping only the highest power of L at every loop order. Going up to $h = 1$ corresponds to next-to-leading-logarithmic accuracy, or NLL. In general N^{i}LL corresponds to truncating the series in at $h = i$.

It has long been established that at LL accuracy $\boldsymbol{\mathcal{R}}^{AB}_{\pm}$ are entirely described by the exchange of a single "reggeized" t-channel gluon [106–110]. In the language of complex angular momentum [111], this single-particle exchange is usually referred to as the "Regge-pole" contribution. In this approximation, the amplitudes take the form

$$\boldsymbol{\mathcal{R}}^{AB}_{-} = \left(\frac{s_{12}}{\mu^2}\right)^{\tau_g C_A} \boldsymbol{\mathcal{R}}^{AB}_{0} \approx e^{\tau_g C_A L} \boldsymbol{\mathcal{R}}^{AB}_{0}\,, \qquad \boldsymbol{\mathcal{R}}^{AB}_{+} = 0\,, \tag{3.67}$$

where $\boldsymbol{\mathcal{R}}_0^{AB} \sim 1/x$ is the leading power of $\boldsymbol{\mathcal{R}}^{(0)}$ in the $x \to 0$ limit, and τ_g is the gluon *Regge trajectory*, which is $\mathcal{O}(\alpha_s)$ and only depends on the t-channel invariant s_{13}. A derivation of this result can be found e.g. in ref. [104], where the Wilson-line formalism for the Balitsky-JIMWLK evolution is used. Since τ_g is scaleless, s_{13} must always appear in the combination $-s_{13}/\mu^2$, which prompts us to set $\mu^2 = -s_{13}$. In anticipation of the perturbative corrections arising from sub-leading contributions, we also define the expansion

$$\tau_g = \sum_{n=1} \left(\frac{\alpha_s}{4\pi}\right)^n \tau_n \,. \tag{3.68}$$

To make contact with standard terminology, eq. (3.67) exhibits Regge scaling in the high-energy limit $s_{12} \to +\infty$, *i.e.* it takes the form of a pure power law $(s_{12})^y$. At leading order $y = \alpha_s \tau_1 C_A/4\pi$.

To generalise our description of the high-energy limit to higher orders in the logarithmic expansion, it is convenient to define the colour operators [112, 113]

$$\begin{aligned} \mathbf{T}_s^2 &= (\mathbf{T}_1+\mathbf{T}_2)^a(\mathbf{T}_1+\mathbf{T}_2)^a, \qquad \mathbf{T}_t^2 = (\mathbf{T}_1+\mathbf{T}_3)^a(\mathbf{T}_1+\mathbf{T}_3)^a, \\ \mathbf{T}_u^2 &= (\mathbf{T}_1+\mathbf{T}_4)^a(\mathbf{T}_1+\mathbf{T}_4)^a, \qquad \mathbf{T}_{s-u}^2 = \frac{1}{2}(\mathbf{T}_s^2 - \mathbf{T}_u^2). \end{aligned} \tag{3.69}$$

Similarly to ref. [80] we rewrite eq. (3.66) by collecting an overall LL exponential as well as the universal factors $Z_{A,B}^c$

$$\boldsymbol{\mathcal{R}}_{\pm}^{AB} = Z_A^c Z_B^c e^{L\mathbf{T}^2\tau_g} \sum_{k=0} \left(\frac{\alpha_s L}{4\pi}\right)^k \boldsymbol{\mathcal{O}}_{\pm,(k)}^{AB}(\alpha_s) \boldsymbol{\mathcal{R}}_0^{AB} \,. \tag{3.70}$$

The Z_i^c account for the factorised IR collinear divergences of the external hard lines. They can be computed directly from eq. (2.94) and can be expanded perturbatively as $Z_i^c = \sum_{\ell=0} \left(\frac{\alpha_s}{4\pi}\right)^\ell Z_i^{c,(\ell)}$. To $O(\alpha_s^2)$ we have

$$\begin{aligned} Z_i^{c,(0)} &= 1 \,, \\ Z_i^{c,(1)} &= -C_i \gamma_1^{\mathrm{K}} \frac{1}{\epsilon^2} + 4\gamma_1^i \frac{1}{\epsilon} \,, \\ Z_i^{c,(2)} &= C_i^2 \frac{(\gamma_1^{\mathrm{K}})^2}{2\epsilon^4} + C_i \left[\frac{1}{\epsilon^3}\gamma_1^{\mathrm{K}}\left(\frac{3\beta_0}{4} - 4\gamma_1^i\right) - \frac{\gamma_2^{\mathrm{K}}}{\epsilon^2}\right] + \frac{2}{\epsilon^2}\gamma_1^i\left(4\gamma_1^i - \beta_0\right) + \frac{8\gamma_2^i}{\epsilon} \,, \end{aligned} \tag{3.71}$$

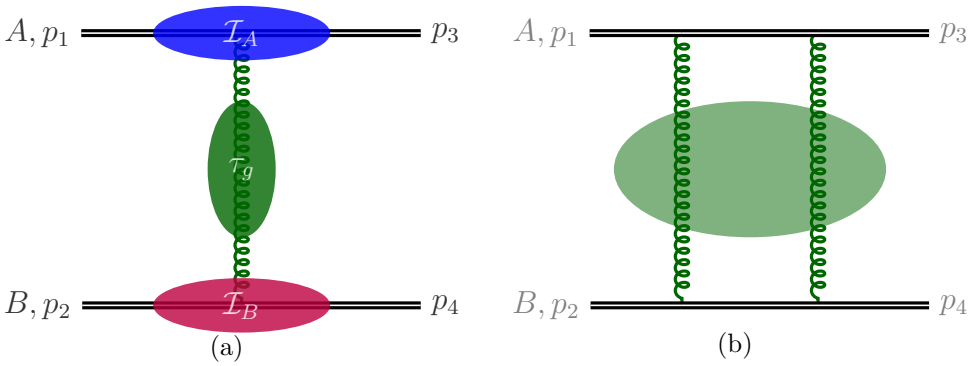

Figure 3.8: Schematic representation of (a) odd and (b) even Regge behaviour in the NLL approximation. The blue and red blobs represent correction to the reggeon-projectile vertex, the green blob corresponds to the perturbative corrections to the Regge trajectory. Diagram (b) is one of two permutations of the reggeon attachments the external lines and the green blob represents rapidity evolution of the multi-reggeon state.

for $i = q, g$. Finally, the $\boldsymbol{\mathcal{O}}$ are colour operators acting on the tree level Regge amplitude. They can also be defined perturbatively as

$$\boldsymbol{\mathcal{O}}^{AB}_{\pm,(k)}(\alpha_s) = \sum_{\ell=0} \left(\frac{\alpha_s}{4\pi}\right)^{\ell} \boldsymbol{\mathcal{O}}^{AB}_{\pm,(k,\ell)} \tag{3.72}$$

and as before powers in ℓ correspond to $\mathrm{N}^{\ell}\mathrm{LL}$ contributions. Because the LL approximation of the amplitudes is entirely predicted by the exponential of eq. (3.70) we find

$$\boldsymbol{\mathcal{O}}^{AB}_{-,(k,0)} = \delta_{k,0}\,, \qquad \boldsymbol{\mathcal{O}}^{AB}_{+,(k,0)} = 0\,. \tag{3.73}$$

One can check that eqs. (3.70) and (3.72) reproduce eq. (3.67) at LL using the fact that the tree level amplitude is a (colour) eigenvector of the t-channel colour operator: $\mathbf{T}_t^2 \boldsymbol{\mathcal{R}}_0^{AB} = C_A \boldsymbol{\mathcal{R}}_0^{AB}$.

At NLL, the odd amplitude maintains its factorised form, however, as in fig. 3.8(a), the vertices between reggeon and external high-energy particles A and B receive perturbative corrections described by so-called *impact factors*. The NLL even amplitude is the first to break (strict) Regge factorisation and it is described by the exchange of two reggeons as illustrated in fig. 3.8(b), a contribution usually referred to as "Regge cut" [80, 104, 105, 110, 114–117]. The colour operators

yielding NLL contributions are [104]

$$\begin{aligned}
\boldsymbol{\mathcal{O}}^{AB}_{-,(k,1)} &= \mathcal{I}^{(1)}_A + \mathcal{I}^{(1)}_B\,,\\
\boldsymbol{\mathcal{O}}^{AB}_{+,(1,1)} &= i\pi\, r_\Gamma \frac{2}{\epsilon}\,\mathbf{T}^2_{s-u}\,,\\
\boldsymbol{\mathcal{O}}^{AB}_{+,(2,1)} &= -i\pi \frac{r_\Gamma^2}{2}\left(\frac{4}{\epsilon^2} + 72\zeta_3\epsilon + 108\zeta_4\epsilon^2 + \mathcal{O}(\epsilon^3)\right)[\mathbf{T}^2_t, \mathbf{T}^2_{s-u}]\,,\\
\boldsymbol{\mathcal{O}}^{AB}_{+,(3,1)} &= i\pi \frac{r_\Gamma^3}{6}\left(\frac{8}{\epsilon^3} - 176\zeta_3 - 264\zeta_4\epsilon - 5712\zeta_5\epsilon^2 + \mathcal{O}(\epsilon^3)\right)[\mathbf{T}^2_t, [\mathbf{T}^2_t, \mathbf{T}^2_{s-u}]]\,,
\end{aligned} \tag{3.74}$$

with the definition

$$r_\Gamma = e^{\epsilon\gamma_E}\frac{\Gamma(1-\epsilon)^2\Gamma(1+\epsilon)}{\Gamma(1-2\epsilon)}\,. \tag{3.75}$$

The objects $\mathcal{I}^{(1)}_{A,B}$ are the one-loop impact factors and are given in appendix A.2.

At NNLL, we focus on the odd-signature amplitude, which receives for the first time contributions from both Regge pole and cuts. In ref. [80], a scheme has been proposed to disentangle the two. We adopt this scheme to study the high-energy behaviour to three loops up to N^{2}LL. The odd-signature colour operators contributing at this order are [105]

$$\begin{aligned}
\boldsymbol{\mathcal{O}}^{AB}_{-,(2,2)} &= \left[\mathcal{I}^{(2)}_A + \mathcal{I}^{(2)}_B + \mathcal{I}^{(1)}_A\mathcal{I}^{(1)}_B\right]\\
&\quad + \frac{2\pi^2}{3} r_\Gamma^2\left(\frac{3}{\epsilon^2} - 18\epsilon\zeta_3 - 27\epsilon^2\zeta_4 + \mathcal{O}(\epsilon)\right)[(\mathbf{T}^2_{s-u})^2 - N_c^2/4]\,,\\
\boldsymbol{\mathcal{O}}^{AB}_{-,(3,2)} &= 64\pi^2 r_\Gamma^3\left(\frac{1}{48\epsilon^2} + \frac{37}{24}\zeta_3 + \mathcal{O}(\epsilon)\right)\mathbf{T}^2_{s-u}[\mathbf{T}^2_t, \mathbf{T}^2_{s-u}]\\
&\quad + 64\pi^2 r_\Gamma^3\left(\frac{1}{24\epsilon^2} + \frac{1}{12}\zeta_3 + \mathcal{O}(\epsilon)\right)[\mathbf{T}^2_t, \mathbf{T}^2_{s-u}]\mathbf{T}^2_{s-u}\,,
\end{aligned} \tag{3.76}$$

where $\mathcal{I}^{(2)}_{A,B}$ are the two-loop impact factors. Their analytic expressions are too lengthy to be reported here and can be found in appendix A.2. The colour structures in eq. (3.76) can be traced to reggeon exchanges of the types in fig. 3.9.

From the discussion above it is clear that for a full description of the N^{2}LL behaviour of two-to-two amplitudes one needs knowledge of the impact factors at one and two loops and of the Regge trajectory up to three loops.

The one and two loop results were already available in the literature [105, 118–121]. A prediction of the large-N_c Regge trajectory in Yang–Mills theory was

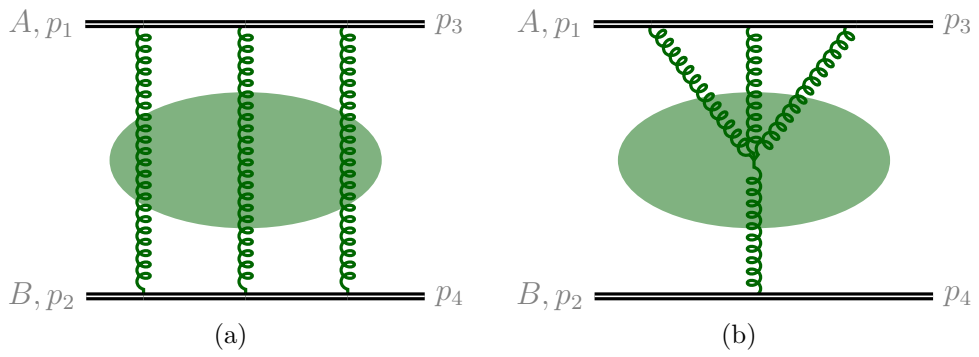

Figure 3.9: Sample reggeon diagrams contributing to the N^{2}LL odd amplitudes. The green blobs represent rapidity evolution of the multi-reggeon states.

computed in ref. [121]. Here, by matching the structure determined by eq. (3.66) with the perturbative expansion of our odd amplitudes, we predicted the three-loop Regge trajectory in full-colour QCD. Explicitly, we find [82, 118]

$$\begin{aligned}
\tau_1 =&\ e^{\epsilon\gamma_E}\frac{\Gamma(1-\epsilon)^2\Gamma(1+\epsilon)}{\Gamma(1-2\epsilon)}\frac{2}{\epsilon} = K_1 + O(\epsilon),\\
\tau_2 =&\ K_2 - \frac{56n_f}{27} + N_c\left(\frac{404}{27} - 2\zeta_3\right) + \epsilon\left[N_c\left(\frac{2428}{81} - 66\zeta_3 - \frac{67\zeta_2}{9} - 3\zeta_4\right)\right.\\
&\left. + n_f\left(12\zeta_3 - \frac{328}{81} + \frac{5\pi^2}{27}\right)\right] + \epsilon^2\left[N_c\left(82\zeta_5 + \frac{142\zeta_2\zeta_3}{3} - \frac{4556\zeta_3}{27} + \frac{14576}{243}\right.\right.\\
&\left.\left. - \frac{404\zeta_2}{27} - \frac{2321\zeta_4}{24}\right) + n_f\left(\frac{680\zeta_3}{27} - \frac{1952}{243} + \frac{56\zeta_2}{27} + \frac{211\zeta_4}{12}\right)\right] + \mathcal{O}(\epsilon^3),\\
\tau_3 =&\ K_3 + N_c^2\left(16\zeta_5 + \frac{40\zeta_2\zeta_3}{3} - \frac{77\zeta_4}{3} - \frac{6664\zeta_3}{27} - \frac{3196\zeta_2}{81} + \frac{297029}{1458}\right)\\
&+ N_c n_f\left(\frac{412\zeta_2}{81} + \frac{2\zeta_4}{3} + \frac{632\zeta_3}{9} - \frac{171449}{2916}\right) + n_f^2\left(\frac{928}{729} - \frac{128\zeta_3}{27}\right)\\
&+ \frac{n_f}{N_c}\left(-4\zeta_4 - \frac{76\zeta_3}{9} + \frac{1711}{108}\right) + \mathcal{O}(\epsilon),
\end{aligned} \tag{3.77}$$

where, as in ref. [80], we defined

$$K(\alpha_s(\mu)) = -\frac{1}{4}\int_\infty^{\mu^2}\frac{d\lambda^2}{\lambda^2}\gamma^{\mathrm{K}}\left(\alpha_s(\lambda^2)\right) = \sum_{\ell\geq 1} K_\ell\left(\frac{\alpha_s}{4\pi}\right)^\ell. \tag{3.78}$$

Its coefficients up to third order are

$$\begin{aligned} K_1 &= \frac{\gamma_0^{\mathrm{K}}}{\epsilon}\,, \\ K_2 &= \frac{2\gamma_1^{\mathrm{K}}}{\epsilon} - \frac{\beta_0\gamma_0^{\mathrm{K}}}{2\epsilon^2}\,, \\ K_3 &= \frac{16\gamma_2^{\mathrm{K}}}{3\epsilon} - \frac{4\beta_0\gamma_1^{\mathrm{K}} + 4\beta_1\gamma_0^{\mathrm{K}}}{3\epsilon^2} + \frac{\beta_0^2\gamma_0^{\mathrm{K}}}{3\epsilon^3}\,. \end{aligned} \tag{3.79}$$

We point out that a single three-loop amplitude among the processes in eq. (3.1) is required for the extraction of τ_3. Once it has been determined, all ingredients are available for the full prediction of the N^{2}LL Regge limit of the other channels. For instance, one could use the simpler $qQ \to qQ$ amplitude to extract the three-loop trajectory, and then fully predict the amplitude for $qg \to qg$ and $gg \to gg$ in the high-energy limit. This serves as a powerful consistency check of our results as well as a non-trivial test of the universality of high-energy factorization in QCD.

4

Two-Loop Five-Gluon Scattering

Contents

4.1 Introduction 79
4.2 Colour Decomposition 80
4.3 Helicity Amplitudes 82
4.4 Loop Integrals 87
4.5 Results 92

4.1 Introduction

In this chapter we turn to two-loop scattering amplitudes of five particles in QCD which were recently obtained via two independent calculations in ref. [122–124]. Here we specifically focus on gluon scattering:

$$0 \to g(p_1) + g(p_2) + g(p_3) + g(p_4) + g(p_5)\,. \tag{4.1}$$

All external momenta are taken to be outgoing and massless:

$$0 = p_1^\mu + p_2^\mu + p_3^\mu + p_4^\mu + p_5^\mu, \quad p_i^2 = 0. \tag{4.2}$$

as well as exactly in four dimensions. Due to the cyclic symmetry of the process, an ideal set of invariants to parametrise the kinematics are the Mandelstam variables

$$s_{12},\ s_{23},\ s_{34},\ s_{45},\ s_{51}. \tag{4.3}$$

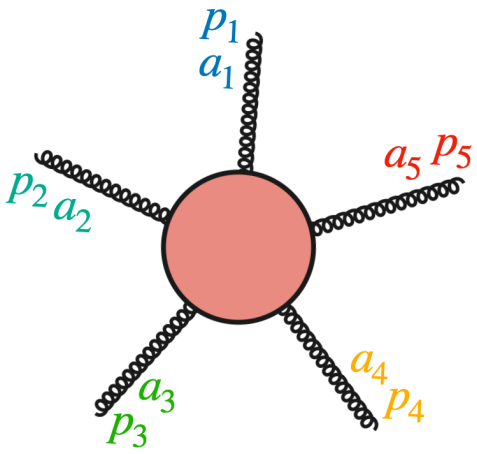

Figure 4.1: Five-gluon scattering. The p_i denote the (outgoing) momenta and the a_i are the adjoint-representation $SU(N_c)$ colour indices.

Physical scattering processes can be obtained by changing sign to the momenta of incoming particles. In particular $gg \to ggg$ corresponds to the region in Mandelstam space defined by

$$s_{12}, s_{34}, s_{45} > 0, \quad s_{23}, s_{51} < 0. \tag{4.4}$$

In order to fully describe the complex kinematic space, relevant for analytic continuation of the Feynman integrals involved in five-point amplitudes, it is useful to define the quantity

$$\mathrm{Tr}_5 = 4i\epsilon_{\mu\nu\rho\sigma} p_1^\mu p_2^\nu p_3^\rho p_4^\sigma \,, \tag{4.5}$$

which has non-trivial transformation properties under parity, inherited from its definition through the Levi-Civita tensor.

4.2 Colour Decomposition

We write the UV-renormalised scattering amplitude for the process of eq. (4.1) as

$$\mathcal{A} = (4\pi\alpha_s)^{\frac{3}{2}} \sum_{i=1}^{44} \mathcal{A}^{[i]} \mathcal{C}_{[i]} = (4\pi\alpha_s)^{\frac{3}{2}} \boldsymbol{\mathcal{A}} \cdot \boldsymbol{\mathcal{C}} \,, \tag{4.6}$$

where the first half of the colour tensors read

$$\begin{aligned}
\mathcal{C}_{[1]} &= \mathrm{Tr}[T^{a_1}T^{a_2}T^{a_3}T^{a_4}T^{a_5}],\ \mathcal{C}_{[2]} = \mathrm{Tr}[T^{a_1}T^{a_2}T^{a_3}T^{a_5}T^{a_4}],\\
\mathcal{C}_{[3]} &= \mathrm{Tr}[T^{a_1}T^{a_2}T^{a_4}T^{a_3}T^{a_5}],\ \mathcal{C}_{[4]} = \mathrm{Tr}[T^{a_1}T^{a_2}T^{a_4}T^{a_5}T^{a_3}],\\
\mathcal{C}_{[5]} &= \mathrm{Tr}[T^{a_1}T^{a_2}T^{a_5}T^{a_3}T^{a_4}],\ \mathcal{C}_{[6]} = \mathrm{Tr}[T^{a_1}T^{a_2}T^{a_5}T^{a_4}T^{a_3}],\\
\mathcal{C}_{[7]} &= \mathrm{Tr}[T^{a_1}T^{a_3}T^{a_2}T^{a_4}T^{a_5}],\ \mathcal{C}_{[8]} = \mathrm{Tr}[T^{a_1}T^{a_3}T^{a_2}T^{a_5}T^{a_4}],\\
\mathcal{C}_{[9]} &= \mathrm{Tr}[T^{a_1}T^{a_3}T^{a_4}T^{a_2}T^{a_5}],\ \mathcal{C}_{[10]} = \mathrm{Tr}[T^{a_1}T^{a_3}T^{a_5}T^{a_2}T^{a_4}],\\
\mathcal{C}_{[11]} &= \mathrm{Tr}[T^{a_1}T^{a_4}T^{a_2}T^{a_3}T^{a_5}],\ \mathcal{C}_{[12]} = \mathrm{Tr}[T^{a_1}T^{a_4}T^{a_3}T^{a_2}T^{a_5}],\\
\mathcal{C}_{[13]} &= \mathrm{Tr}[T^{a_1}T^{a_2}]\mathrm{Tr}[T^{a_3}T^{a_4}T^{a_5}],\ \mathcal{C}_{[14]} = \mathrm{Tr}[T^{a_4}T^{a_5}]\mathrm{Tr}[T^{a_1}T^{a_2}T^{a_3}],\\
\mathcal{C}_{[15]} &= \mathrm{Tr}[T^{a_3}T^{a_5}]\mathrm{Tr}[T^{a_1}T^{a_2}T^{a_4}],\ \mathcal{C}_{[16]} = \mathrm{Tr}[T^{a_3}T^{a_4}]\mathrm{Tr}[T^{a_1}T^{a_2}T^{a_5}],\\
\mathcal{C}_{[17]} &= \mathrm{Tr}[T^{a_1}T^{a_3}]\mathrm{Tr}[T^{a_2}T^{a_4}T^{a_5}],\ \mathcal{C}_{[18]} = \mathrm{Tr}[T^{a_2}T^{a_5}]\mathrm{Tr}[T^{a_1}T^{a_3}T^{a_4}],\\
\mathcal{C}_{[19]} &= \mathrm{Tr}[T^{a_2}T^{a_4}]\mathrm{Tr}[T^{a_1}T^{a_3}T^{a_5}],\ \mathcal{C}_{[20]} = \mathrm{Tr}[T^{a_1}T^{a_4}]\mathrm{Tr}[T^{a_2}T^{a_3}T^{a_5}],\\
\mathcal{C}_{[21]} &= \mathrm{Tr}[T^{a_2}T^{a_3}]\mathrm{Tr}[T^{a_1}T^{a_4}T^{a_5}],\ \mathcal{C}_{[22]} = \mathrm{Tr}[T^{a_1}T^{a_5}]\mathrm{Tr}[T^{a_2}T^{a_3}T^{a_4}],
\end{aligned} \tag{4.7}$$

and the other half are defined by reversing the traces above:

$$\mathcal{C}_{22+c} \equiv \mathcal{C}_c|_{\mathrm{Tr}[\bullet]\to\mathrm{Tr}[(\bullet)^T]}\ , \qquad c = 1,\ldots,22\,. \tag{4.8}$$

Here T denotes transposition of the string of generators inside the trace.

Denoting by $\boldsymbol{\lambda} = (\lambda_1, \lambda_2, \lambda_3, \lambda_4, \lambda_5)$ the list of signs of the helicities of the five incoming external gluons, the 16 parity independent amplitudes which need to be computed for this process are

$$\begin{aligned}
\boldsymbol{\lambda} = &(+,+,+,+,+),\ (-,+,+,+,+),\ (+,-,+,+,+),\ (+,+,-,+,+),\\
&(+,+,+,-,+),\ (+,+,+,+,-),\ (-,-,+,+,+),\ (-,+,-,+,+),\\
&(-,+,+,-,+),\ (-,+,+,+,-),\ (+,-,-,+,+),\ (+,-,+,-,+),\\
&(+,-,+,+,-),\ (+,+,-,-,+),\ (+,+,-,+,-),\ (+,+,+,-,-).
\end{aligned} \tag{4.9}$$

However, due to the permutation symmetries of the partial amplitudes we can

restrict our efforts to the combinations of colour and helicity configurations below:

$$\mathrm{Tr}[T^{a_1}T^{a_2}T^{a_3}T^{a_4}T^{a_5}] \to \begin{cases}(+,+,+,+,+)\\(-,+,+,+,+)\\(-,-,+,+,+)\\(-,+,-,+,+)\end{cases}$$

and

$$\mathrm{Tr}[T^{a_1}T^{a_2}]\mathrm{Tr}[T^{a_3}T^{a_4}T^{a_5}] \to \begin{cases}(+,+,+,+,+)\\(-,+,+,+,+)\\(-,-,+,+,+)\\(-,+,-,+,+)\\(+,+,+,+,-)\\(+,+,+,-,-)\end{cases} \tag{4.10}$$

This reduces the number of objects to be computed from $44 \times 16 = 704$ to only 10.

In particular, reality conditions on the colour tensors of gluon amplitudes imply

$$\mathcal{A}^{[i+22]} = -\mathcal{A}^{[i]}\,, \tag{4.11}$$

allowing us to write the amplitude as

$$\mathcal{A} = (4\pi\alpha_s)^{\frac{3}{2}} \sum_{i=1}^{22} \mathcal{A}^{[i]}\tilde{\mathcal{C}}_{[i]}\,, \qquad \tilde{\mathcal{C}}_{[i]} = \mathcal{C}_{[i]} - \mathcal{C}_{[i+22]}\,. \tag{4.12}$$

4.3 Helicity Amplitudes

In order to compute the primitive amplitudes of eq. (4.10) one can use the tensor-projection method described in section 2.1.2. Here I will describe a different (though equivalent) approach which allows us to directly evaluate helicity amplitudes in tHV, one configuration independently from the other. In ref. [122] both methods were used for the computation of all two-loop helicity amplitudes and full agreement was found.

Given a helicity configuration $\boldsymbol{\lambda}$, we can factor all external gluon polarisation vectors from the partial amplitudes

$$\boldsymbol{\mathcal{A}}_{\boldsymbol{\lambda}} = \boldsymbol{\mathcal{A}}_{\mu_1\mu_2\mu_3\mu_4\mu_5}\epsilon^{\mu_1}_{\lambda_1}\epsilon^{\mu_2}_{\lambda_2}\epsilon^{\mu_3}_{\lambda_3}\epsilon^{\mu_4}_{\lambda_4}\epsilon^{\mu_5}_{\lambda_5} \tag{4.13}$$

and as before use

$$\epsilon^{\mu_i}_{-} = \frac{[q_i|\mu_i|i\rangle}{\sqrt{2}[i|q_i]}, \qquad \epsilon^{\mu_i}_{i,+} = \frac{[i|\mu_i|q_i\rangle}{\sqrt{2}\langle q_i|i\rangle} \tag{4.14}$$

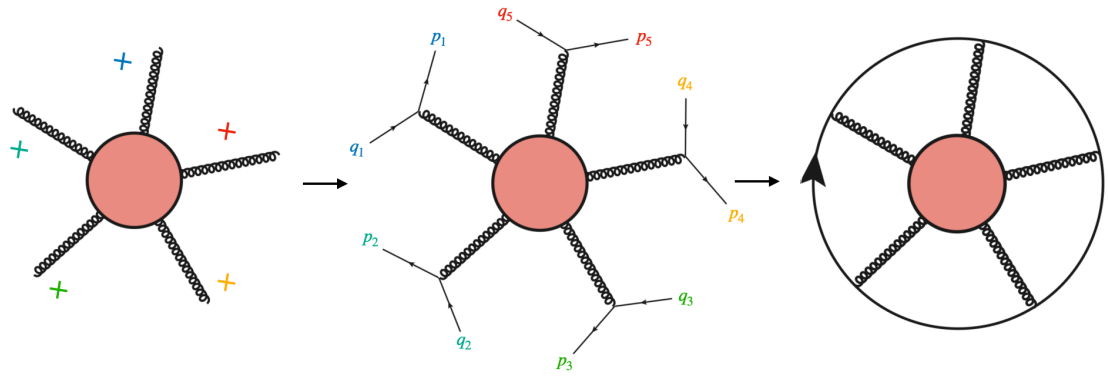

Figure 4.2: Graphical representation of the helicity projection procedure for the all-plus amplitude. The middle figure corresponds to eq. (4.15), where gluon polarisation vectors have been expressed using the spinor helicity formalism, but the reference vectors q_i have not yet been fixed. The closed circle (right) represents the trace in the second line of eq. (4.16).

to fix the helicities. The reference vectors q_i can then be chosen in a helicity-dependent way to "link" as many spinor chains as possible. For instance in the all-plus case we get

$$\epsilon_+^{\mu_1}\epsilon_+^{\mu_2}\epsilon_+^{\mu_3}\epsilon_+^{\mu_4}\epsilon_+^{\mu_5} = \frac{1}{4\sqrt{2}}\frac{[1|\mu_1|q_1\rangle}{\langle q_1|1\rangle}\frac{[2|\mu_2|q_2\rangle}{\langle q_2|2\rangle}\frac{[3|\mu_3|q_3\rangle}{\langle q_3|3\rangle}\frac{[4|\mu_4|q_4\rangle}{\langle q_4|4\rangle}\frac{[5|\mu_5|q_5\rangle}{\langle q_5|5\rangle} \tag{4.15}$$

which prompts us to make the cyclic choice $q_i = p_{i+1}$, with $p_6 = p_1$, yielding

$$\begin{aligned}\epsilon_+^{\mu_1}\epsilon_+^{\mu_2}\epsilon_+^{\mu_3}\epsilon_+^{\mu_4}\epsilon_+^{\mu_5} &= \frac{1}{4\sqrt{2}}\frac{[1|\mu_1|2\rangle}{\langle 2|1\rangle}\frac{[2|\mu_2|3\rangle}{\langle 3|2\rangle}\frac{[3|\mu_3|4\rangle}{\langle 4|3\rangle}\frac{[4|\mu_4|5\rangle}{\langle 5|4\rangle}\frac{[5|\mu_5|1\rangle}{\langle 1|5\rangle} \\ &= -\frac{1}{4\sqrt{2}}\frac{\mathrm{Tr}_-[\not{p}_1\gamma^{\mu_1}\not{p}_2\gamma^{\mu_2}\not{p}_3\gamma^{\mu_3}\not{p}_4\gamma^{\mu_4}\not{p}_5\gamma^{\mu_5}]}{\langle 12\rangle\langle 23\rangle\langle 34\rangle\langle 45\rangle\langle 51\rangle}\,,\end{aligned} \tag{4.16}$$

where $\mathrm{Tr}_\pm[\Gamma] = \frac{1}{2}\mathrm{Tr}[(1\pm\gamma_5)\Gamma]$. For the $(-,-,+,+,+)$ MHV amplitude the natural reference-vector choice would be different, reflecting the symmetry of the amplitude. In this case we would fix $q_1 = p_2, q_2 = p_1, q_3 = p_4, q_4 = p_5, q_5 = p_3$ and find

$$\epsilon_-^{\mu_1}\epsilon_-^{\mu_2}\epsilon_+^{\mu_3}\epsilon_+^{\mu_4}\epsilon_+^{\mu_5} = -\frac{1}{4\sqrt{2}}\frac{\mathrm{Tr}_+[\not{p}_1\gamma^{\mu_1}\not{p}_2\gamma^{\mu_2}]\mathrm{Tr}_-[\not{p}_3\gamma^{\mu_3}\not{p}_4\gamma^{\mu_4}\not{p}_5\gamma^{\mu_5}]}{[12][21]\langle 34\rangle\langle 45\rangle\langle 53\rangle}\,. \tag{4.17}$$

Similarly for the other MHV configurations we can choose the reference momenta so that

$$\epsilon_-^{\mu_1}\epsilon_+^{\mu_2}\epsilon_-^{\mu_3}\epsilon_+^{\mu_4}\epsilon_+^{\mu_5} = -\frac{1}{4\sqrt{2}}\frac{\mathrm{Tr}_+[\not{p}_1\gamma^{\mu_1}\not{p}_3\gamma^{\mu_3}]\mathrm{Tr}_-[\not{p}_2\gamma^{\mu_2}\not{p}_4\gamma^{\mu_4}\not{p}_5\gamma^{\mu_5}]}{[13][31]\langle 24\rangle\langle 45\rangle\langle 52\rangle}\,, \tag{4.18}$$

$$\epsilon_+^{\mu_1}\epsilon_+^{\mu_2}\epsilon_+^{\mu_3}\epsilon_-^{\mu_4}\epsilon_-^{\mu_5} = -\frac{1}{4\sqrt{2}}\frac{\mathrm{Tr}_+[\not{p}_4\gamma^{\mu_4}\not{p}_5\gamma^{\mu_5}]\mathrm{Tr}_-[\not{p}_1\gamma^{\mu_1}\not{p}_2\gamma^{\mu_2}\not{p}_3\gamma^{\mu_3}]}{[45][54]\langle 12\rangle\langle 23\rangle\langle 31\rangle}\,. \tag{4.19}$$

Finally, in the single-minus cases the traces can be completed as follows:

$$\epsilon_-^{\mu_1}\epsilon_+^{\mu_2}\epsilon_+^{\mu_3}\epsilon_+^{\mu_4}\epsilon_+^{\mu_5} = -\frac{1}{4\sqrt{2}}\frac{\mathrm{Tr}_+[\not{p}_1\gamma^{\mu_1}\not{p}_2\not{p}_3]\mathrm{Tr}_-[\not{p}_2\gamma^{\mu_2}\not{p}_3\gamma^{\mu_3}\not{p}_4\gamma^{\mu_4}\not{p}_5\gamma^{\mu_5}]}{[1231]\langle 23\rangle\langle 34\rangle\langle 45\rangle\langle 52\rangle}\,, \tag{4.20}$$

$$\epsilon_+^{\mu_1}\epsilon_+^{\mu_2}\epsilon_+^{\mu_3}\epsilon_+^{\mu_4}\epsilon_-^{\mu_5} = -\frac{1}{4\sqrt{2}}\frac{\mathrm{Tr}_+[\not{p}_5\gamma^{\mu_5}\not{p}_2\not{p}_3]\mathrm{Tr}_-[\not{p}_1\gamma^{\mu_1}\not{p}_2\gamma^{\mu_2}\not{p}_3\gamma^{\mu_3}\not{p}_4\gamma^{\mu_4}]}{[5235]\langle 12\rangle\langle 23\rangle\langle 34\rangle\langle 41\rangle}\,. \tag{4.21}$$

The traces $\mathrm{Tr}_\pm$ can then be directly evaluated yielding explicit helicity projection tensors written in terms of the external momenta, the four-dimensional metric $\overline{g}^{\mu\nu}$ and the four dimensional Levi-Civita tensor $\epsilon^{\mu\nu\rho\sigma}$, which can be directly applied to the amplitude by plugging the result in eq. (4.13).

However, in order to obtain a representation of the helicity amplitudes whose loop integrals fall within the standard class of Feynman integrals, we need to take care when dealing with $\overline{g}^{\mu\nu}$ and $\epsilon^{\mu\nu\rho\sigma}$. The problem stems from the fact that these are strictly four-dimensional quantities and lead to integrands which are not Lorentz invariant in d dimensions. However it turns out that they can always be replaced in favour of the standard metric and a set of independent external momenta. The four-dimensional metric can be replaced by

$$\overline{g}^{\mu\nu} = g^{\mu\nu} - \frac{G\begin{pmatrix}\mu\ 1\ 2\ 3\ 4\\ \nu\ 1\ 2\ 3\ 4\end{pmatrix}}{G\begin{pmatrix}1\ 2\ 3\ 4\end{pmatrix}}\,, \tag{4.22}$$

that is by the d-dimensional metric to which we have subtracted the (-2ϵ)-dimensional metric written as a ratio of Gram determinants of the four independent external momenta. The Levi-Civita tensor can instead be dealt with by first removing powers higher than one via the identity

$$\epsilon_{\mu_1\mu_2\mu_3\mu_4}\epsilon_{\nu_1\nu_2\nu_3\nu_4} = -\begin{vmatrix} g_{\mu_1\nu_1} & g_{\mu_1\nu_2} & g_{\mu_1\nu_3} & g_{\mu_1\nu_4}\\ g_{\mu_2\nu_1} & g_{\mu_2\nu_2} & g_{\mu_2\nu_3} & g_{\mu_2\nu_4}\\ g_{\mu_3\nu_1} & g_{\mu_3\nu_2} & g_{\mu_3\nu_3} & g_{\mu_3\nu_4}\\ g_{\mu_4\nu_1} & g_{\mu_4\nu_2} & g_{\mu_4\nu_3} & g_{\mu_4\nu_4}\end{vmatrix}\,, \tag{4.23}$$

and then substituting any left-over with the relation

$$\epsilon^{\mu\nu\rho\sigma} = -\frac{4i}{\mathrm{Tr}_5}G\begin{pmatrix}\mu\ \nu\ \rho\ \sigma\\ 1\ 2\ 3\ 4\end{pmatrix}\,, \tag{4.24}$$

where Tr_5 was introduced in eq. (4.5).

In practice this means we can evaluate each helicity amplitude independently[1] in a way that allows us to fix the reference momenta in a helicity-dependent way and entirely by-passing the tensor projection method. Importantly, one can do the above while still obtaining loop integrals which can be evaluated with standard techniques.

Following chapter 2, we can express helicity amplitudes in terms of a little-group invariant helicity amplitude $\boldsymbol{\mathcal{H}}$

$$\boldsymbol{\mathcal{A}}|_{\boldsymbol{\lambda}} = \boldsymbol{\mathcal{H}}_{\boldsymbol{\lambda}}\, s_{\boldsymbol{\lambda}}, \tag{4.25}$$

where we defined the spinor factors

$$\begin{aligned}
s_{+++++} &= \frac{2s_{12}^2/3}{\langle 12\rangle\langle 23\rangle\langle 34\rangle\langle 45\rangle\langle 51\rangle}\,, \quad s_{-++++} = \frac{[21]\langle 12\rangle^4\langle 13\rangle^3}{\langle 15\rangle^2\langle 23\rangle^5\langle 14\rangle^2}\,,\\
s_{--+++} &= \frac{4\langle 12\rangle^4}{\langle 12\rangle\langle 23\rangle\langle 34\rangle\langle 45\rangle\langle 51\rangle}\,, \quad s_{-+-++} = \frac{4\langle 13\rangle^4}{\langle 12\rangle\langle 23\rangle\langle 34\rangle\langle 45\rangle\langle 51\rangle}\,,\\
s_{++++-} &= \frac{[51]\langle 15\rangle^4\langle 25\rangle^3}{\langle 54\rangle^2\langle 12\rangle^5\langle 53\rangle^2}\,, \quad s_{+++--} = \frac{4\langle 45\rangle^4}{\langle 12\rangle\langle 23\rangle\langle 34\rangle\langle 45\rangle\langle 51\rangle}\,.
\end{aligned} \tag{4.26}$$

While the formal colour and helicity decomposition of helicity amplitude eq. (4.25) holds at all orders in perturbation theory, in order to explicitly compute the $\boldsymbol{\mathcal{H}}_{\boldsymbol{\lambda}}$ one can perform a perturbative expansion in the coupling α_s:

$$\boldsymbol{\mathcal{H}}_{\boldsymbol{\lambda}} = \sum_{\ell=0} \alpha_s^{\ell}\, \boldsymbol{\mathcal{H}}_{\boldsymbol{\lambda}}^{(\ell)}\,. \tag{4.27}$$

where each $\boldsymbol{\mathcal{H}}_{\boldsymbol{\lambda}}^{(\ell)}$ is computed from the corresponding ℓ-loop Feynman diagrams. From eq. (4.10) we read that only the colour components $\mathcal{H}_{\boldsymbol{\lambda}}^{[1],(\ell)}$ and $\mathcal{H}_{\boldsymbol{\lambda}}^{[13],(\ell)}$ need to be computed for the required helicity configurations, while the remaining 42 components can be obtained by crossing of the external legs. The crossing-independent partial amplitudes in eq. (4.10) can be further decomposed by separating

[1]Differently from the tensor-decomposition method, for which a system involving all relevant tensors must be solved in order to obtain the helicity projectors.

different powers in N_c and n_f:

$$\mathcal{H}^{[1],(\ell)} = N_c^{\ell} \sum_{h=0}^{\lfloor \ell/2 \rfloor} \sum_{k=0}^{\ell} \frac{1}{N_c^{2h}} \left(\frac{n_f}{N_c}\right)^k \mathcal{H}_{h,k}^{[1],(\ell)}\,, \tag{4.28}$$

$$\mathcal{H}^{[13],(\ell)} = N_c^{\ell-1} \sum_{h=0}^{\lfloor (\ell-1)/2 \rfloor} \sum_{k=0}^{\ell} \frac{1}{N_c^{2h}} \left(\frac{n_f}{N_c}\right)^k \mathcal{H}_{h,k}^{[13],(\ell)}\,, \tag{4.29}$$

where we omitted the helicity dependence $\boldsymbol{\lambda}$. The $\mathcal{H}_{h,k}^{[i],(\ell)}$ carry no dependence on the size of the gauge group or the number of quark flavours. In particular, up to two loops we find

$$\begin{aligned}
&\mathcal{H}^{[1],(0)} = \mathcal{H}_{0,0}^{[1],(\ell)}\,, \quad \mathcal{H}^{[13],(0)} = 0\,,\\
&\mathcal{H}^{[1],(1)} = N_c \mathcal{H}_{0,0}^{[1],(1)} + n_f \mathcal{H}_{0,1}^{[1],(1)}\,, \quad \mathcal{H}^{[13],(1)} = \mathcal{H}_{0,0}^{[13],(1)}\,,\\
&\mathcal{H}^{[1],(2)} = N_c^2 \mathcal{H}_{0,0}^{[1],(2)} + N_c n_f \mathcal{H}_{0,1}^{[1],(2)} + n_f^2 \mathcal{H}_{0,2}^{[1],(2)} + \mathcal{H}_{1,0}^{[1],(2)} + \frac{n_f}{N_c} \mathcal{H}_{1,1}^{[1],(2)} + \frac{n_f^2}{N_c^2} \mathcal{H}_{1,2}^{[1],(2)}\,,\\
&\mathcal{H}^{[13],(2)} = N_c \mathcal{H}_{0,0}^{[13],(2)} + n_f \mathcal{H}_{0,1}^{[13],(2)}\,,
\end{aligned} \tag{4.30}$$

where the helicity dependence was left implicit. It should be noted that the over-completeness relations mentioned in section 2.2 provide a further constraint on the partial five-gluon two-loop amplitudes which allows us to express $\mathcal{H}_{0,0}^{[13],(2)}$ as a linear combination of crossings of $\mathcal{H}_{0,0}^{[1],(\ell)}$ and $\mathcal{H}_{1,0}^{[1],(\ell)}$. Nevertheless in ref. [122] we computed an over-complete set of partial amplitude and used this relation as a check of our results.

As a final remark, we point out that because of the existence of the parity-odd little-group invariant Tr_5 defined in eq. (4.5), all $\mathcal{H}_{h,k}^{[i],(\ell)}$ can be split into a parity-even and a parity-odd part:

$$\mathcal{H}_{h,k}^{[i],(\ell)} = \mathcal{E}_{h,k}^{[i],(\ell)} + \mathrm{Tr}_5\, \mathcal{O}_{h,k}^{[i],(\ell)}\,, \tag{4.31}$$

where the $\mathcal{E}$ and $\mathcal{O}$ do not change sign under parity. After helicity projection has been completed, one can explicitly separate the two contributions which never mix during the rest of the calculation. Practically, during this computation, all the various ways mentioned above of splitting the amplitudes in building blocks proved to be an extremely useful to manage the complexity of the calculation.

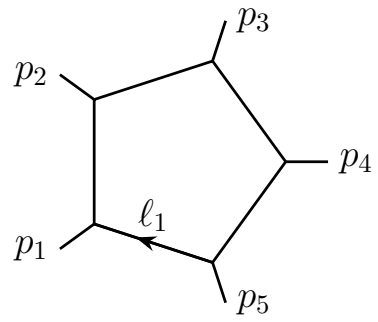

Figure 4.3: Massless Pentagon

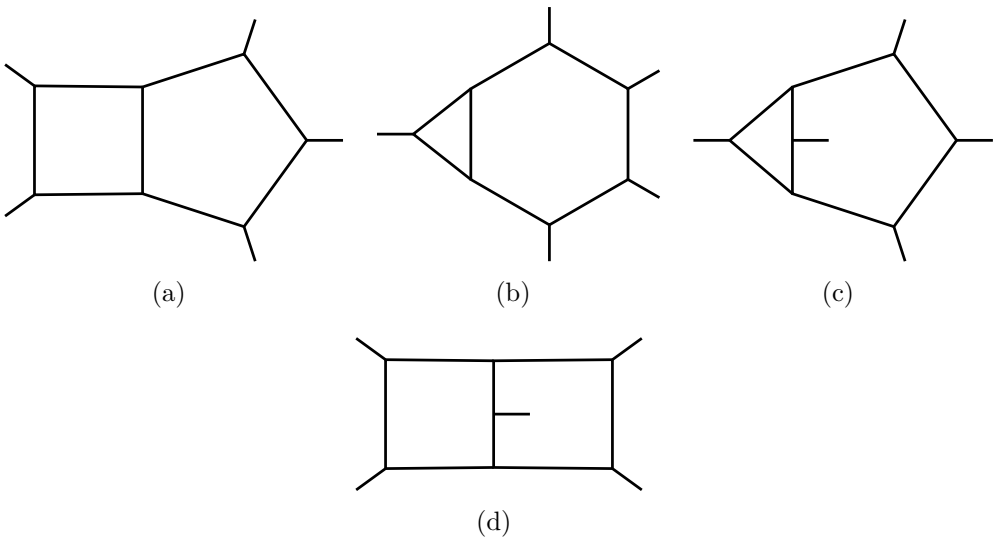

Figure 4.4: Two-loop topologies for five-point massless scattering: penta-box (a), five-point beetle (b), hexa-box (c) and double pentagon (d).

4.4 Loop Integrals

As a result of the previous sections, we defined the scalar quantities $\mathcal{H}_{h,k}^{[i],(\ell)}$, which carry the whole information about the scattering amplitude and are entirely written in terms of scalar Feynman integrals. All integrals appearing at one loop belong to the pentagon topology of fig. 4.3

$$\mathcal{I}^{\text{Pentagon}}_{\nu_1,\ldots,\nu_5} = \int \mathfrak{D}\ell \frac{1}{\mathcal{D}_1^{\nu_1}\ldots\mathcal{D}_5^{\nu_5}} \tag{4.32}$$

and to the topologies obtained from it by crossing the external legs. At two loops the four topologies of fig. 4.4 appear, however the beetle integral (b) is reducible to sub-sectors of (a). Integrals in the penta-box topology are planar, while the

Family	Pentagon	PL_5	NPL_5 – check
$\mathcal{D}_1$	ℓ_1^2	ℓ_1^2	ℓ_1^2
$\mathcal{D}_2$	$(\ell_1+p_1)^2$	$(\ell_1+p_1)^2$	$(\ell_1+p_1)^2$
$\mathcal{D}_3$	$(\ell_1+p_1+p_2)^2$	$(\ell_1+p_1+p_2)^2$	$(\ell_1+p_1+p_2)^2$
$\mathcal{D}_4$	$(\ell_1+p_1+p_2+p_3)^2$	$(\ell_1+p_1+p_2+p_3)^2$	$(\ell_1+p_1+p_2+p_3)^2$
$\mathcal{D}_5$	$(\ell_2+p_1+p_2+p_3+p_4)^2$	$(\ell_1+p_1+p_2+p_3+p_4)^2$	$(\ell_1-\ell_2-p_4)^2$
$\mathcal{D}_6$	–	ℓ_2^2	ℓ_2^2
$\mathcal{D}_7$	–	$(\ell_2+p_1)^2$	$(\ell_2+p_1)^2$
$\mathcal{D}_8$	–	$(\ell_2+p_1+p_2)^2$	$(\ell_2+p_1+p_2)^2$
$\mathcal{D}_9$	–	$(\ell_2+p_1+p_2+p_3)^2$	$(\ell_2+p_1+p_2+p_3)^2$
$\mathcal{D}_{10}$	–	$(\ell_2+p_1+p_2+p_3+p_4)^2$	$(\ell_2+p_1+p_2+p_3+p_4)^2$
$\mathcal{D}_{11}$	–	$(\ell_1-\ell_2)^2$	$(\ell_1-\ell_2)^2$

Table 4.1: Integral families for five-point massless scattering up to two loops.

hexa-box and double pentagon topologies contain the non-planar integrals needed for the evaluation of the amplitude beyond the leading-colour approximation.

The propagator-denominator (PD) representation for Feynman integrals defined in section 2.3.1 allows us to express all needed integrals in terms of only two integral families $\mathfrak{f} = \{\mathrm{PL}_5, \mathrm{NPL}_5\}$, each with 11 propagators, which can be written as

$$\mathcal{I}^{\mathfrak{f}}_{\nu_1,\ldots,\nu_{11}} = \int \mathfrak{D}^2\ell \, \frac{1}{\mathcal{D}_1^{\nu_1}\ldots\mathcal{D}_{11}^{\nu_{11}}} \,. \tag{4.33}$$

The list of propagators for all families up to two loops can be found in table 4.1 and the required crossed families are obtained from these via permutation of the external momenta. A set of canonical master integrals for these integral families was computed in refs. [125–130] via the method of differential equations, and expressed as a Laurent series in the dimensional regulator ϵ. A uniform representation in terms of massless *pentagon functions* was given in ref. [131].

The methodology followed for the simplification of the amplitudes for the process $0 \to ggggg$ is similar to the one described in chapter 3, though its implementation presented different challenges. Sector relations and sector symmetries were obtained using `Reduze 2` [36, 84]. Inserting them into the amplitudes reduced the initial number of integrals from $\mathcal{O}(10^6)$ to $\mathcal{O}(10^4)$. The disk-size of the scattering amplitudes also shrunk by one order of magnitude from ~ 1 TB to ~ 100 GB. IBP

reduction for the reduced set of integrals was then achieved using the public code `Kira` [132, 133] and, specifically for the non-planar topologies, the code `Finred`.

Although the number of integrals to reduce here was substantially smaller compared to the three-loop four-point amplitudes presented in chapter 3, the multi-scale kinematics of five-point amplitudes is responsible for a large swell of intermediate expressions, in particular in the non-planar sectors, where all channels contribute simultaneously and one encounters individual IBP identities with disk-sizes of up to 3 GB [134–136].

Our approach to deal with the complexity of the rational coefficients of these amplitudes is based on the initial observation [135, 136] that partial-fraction decomposition can reduce expression size for single IBPs of various orders of magnitude. The same turns out to happen at the amplitude level, transforming a seemingly un-treatable problem into an achievable computation.

We perform IBP reduction for a minimal subset of integrals and decompose the resulting integral coefficients into multivariate partial fractions. The problem of multivariate partial fractioning can be addressed via computational algebraic geometry. The first step is to determine the full list of potential numerator and denominator factors appearing in the rational functions we want to simplify. Working at the level of the rational coefficients in the even and odd components defined in eq. (4.31), we find that the space of numerators is simply given by the set of linearly independent Mandelstam invariants eq. (4.3) while the most general list of denominators can be written as

$$\begin{aligned}
\{d_{i=1,\ldots,10}\} &= \{s_{12},\ s_{23},\ s_{34},\ s_{45},\ s_{51},\ s_{13},\ s_{14},\ s_{24},\ s_{25},\ s_{35}\}\,, \\
\{d_{i=11,\ldots,25}\} &= \{(s_{12}+s_{23}),\ (s_{23}+s_{34}),\ (s_{34}+s_{45}),\ (s_{45}+s_{51}), \\
&\qquad (s_{51}+s_{12}),\ (s_{12}+s_{34}),\ (s_{23}+s_{45}),\ (s_{34}+s_{51}), \\
&\qquad (s_{45}+s_{12}),\ (s_{51}+s_{23}),\ (s_{12}+s_{45}),\ (s_{23}+s_{51}), \\
&\qquad (s_{34}+s_{12}),\ (s_{45}+s_{23}),\ (s_{51}+s_{34})\}\,, \\
d_{26} &= \mathrm{Tr}_5^2 = G\left(1\ 2\ 3\ 4\right)\,,
\end{aligned} \tag{4.34}$$

where the subsets $\{d_{i=1,\ldots,10}\}$, $\{d_{i=11,\ldots,25}\}$ and $\{d_{26}\}$ are closed under permutations of the external momenta. The denominator factors $\{d_{i=1,\ldots,25}\}$ are of degree 1 in the Mandelstam variables, while the Gram determinant of d_{26} is of degree 4. Then any rational function R can be written as

$$R = \sum_{\substack{\vec{a}\in\mathbb{N}^5 \\ \vec{b}\in\mathbb{N}^{26}}} r(\vec{a},\vec{b})\; s_{12}^{a_1} s_{23}^{a_2} s_{34}^{a_3} s_{45}^{a_4} s_{51}^{a_5} \prod_{i=1}^{26} \frac{1}{d_i^{b_i}} \tag{4.35}$$

with $r(\vec{a},\vec{b})$ rational numbers. The next step is to introduce auxiliary variables $\tilde{d}_i$ defined by $1 - \tilde{d}_i d_i = 0$, in terms of which the rational function above becomes

$$R = \sum_{\substack{\vec{a}\in\mathbb{N}^5 \\ \vec{b}\in\mathbb{N}^{26}}} r(\vec{a},\vec{b})\; s_{12}^{a_1} s_{23}^{a_2} s_{34}^{a_3} s_{45}^{a_4} s_{51}^{a_5} \prod_{i=1}^{26} \tilde{d}_i^{b_i}\,. \tag{4.36}$$

We can then define the polynomial ring

$$\mathfrak{R} = \mathbb{Q}[s_{12}, s_{23}, s_{34}, s_{45}, s_{51}, \tilde{d}_1, \ldots, \tilde{d}_{26}]\,, \quad R \in \mathfrak{R} \tag{4.37}$$

and the ideal

$$\mathfrak{I} = \langle 1 - \tilde{d}_1 d_1, \ldots, 1 - \tilde{d}_{26} d_{26} \rangle\,. \tag{4.38}$$

Finally, provided we have defined a total monomial ordering $\geq_{\mathfrak{R}}$ in $\mathfrak{R}$ (which we will mostly leave implicit below), we can compute a Gröbner basis g of $\mathfrak{I}$ and reduce R with respect to g:

$$red(R,g)_{\geq_{\mathfrak{R}}} = \bar{R} = \sum_i \bar{r}_i\, m_i\,, \tag{4.39}$$

where $\bar{r}_i$ are rational numbers which depend on the choice of monomial ordering and m_i are monomials in $\mathfrak{R}$ which are irreducible with respect to g. The reduced rational function $\bar{R}$ is the desired result: a partial-fractioned representation of the original rational function. Two comments are in order at this point. First, the simplicity of the results one obtains is greatly influenced by the choice of monomial ordering. In any given partial amplitude, one can expect some denominators to be absent, while the presence of the rest is justified by the singularity structure of the amplitude (for more details see refs. [135, 136]). One should therefore choose a monomial ordering

favouring denominators which are (physically) expected in an amplitude, so that as few spurious denominators as possible are introduced. For instance, in the case of the single trace colour ordered amplitude, proportional to $\mathcal{C}_{[1]}$, our choice of ordering was

$$\tilde{d}_{26} > \cdots > \tilde{d}_1 > s_{51} > s_{45} > s_{34} > s_{23} > s_{12}\,. \tag{4.40}$$

Second, for a fixed monomial ordering, the coefficients $\bar{r}_i$ form a ($\mathbb{Q}$-)vector space: once a list of the irreducible monomials has been specified, each rational function R can be identified with a vector $\bar{\boldsymbol{r}}(R) = \{\bar{r}_1, \bar{r}_2, \ldots\}$. This map satisfies

$$\bar{\boldsymbol{r}}(\alpha R_1 + \beta R_2) = \alpha \bar{\boldsymbol{r}}(R_1) + \beta \bar{\boldsymbol{r}}(R_2) \quad \text{for } \alpha, \beta \in \mathbb{Q}\,. \tag{4.41}$$

This is a particularly useful property when performing sum of contributions to the same amplitude. When working with partial-fractioned rational functions one can simply sum the vector coefficients $\bar{\boldsymbol{r}}$ and obtain partial-fractioned expressions for the sums of rational functions. Conversely, if one tries to do the same in common-denominator form large amounts of algebra are usually required to simplify the results. In practice, to perform Gröbner basis computations and polynomial reduction we use `Singular` [137], which proves to be sufficient the denominators set of eq. (4.34).

More specifically, we first derive reduction identities for the un-crossed integral families of table 4.1 and perform a partial-fraction decomposition of their rational functions which reduces their overall size by about two orders of magnitude. We then obtain reduction identities for all crossed families contributing to the amplitudes by permutations of the external invariants. Crossing of the external legs does not preserve monomial ordering and therefore the resulting identities require an additional partial-fractioning step.

Once the simplified reduction identities are inserted into the amplitude, we perform an additional partial-fraction decomposition to simplify the resulting expressions; in addition to the IBP reduction, this proves to be the step with the highest computational cost in our framework. A further level of simplification can then be achieved by expressing the reduced amplitudes in terms of a minimal

number of independent rational functions (see for instance ref. [122] and references therein for more details).

4.5 Results

As a result of the computations described in previous sections one obtains the bare scattering amplitudes for the five-gluon process. Each any of the amplitude components of eq. (4.30) can be UV renormalised following eq. (2.89). The resulting renormalised colour components can then be explicitly written as

$$\mathcal{R}^{[i],(\ell)}_{h,k} = \sum_{m=-2\ell}^{4-2\ell} \sum_{w=0}^{m} \frac{1}{\epsilon^m} (R^E_{m,w,j} + \mathrm{Tr}_5\, R^O_{m,w,j}) F^{(w)}_j \,, \tag{4.42}$$

where $R^E_{m,w,j}, R^O_{m,w,j}$ are rational functions[2] of the invariants s_{ij}, expressed as polynomials in $\mathfrak{R}$, and the $F^{(w)}_j$ are weight-w pentagon functions defined in ref. [131]. The $4-2\ell$ upper bound represents a truncation of higher powers of ϵ which still allows one to obtain the $\mathcal{O}(\epsilon^0)$ contribution to finite remainders.

We performed numerous checks on our results. First, we observed that the IR poles of the UV-renormalised amplitude components (4.42) are fully predicted by eqs. (2.90) and (2.100). We also verified the one- and two-loop $U(1)$ decoupling identities as well as the generalized colour-trace identities described in [34]. We also computed a redundant set of single-trace partial amplitudes; crossing relations among them allowed us to verify the consistency of our calculation.

We also compared our tree-level and one-loop results against existing analytic calculations [138, 139] as well as `OpenLoops2` [103], by numerically evaluating all helicity configurations and summing over colour degrees of freedom.

We also found perfect agreement with the analytic two-loop full-colour all-plus gluon amplitude of ref. [140] and with the numerical benchmarks in the leading-colour approximation provided in ref. [141].

Finally, we verified that our results agree numerically to high precision with those provided by a similar concurrent calculation presented in ref. [123].

[2]The dependence of the rational functions on the colour component indices i, k, h as well as on the loop order and helicity configuration is left implicit.

Though the definitions in eq. (2.101) would provide a valid set of IR-subtracted finite remainders, we decided to present our results in a slightly different IR-subtraction scheme in order to match pre-existing literature. In particular, we used Catani's subtraction operators [142]

$$\begin{aligned}
\boldsymbol{\mathcal{I}}_1^c(\epsilon) &= \frac{e^{\epsilon\gamma_E}}{\Gamma(1-\epsilon)} \sum_i \left(\frac{1}{\epsilon^2} - \frac{\gamma_0^i}{2\epsilon}\frac{1}{\mathbf{T}_i^2}\right) \sum_{i\neq j} \frac{\mathbf{T}_i\cdot\mathbf{T}_j}{2} \left(\frac{\mu^2}{-s_{ij}}\right)^{\epsilon} , \\
\boldsymbol{\mathcal{I}}_2^c(\epsilon) &= \frac{e^{-\epsilon\gamma_E}\Gamma(1-2\epsilon)}{\Gamma(1-\epsilon)} \left(\frac{\gamma_1^{\text{cusp}}}{8} + \frac{\beta_0}{2\epsilon}\right) \boldsymbol{\mathcal{I}}_1^c(2\epsilon) - \frac{1}{2}\boldsymbol{\mathcal{I}}_1^c(\epsilon)\left(\boldsymbol{\mathcal{I}}_1^c(\epsilon) + \frac{\beta_0}{\epsilon}\right) + \frac{1}{\epsilon}\boldsymbol{\mathcal{H}}_2 ,
\end{aligned} \tag{4.43}$$

where the colour operator $\boldsymbol{\mathcal{H}}_2$ is given by

$$\begin{aligned}
\boldsymbol{\mathcal{H}}_2 = &\frac{1}{16}\sum_i \left(\gamma_1^i - \frac{1}{4}\gamma_1^{\text{cusp}}\gamma_0^i + \frac{\pi^2}{16}\beta_0\gamma_0^{\text{cusp}}C_i\right) \\
&+ \frac{if^{abc}}{24}\sum_{(i,j,k)} \mathbf{T}_i^a\mathbf{T}_j^b\mathbf{T}_k^c \log\frac{-s_{ij}}{-s_{jk}}\log\frac{-s_{jk}}{-s_{ki}}\log\frac{-s_{ki}}{-s_{ij}} \\
&- \frac{if^{abc}}{128}\gamma_0^{\text{cusp}}\sum_{(i,j,k)} \mathbf{T}_i^a\mathbf{T}_j^b\mathbf{T}_k^c \left(\frac{\gamma_0^i}{C_i} - \frac{\gamma_0^j}{C_j}\right)\log\frac{-s_{ij}}{-s_{jk}}\log\frac{-s_{ki}}{-s_{ij}} ,
\end{aligned} \tag{4.44}$$

as reported in ref. [61].

In terms of eqs. (4.43) and (4.44) we defined the following finite remainders

$$\begin{aligned}
\mathcal{F}_c^{(0)} &= \mathcal{R}^{(0)} , \\
\mathcal{F}_c^{(1)} &= \mathcal{R}^{(1)} - \boldsymbol{\mathcal{I}}_1^c\,\mathcal{R}^{(0)} , \\
\mathcal{F}_c^{(2)} &= \mathcal{R}^{(2)} - \boldsymbol{\mathcal{I}}_1^c\,\mathcal{R}^{(1)} - \boldsymbol{\mathcal{I}}_2^c\,\mathcal{R}^{(0)} .
\end{aligned} \tag{4.45}$$

`Mathematica`-readable expressions corresponding to the finite remainders of the partial amplitudes of eq. (4.10) can be found at [143].

In order to reconstruct the full amplitude from the results of the primitive amplitudes, we employ crossing symmetry and parity transformations similarly to section 3.5. The analytic continuation of each pentagon function individually is non-trivial but also not necessary. In fact, the information needed to perform the required continuation is available implicitly in the results provided by ref. [131], where all master integrals are evaluated for all 120 permutations of the external invariants in terms of a minimal set of pentagon functions. In practice, we took every uncrossed master integral and applied the required crossing on its analytic expression

by formally crossing all appearing pentagon functions. We then equated these formal expressions to the explicit results for the crossed master integrals, which are written in terms of uncrossed pentagon functions. Repeating this for all master integrals for a given crossing, we obtained a linear system of equations, which we solved using `FiniteFlow` [89]. This allowed us to express the crossed pentagon functions in terms of the uncrossed ones. Typically, the system is under-determined and some crossed pentagon functions remain unsolved for. Nevertheless, since the results in ref. [131] are sufficient to represent any crossing of the amplitudes, all formally crossed pentagon functions remaining after solving the system must cancel upon inserting the solution into the amplitude. We verified this cancellation explicitly for each crossing required to obtain the helicity and colour ordered amplitudes for all partonic sub-channels. This provided a strong check of the consistency of our procedure.

5 Infrared-Finite Integrals

Contents

5.1 Introduction 95
5.2 Dimension-Independent Integral Relations 97
5.3 IR-finite Feynman Integrals 100
5.3.1 Ideals of IR-finite Integrals 102
5.3.2 IR Power Counting 102
5.3.3 Example: Massless Box 105
5.3.4 Evanescent Integrands 109
5.3.5 Example: Massless Pentagon 111
5.4 Examples of Finite Ideals 112
5.4.1 Planar Double Box 112
5.4.2 Ladder Integrals: an All-Loops Conjecture 119
5.4.3 Non-Planar Double Box 121
5.4.4 Two-Loop Beetle 124
5.4.5 Two-Loop Four-Gluon Helicity Amplitudes 125

5.1 Introduction

Scattering amplitudes have many different representations. In previous chapters I described a practical method to obtain representations in terms of minimal sets of master integrals. It is known that this method does not always yield the most compact from of amplitudes and can often obscure the some features of amplitudes. A great reduction in complexity is usually obtained by Laurent-expanding the master

integrals in the dimensional regulator ϵ via the method of differential equations of section 2.3.5. This has two benefits: it makes the loop divergences of the amplitude manifest as poles in ϵ and it allows one to numerically evaluate[1] the amplitude for explicit values of the external kinematics.

In this chapter we make a first step towards a different approach. The aim will be to obtain representations of scattering amplitudes where IR and UV singularities are faithfully represented in loop-momentum space.

More concretely, with Yang–Mills theories in mind, we would like to make IR factorisation manifest by finding an integrand-level representation of the form

$$\mathcal{A} = \mathcal{A}_{\text{hard}} + \mathcal{A}_{\text{IR}} \tag{5.1}$$

where $\mathcal{A}_{\text{IR}}$ contains all IR divergences.

Already at this level it becomes clear that a representation of the type in eq. (5.1) cannot be obtained by fully relying on IBP identities as is normally done. This is because of relations like

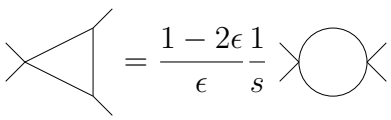

(5.2)

where the double IR (soft and collinear) divergence of the triangle has been traded for an explicit pole in ϵ and a UV divergence of the bubble. More in general, the IR-UV mixing induced by IBP relations spoils the physical properties of the integrand and has to be avoided.

Below we will tackle this problem by studying a subset of IBPs whose coefficients do not depend on the space-time dimensions d and therefore automatically exclude relations similar to eq. (5.2). However it should be noted that this does not completely solve the IR-UV mixing problem. In fact, due to the fact that scaleless integrals vanish in dimensional regularisation, the equation

(5.3)

[1] provided that an efficient code for the numerical evaluation of the class of iterated integrals in question has been developed.

would still be included in the set we consider, as it does not explicitly depend on d. However, it is a source of UV-IR mixing because the bubble integral above is both UV and IR divergent and schematically $0 = 1/\epsilon_{UV} - 1/\epsilon_{IR}$. For the moment we will ignore this type of mixing.

Assuming for the moment that we know how to find all relations among Feynman integrals which do not mix their IR and UV behaviour, the next question is how to choose the corresponding set of master integrals. Eq. (5.1) suggests that a good basis of integrals should have definite IR (and UV) properties. In particular we might ask what is the set of integrals which can appear in $\mathcal{A}_{\text{hard}}$. By definition they should be IR-finite, meaning that all IR singularities of the propagators should be integrable. Once the set of all IR-finite integrals is known, one can use them to identify a complete basis of IR-divergent integrals which can be used to represent $\mathcal{A}_{\text{IR}}$.

The remainder of this chapter is organised as follows. In section section 5.2 we will discuss the set of IBP relations whose coefficients do not depend on the space-time dimensions d and which represent a good starting point to remove the aforementioned UV-IR mixing. In section 5.3 we will shift our attention to the determination of IR-finite integrals. Finally in section 5.4.5 we will provide a proof-of-concept example of the combination of ideas developed in sections 5.2 and 5.3.

5.2 Dimension-Independent Integral Relations

In this section we will describe a method to obtain IBP relations among Feynman integrals whose coefficients do not depend on the space-time dimensions d.[2] Our motivation comes from the fact that such systems of IBPs induce a far smaller degree of UV-IR mixing, the only effect coming from the vanishing of scaleless integrals like in eq. (5.3). Restricting ourselves to a subset of IBPs has the clear

[2]It would also be possible to take a more refined approach, allowing reduction identities to explicitly depend on d, but asking that all coefficients should be regular as $d \to 4$. Because identities of the type eq. (5.2) would still be forbidden, we expect equivalent UV-IR properties but a smaller number of master integrals. In the following we explore the idea of d-independent IBP reduction and leave relations regular in the $d \to 4$ limit for future investigation.

disadvantage of increasing the number of master integrals for any given process. However, because d-independent integral relations preserve the UV/IR properties of amplitudes, we might expect to find more representations which are more compact and physically meaningful for a suitable choice of master integrals.

Let us refer to integrals appearing in a given topology or integral family (see section 2.3) as $\mathcal{I}_i$, with $i \in \mathbb{N}$ and with each integral defined as in eq. (2.43) for some set of propagators and with a scalar numerator whose coefficients are independent of d. Then our goal is to find all IBP reduction identities whose rational coefficients are independent of d:

$$\sum_{i \in \mathcal{S}'} C_i(\vec{s})\, \mathcal{I}_i = 0 \tag{5.4}$$

Denoting by $\mathcal{M}_i^{(d)}$ the master integrals obtained via standard IBPs, all integrals can be reduced as

$$\mathcal{I}_i = \sum_j c_{ij}(\vec{s}, d)\, \mathcal{M}_j^{(d)}\,. \tag{5.5}$$

Let us now assume that the master integrals in question have been chosen[3] so that the dependence on d of the reduction coefficients is factorised from the kinematics so that rational functions in d can be partial fractioned to yield

$$c_{ij}(\vec{s}, d) = \sum_{d^* \in \mathbb{Q}} \sum_{k>0} \frac{c_{ij}^{(d^*,k)}(\vec{s})}{(d-d^*)^k} + \sum_{k \geq 0} b_{ij}^{(k)}(\vec{s})\, d^k\,. \tag{5.6}$$

In order to find all d-independent relations among a given set of integrals $\mathcal{I}_i$ with $i = 1, \ldots, N$, we can start by writing an ansatz relation

$$\sum_{i=1}^{N} C_i(\vec{s})\, \mathcal{I}_i = 0\,. \tag{5.7}$$

and plug in the reduction identities eqs. (5.5) and (5.6)

$$\sum_{i=1}^{N} \sum_j \sum_{d^* \in \mathbb{Q}} \sum_{k>0} \left(\frac{c_{ij}^{(d^*,k)}(\vec{s})}{(d-d^*)^k} + \sum_{k \geq 0} b_{ij}^{(k)}(\vec{s})\, d^k \right) C_i(\vec{s})\, \mathcal{M}_j^{(d)} = 0\,. \tag{5.8}$$

[3]We are making the assumption that such a basis exists for the integrals appearing in amplitudes we are interested in.

Because all coefficients C_i are independent of d and the coefficient of each master integral $\mathcal{M}_j^{(d)}$ must vanish independently we find the equations

$$\begin{cases} \sum_{i=1}^{N} c_{ij}^{(d^*,k)}(\vec{s})\, C_i(\vec{s}) & = 0\,, \\ \sum_{i=1}^{N} b_{ij}^{(k)}(\vec{s})\, C_i(\vec{s}) & = 0\,. \end{cases} \tag{5.9}$$

The system of equations above is typically under-constrained: one can express all C_i in terms of subset, which we denote by $\overline{C}_j$, but not completely solve the system. We can express this as

$$C_i = \sum_{j=1}^{\overline{N}} M_{ij}^{C} \overline{C}_j\,, \tag{5.10}$$

with $\overline{N} < N$. Plugging eq. (5.10) into eq. (5.7) we find the d-independent relations

$$\sum_{i=1}^{N} M_{ij}^{C} \overline{C}_j\, \mathcal{I}_i = 0\,, \qquad j = 1, \ldots, \overline{N}\,. \tag{5.11}$$

We can then proceed to find the solution of eq. (5.11) in terms of a (larger) set of master integrals $\mathcal{M}_j^{(4)}$:

$$\mathcal{I}_i = \sum_j C'_{ij}(\vec{s})\, \mathcal{M}_j^{(4)}\,. \tag{5.12}$$

Let us now make two comments.

First, the procedure described above allows one to find all d-independent relations among Feynman integrals, but relies on the full IBP reduction. Because reduction identities are very often a bottleneck for state-of-the-art computations, it might be desirable to find an alternative way of obtaining the relations (5.12).

Second, the set of master integrals $\mathcal{M}_j^{(4)}$ is usually not finite. As the rank of integrals considered is increased, the number of master integrals grows accordingly, as it happens in the context of one-loop integrand reduction. Though this might seem problematic at first, the rank of Feynman integrals appearing in scattering amplitudes is always bounded by renormalisability which automatically forbids the appearance of an infinite number of master integrals.

5.3 IR-finite Feynman Integrals

The problem of classifying all finite integrals for a given graph can be solved by finding all numerators $\mathcal{N}$ that make the integral (2.43) finite. Our goal is to identify the general form of $\mathcal{N}$. As discussed in section 2.3, we will focus on numerators which are invariant under the full d-dimensional Lorentz group. In particular, following the tensor decomposition method of section 2.1.2, we can simply consider polynomials of scalar products of internal end external momenta: $\ell_i \cdot p_j$ and $\ell_i \cdot \ell_j$.

This allows us to write any numerator in the form

$$\mathcal{N}(\ell_i) = \sum_{\vec{r}} c_{\vec{r}} \prod_a t_a^{r_a} \,, \tag{5.13}$$

where the t_a belong to the list of allowed scalar products described above

$$t_a \in \{\ell_i \cdot p_j\} \cup \{\ell_i \cdot \ell_j\} \,, \tag{5.14}$$

and $\vec{r}$ are vectors of non-negative integer numbers representing the powers of each monomial. The coefficients c are rational functions of the kinematic invariants. In this chapter, we will use the notation $p_{i\ldots j} \equiv p_i + \cdots + p_j$, and use as kinematic invariants the Mandelstam variables $s_{i\ldots j} = p_{i\ldots j}^2$. Though the methods described are applicable to Feynman integrals involving internal and external masses, here we will focus on purely massless cases.

In a slight abuse of language, we will refer to the total degree of a term in $\mathcal{N}$ in the loop momenta as *rank*; the rank of a numerator is the maximum rank of any of its terms.

The numerator representation given by eqs. (5.13) and (5.14) is not unique. For our purposes, it will be useful to consider an alternative representation built using a van Neerven–Vermaseren basis, which we define below. We first define the generalized Gram determinant of two sets of R vectors in d dimensions

$$\begin{aligned} G\begin{pmatrix} p_1 & \cdots & p_R \\ q_1 & \cdots & q_R \end{pmatrix} &\equiv \det(2p_i \cdot q_j) \,, \\ G\begin{pmatrix} p_1 & \cdots & p_R \end{pmatrix} &\equiv G\begin{pmatrix} p_1 & \cdots & p_R \\ p_1 & \ldots & p_R \end{pmatrix} \,. \end{aligned} \tag{5.15}$$

We define a Gram with a free index

$$G\begin{pmatrix} p_1 & \cdots \mu \cdots & p_R \\ q_1 & \dots & q_R \end{pmatrix} \equiv \frac{\partial}{\partial w_\mu} G\begin{pmatrix} p_1 & \cdots w \cdots & p_R \\ q_1 & \dots & q_R \end{pmatrix} . \tag{5.16}$$

Next, suppose that the space of external momenta for an n-point process is spanned by a basis $p_1, \ldots, p_R$, where $R = \min(n-1, 4)$ in four dimensions. The well-known van Neerven–Vermaseren basis can be defined as

$$v_i^\mu \equiv \frac{G\begin{pmatrix} p_1 & \dots & \mu & \dots & p_R \\ p_1 & \dots & p_i & \dots & p_R \end{pmatrix}}{G\left(p_1 \; \dots \; p_R\right)} , \tag{5.17}$$

which has the important property

$$v_i \cdot p_j = \delta_{ij} \quad \text{for } 1 \leq j \leq R , \tag{5.18}$$

and allows us to decompose any external momentum w^μ as

$$w^\mu = \sum_{j=1}^{R} (v_j \cdot w)\, p_j^\mu + \hat{w}^\mu , \tag{5.19}$$

with $p_i \cdot \hat{w} = 0$ for $i = 1, \ldots, R$. The remainder $\hat{w}$ satisfies $\hat{w}^2 \leq 0$. In the rest of this chapter we will reserve the "hat" symbol for out-of-plane components of momenta.

We also introduce $\hat{\ell}_i$, the out-of-plane part of the loop momentum ℓ_i orthogonal to all external momenta p_j. When considering an n-point process with $n > 4$, this part is strictly ϵ-dimensional. Using eq. (5.19) we can then write the scalar products in eq. (5.14) as linear combinations of those in the set

$$t_a \in \{\ell_i \cdot v_j\} \cup \{\hat{\ell}_i \cdot \hat{\ell}_j\} , \tag{5.20}$$

which span the same space as the one generated by eq. (5.14), but greatly simplify the identification of IR-finite numerators. This alternate basis will allow us to generalize our analysis more easily than the standard basis in eq. (5.14). It is convenient to define the notation

$$\nu_{ij} \equiv \hat{\ell}_i \cdot \hat{\ell}_j = \frac{G\begin{pmatrix} l_i & p_1 & \dots & p_R \\ l_j & p_1 & \dots & p_R \end{pmatrix}}{G\left(p_1 \; \dots \; p_R\right)} . \tag{5.21}$$

Conveniently, all definitions above can be continued to d continuous space-time dimensions, whenever necessary.

5.3.1 Ideals of IR-finite Integrals

Suppose we have the set of all IR-finite numerators $\widetilde{\mathcal{W}}$. Multiplying any IR-finite numerator $f \in \widetilde{\mathcal{W}}$ by any polynomial p in the variables of eq. (5.20) yields another IR-finite numerator:

$$pf \in \widetilde{\mathcal{W}}\,. \tag{5.22}$$

This is the defining property of an *ideal*; it implies that there exists a (non-unique) minimal set of polynomials $f_1, f_2, \cdots \in \mathcal{W}$ which generate $\widetilde{\mathcal{W}}$:

$$\widetilde{\mathcal{W}} = \langle f_1, f_2, \dots \rangle\,. \tag{5.23}$$

This means that any IR-finite polynomial can be written as a linear combination of $f_1, f_2, \dots$ with polynomial coefficients, and vice versa, any such combination is IR-finite. Furthermore, polynomial ideals are finitely generated and, as we shall see, only a small number of generators are required to describe IR-finite numerators. This allows us to capture all information on $\widetilde{\mathcal{W}}$ in a very compact form.

Let us now see how to determine the list of generators f_i for any integral topology.

5.3.2 IR Power Counting

In section 2.3.6 we saw how, at least in simple cases, one can solve the Landau equations eq. (2.78) to find regions of loop-momentum space where Feynman integrals might develop IR singularities.

Solutions of the Landau equations turn out to impose two types of constraints on the loop momenta: *soft* constraints take the form $q_e(\ell, p) = 0$, where $q_e(\ell, p)$ is the momentum of a massless line, while *collinear* constraints require $q_e(\ell, p) = xp_i$, where p_i is an external massless momentum, and the proportionality coefficient $x \in (0, 1)$ is the ratio of unconstrained α parameters, such as $\alpha_1/(\alpha_1 + \alpha_2)$.

Following Anastasiou and Sterman [144], one can use the IR power-counting technique of Libby and Sterman [145–147] to determine the behavior of the integral near a

divergent surface described by soft and collinear constraints. Namely, we parametrize the vicinity of the divergent surface by modifying the constraints as follows:

$$\begin{aligned} q_e^\mu(\ell,p) = 0 \qquad &\to \quad q_e^\mu(\ell,p) = \lambda\sigma_e^\mu\,, \\ q_e^\mu(\ell,p) = x_e p_i^\mu \quad &\to \quad q_e^\mu(\ell,p) = x_e p_i^\mu + \lambda\eta_i^\mu + \lambda^{1/2} q_e^{\perp,\mu}\,. \end{aligned} \tag{5.24}$$

Here, σ_e is a unit euclidean-norm vector while η_i and $q_e^\perp$ satisfy

$$q_e^\perp \cdot p_i = \eta_i^2 = q_e^\perp \cdot \eta_i = 0 \quad \text{and} \quad \hat{\eta}_i = 0\,. \tag{5.25}$$

Solving the modified set of constraints for the loop momenta, we obtain a scaling rule of the form $\ell_i = \ell_i(\lambda)$, which can be used to find IR-finite numerators. For every divergent configuration of the loop momenta, we can substitute the scaling rules of eq. (5.24) into the integration measure, which yields[4]

$$\begin{aligned} \text{soft:} \quad & \mathrm{d}^d\ell = \mathrm{d}\Omega_d\, \mathrm{d}\lambda\, \lambda^{d-1} \sim \mathrm{d}\lambda\, \lambda^{d-1}\,, \\ \text{collinear:} \quad & \mathrm{d}^d\ell = \frac{1}{2}\mathrm{d}x_e\, \mathrm{d}{q_e^\perp}^2\, \mathrm{d}\Omega_{d-2}\, (p_i\cdot\eta_i)\, \mathrm{d}\lambda\, \lambda^{d/2-1} \sim \mathrm{d}\lambda\, \lambda^{d/2-1}\,, \end{aligned} \tag{5.26}$$

as well as into the integrand ansatz

$$\frac{\mathcal{N}(\ell_i)}{\mathcal{D}_1^{\nu_1}\cdots\mathcal{D}_E^{\nu_E}} \tag{5.27}$$

with the numerator given by eqs. (5.13) and (5.20). Assuming that the overall scaling in λ of measure and propagators is $\mathrm{d}\lambda\,\lambda^{-\omega_{IR}}$ with $\omega_{IR} \geq 1$, we Taylor-expand the numerator in λ and retain only powers leading to divergences

$$\mathcal{N}(\ell_i) = \sum_{i=0}^{\omega_{IR}} \lambda^i J_i + \mathcal{O}(\lambda^{\omega_{IR}+1})\,. \tag{5.28}$$

The coefficients J_i of divergent powers of λ are in general polynomials in the quantities

$$\begin{aligned} &\ell_i\cdot v_j,\ \ \nu_{ij},\ \ \hat{\ell}_i\cdot\hat{\sigma}_e,\ \ \hat{\ell}_i\cdot\hat{q}_j^\perp,\ \ v_i\cdot q_j^\perp,\ \ v_i\cdot\eta_j, \\ &v_i\cdot\sigma_e,\ \ \hat{\sigma}_e\cdot\hat{q}_j^\perp,\ \ \hat{q}_i^\perp\cdot\hat{q}_j^\perp,\ \ \hat{\sigma}_{e_1}\cdot\hat{\sigma}_{e_2},\ \ x_e, \end{aligned} \tag{5.29}$$

with coefficients depending on the ansatz parameters $c_{\vec{r}}$, and ℓ_i being the unconstrained loop momenta. We remind the reader that the "hat" notation was defined

[4]We denote the solid angle measure by $\mathrm{d}\Omega_d$.

above in eq. (5.19). The set of monomials in eq. (5.29) is determined by substituting the modified constraints of eq. (5.24) into the ansatze of eqs. (5.13) and (5.20).

However, not all monomials in eq. (5.29) are independent. We can find relations by applying the decomposition of eq. (5.19) to each of the vectors appearing in eq. (5.25). We find

$$\sum_{j=1}^{R}(p_i\cdot p_j)\, v_j\cdot q_e^{\perp} \;=\; \sum_{j,h=1}^{R}(p_j\cdot p_h)\, v_j\cdot\eta_i\; v_h\cdot\eta_i \;=\; \sum_{j,h=1}^{R}(p_j\cdot p_h)\, v_j\cdot q_e^{\perp}\; v_h\cdot\eta_i \;=0\,, \quad (5.30)$$

with i labelling a massless external momentum p_i. The first is a relation among degree-1 monomials while the other two are among degree-2 monomials. We take these relations into account and require that the coefficient of every independent monomial should vanish. The solution of the associated system of equations leads us to a set of constraints on the ansatz parameters.

The $p_i \cdot p_j$ factors appearing in eq. (5.30) are the only kinematics-dependent objects which enter the system of linear equations induced by the IR finiteness constraints. Moreover, they are only relevant when power-like collinear singularities are present. In practice one can first solve the system of equations which does not involve these $p_i \cdot p_j$ and then solve a much smaller system coming from the sub-leading contributions of the numerator which may possibly depend on the $p_i \cdot p_j$. This greatly simplifies the determination of IR-finite numerators and allows us to compute them for four-point topologies up to four loops on a laptop[5].

Repeating the procedure above for all IR-divergent surfaces, we find the most general numerator consistent with IR finiteness for a given ansatz. Denoting the space of IR-finite numerators by $\mathcal{W}$, any element $f \in \mathcal{W}$ can then be written in the form,

$$f(\ell) = \sum_i g_i\, \mathcal{N}_i(\ell)\,, \quad (5.31)$$

where the $\mathcal{N}_i$ are polynomials in the independent monomials in eq. (5.20) and the g_i are unconstrained coefficients independent of the loop momenta.

To guarantee IR finiteness, following ref. [144], one must check not only the divergent surfaces found from the Landau analysis, but also sub-surfaces. The latter

[5]In practice when the problem involves large systems of (linear) equations one can use for instance `FiniteFlow` [89] to obtain a solution efficiently.

do not always show up as separate solutions of the Landau equations. In particular, a solution with a soft constraint may be a special case of a solution with a collinear constraint when the proportionality coefficient x_e reaches its boundary value of 0 or 1. To include the sub-surfaces we also consider each solution of the Landau equations where x_e have been set to 0 or 1 in all possible combinations. This is necessary only when the degree of divergence of a subsurface is greater than that of any of the parent surfaces. An example of this would be a set of surfaces associated to logarithmic divergences intersecting on a subsurface which leads to a power-like divergence, as in the case of the massless non-planar double box, see section 5.4.3.

In order to determine the generators f_i of IR-finite integrals one can compute the reduced Gröbner basis of the ideal generated by all the $\mathcal{N}_i$ of eq. (5.31). Because the ideal of IR-finite integrals is finitely generated, one can perform the procedure above using a truncated ansatz, by retaining only terms in eq. (5.13) below a certain maximum rank r_{max}. In practice we observe that r_{max} is usually quite small. In fact, r_{max} often turns out to be below the degree of UV-convergence of the integral topology, yielding a set of fully UV-finite generators. Inspired by this, in the following we use UV-convergence of the numerator as a criterion for the truncation of the ansatz.

5.3.3 Example: Massless Box

To illustrate the procedure described in the previous sections, let us consider the one-loop massless box integral, depicted in fig. 5.1, as a simple example. We define the momenta,

$$q_1 = \ell, \quad q_2 = \ell - p_1, \quad q_3 = \ell - p_{12}, \quad q_4 = \ell - p_{123}\,. \tag{5.32}$$

We start by writing down the most general ansatz for a UV-finite numerator as described in section 2.3.6. Superficial convergence imposes a maximum degree

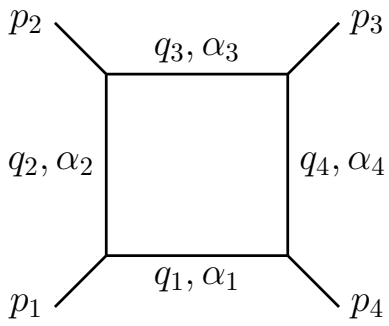

Figure 5.1: The massless one-loop box graph.

$r_{\max} = 3$. As there are no sub-integrations to consider the ansatz reads,

$$\begin{aligned}\mathcal{N}(\ell) = c_0 &+ c_1\,\ell\cdot v_1 + c_2\,\ell\cdot v_2 + c_3\,\ell\cdot v_3 + c_4\,\hat{\ell}^2 + c_5\,(\ell\cdot v_1)^2 + c_6\,\ell\cdot v_1\,\ell\cdot v_2 \\ &+ c_7\,(\ell\cdot v_2)^2 + c_8\,\ell\cdot v_1\,\ell\cdot v_3 + c_9\,\ell\cdot v_2\,\ell\cdot v_3 + c_{10}\,(\ell\cdot v_3)^2 + c_{11}\,\hat{\ell}^2\,\ell\cdot v_1 \\ &+ c_{12}\,\hat{\ell}^2\,\ell\cdot v_2 + c_{13}\,\hat{\ell}^2\,\ell\cdot v_3 + c_{14}\,(\ell\cdot v_1)^3 + c_{15}\,(\ell\cdot v_1)^2\,\ell\cdot v_2 \\ &+ c_{16}\,\ell\cdot v_1\,(\ell\cdot v_2)^2 + c_{17}\,(\ell\cdot v_2)^3 + c_{18}\,(\ell\cdot v_1)^2\,\ell\cdot v_3 + c_{19}\,\ell\cdot v_1\,\ell\cdot v_2\,\ell\cdot v_3 \\ &+ c_{20}\,(\ell\cdot v_2)^2\,\ell\cdot v_3 + c_{21}\,\ell\cdot v_1\,(\ell\cdot v_3)^2 + c_{22}\,\ell\cdot v_2\,(\ell\cdot v_3)^2 + c_{23}\,(\ell\cdot v_3)^3\,.\end{aligned} \tag{5.33}$$

Moving to the IR analysis, we start by computing the auxiliary quantities (see eq. (2.51)),

$$\begin{aligned}A_{11} &= \alpha_1 + \alpha_2 + \alpha_3 + \alpha_4\,, \\ B_1^\mu &= (\alpha_2 + \alpha_3 + \alpha_4)\,p_1^\mu + (\alpha_3 + \alpha_4)\,p_2^\mu + \alpha_4\,p_3^\mu\,,\end{aligned} \tag{5.34}$$

so that the Symanzik polynomials for this diagram are,

$$\mathcal{U} = \alpha_1 + \alpha_2 + \alpha_3 + \alpha_4\,, \qquad \mathcal{F} = s\,\alpha_1\alpha_3 + t\,\alpha_2\alpha_4\,. \tag{5.35}$$

Solving $\mathcal{F} = 0$ monomial by monomial, and then using eq. (2.79) together with eq. (5.34), we obtain four solutions corresponding to divergent surfaces of collinear type. Intersecting these surfaces, or equivalently setting the proportionality coefficients to 0 or 1, we find four soft sub-surfaces. We list the results in table 5.1.

To each of the singular configurations we associate a modified constraint $\ell = \ell(\lambda)$ as decribed in eq. (5.24) and substitute it into the momentum-space representation of the integral,

$$\mathrm{Box}[\mathcal{N}(\ell)] = \int \mathrm{d}^d\ell\,\frac{\mathcal{N}(\ell)}{\mathcal{D}_1\,\mathcal{D}_2\,\mathcal{D}_3\,\mathcal{D}_4}\,. \tag{5.36}$$

Table 5.1: Solutions of the Landau equations for the 1-loop box and the corresponding IR divergent surfaces and sub-surfaces. Teal dotted lines indicate collinear sub-diagrams while red dashed lines represent soft propagators.

surface	solution of $\mathcal{F}=0$	momentum constraint	subsurface	momentum constraint
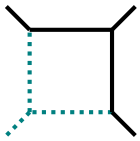 (C_1)	$\alpha_3=\alpha_4=0$	$q_1=\frac{\alpha_2}{\alpha_1+\alpha_2}p_1$	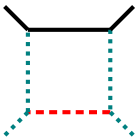 $(S_1)=(C_4)\cap(C_1)$	$q_1=0$
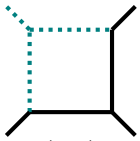 (C_2)	$\alpha_4=\alpha_1=0$	$q_2=\frac{\alpha_3}{\alpha_2+\alpha_3}p_2$	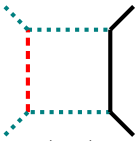 $(S_2)=(C_1)\cap(C_2)$	$q_2=0$
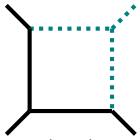 (C_3)	$\alpha_1=\alpha_2=0$	$q_3=\frac{\alpha_4}{\alpha_3+\alpha_4}p_3$	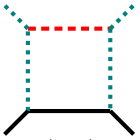 $(S_3)=(C_2)\cap(C_3)$	$q_3=0$
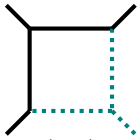 (C_4)	$\alpha_2=\alpha_3=0$	$q_4=\frac{\alpha_1}{\alpha_4+\alpha_1}p_4$	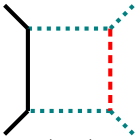 $(S_4)=(C_3)\cap(C_4)$	$q_4=0$

Using the integration-measure scalings (5.26) together with the scaling of the propagators $\mathcal{D}_e=q_e^2+i\varepsilon$ we find that Box[1] behaves as $\mathrm{d}\lambda\ \lambda^{-1+\mathcal{O}(\epsilon)}$ near $d=4$ for all the soft and collinear configurations of table 5.1. Because of the logarithmic nature of these singularities we need to expand the numerator only to $\mathcal{O}(\lambda^0)$ to obtain singular contributions to the integral. To this order in λ we find that the monomials $\{\hat{\ell}^2,\ \ell\cdot v_1,\ \ell\cdot v_2,\ \ell\cdot v_3\}$ take the values:

$$\begin{gathered}C_1:\ \{0,x_1,0,0\}\,,\quad C_2:\ \{0,1,x_2,0\}\,,\quad C_3:\ \{0,1,1,x_3\}\,,\quad C_4:\ \{0,x_4,x_4,x_4\}\,,\\ S_1:\ \{0,0,0,0\}\,,\quad S_2:\ \{0,1,0,0\}\,,\quad S_3:\ \{0,1,1,0\}\,,\quad S_4:\ \{0,1,1,1\}\,,\end{gathered}\tag{5.37}$$

where the x_e stand for the collinear-fraction parameters which can be read off from table 5.1 for the different collinear regions.

Let us study these configurations, extracting the corresponding constraints on

the numerator. Substituting the collinear configurations into eq. (5.33) and setting the result to zero for every value of the x_e we find the equations,

$$\begin{aligned}
&C_1 : c_0 \;=\; c_1 \;=\; c_5 \;=\; c_{14} \;=\; 0\,,\\
&C_2 : c_0 + c_1 + c_5 + c_{14} \;=\; c_2 + c_6 + c_{15} \;=\; c_7 + c_{16} \;=\; c_{17} \;=\; 0\,,\\
&C_3 : c_0 + c_1 + c_2 + c_5 + c_6 + c_7 + c_{14} + \cdots + c_{17} \;=\\
&\qquad c_3 + c_8 + c_9 + c_{18} + c_{19} + c_{20} \;=\; c_{10} + c_{21} + c_{22} \;=\; c_{23} \;=\; 0\,,\\
&C_4 : c_0 \;=\; c_1 + c_2 + c_3 \;=\; c_5 + \cdots + c_{10} \;=\; c_{14} + \cdots + c_{23} \;=\; 0\,.
\end{aligned} \tag{5.38}$$

As anticipated these equations do not depend on the external kinematic invariants s_{ij}. Moving on, for each soft region S_i we get the following constraints:

$$\begin{aligned}
&S_1 : c_0 \;=\; 0\,,\\
&S_2 : c_0 + c_1 + c_5 + c_{14} \;=\; 0\,,\\
&S_3 : c_0 + c_1 + c_2 + c_5 + c_6 + c_7 + c_{14} + \cdots + c_{17} \;=\; 0\,,\\
&S_4 : c_0 + \cdots + c_3 + c_5 + \cdots + c_{10} + c_{14} + \cdots + c_{23} \;=\; 0\,.
\end{aligned} \tag{5.39}$$

One can check that these constraints are satisfied automatically if eq. (5.38) holds. This comes as no surprise, because in this case soft subsurfaces have the same degree of divergence as their parent surfaces corresponding to collinear regions (see discussion at the end of section 5.3.2). Therefore, cancellation of collinear divergences is sufficient for IR-finiteness.

The constraints in eqs. (5.38) and (5.39) entirely fix 12 coefficients in the ansatz of eq. (5.33). Therefore, within the space of UV-finite numerators of eq. (5.33), described by 24 independent monomials, the subset of IR-finite integrals has 12 degrees of freedom.

In general, the results of a UV–IR analysis such as the one presented above can be summarized by simply listing the generators of the ideal of IR-finite numerators. A set of generators can be found using standard techniques of computational algebraic geometry, such as Gröbner bases. In the case of the massless one-loop box there are only three rank-two generators: $\hat{\ell}^2$, $(\ell - p_1)\cdot v_1\ \ell\cdot(v_2 - v_3)$ and $\ell\cdot v_3\ \ell\cdot(v_1 - v_2)$. Using them we can write the most general UV- and IR-finite

numerator for the massless one-loop box as,

$$\begin{aligned}\mathcal{N}(\ell) = &[b_1 \,+\, b_2\,\ell\cdot v_1 \,+\, b_3\,\ell\cdot v_2 \,+\, b_4\,\ell\cdot v_3]\;(\ell - p_1)\cdot v_1\;\ell\cdot(v_2 - v_3) \,+\\ &[b_5 \,+\, b_6\,\ell\cdot v_1 \,+\, b_7\,\ell\cdot v_2 \,+\, b_8\,\ell\cdot v_3]\;\ell\cdot v_3\;\ell\cdot(v_1 - v_2) \,+\\ &[b_9 \,+\, b_{10}\,\ell\cdot v_1 \,+\, b_{11}\,\ell\cdot v_2 \,+\, b_{12}\,\ell\cdot v_3]\;\hat{\ell}^2\,,\end{aligned} \tag{5.40}$$

where the b_i are purely functions of the external momenta.

We end our discussion with two comments on eq. (5.40):

1. The generators obtained in the van Neerven–Vermaseren basis of monomials have a straightforward representation in terms of Gram determinants,

$$\begin{aligned}(\ell - p_1)\cdot v_1\;\ell\cdot(v_2 - v_3) &\propto G\begin{pmatrix}\ell - p_1 & 2 & 3\\ 1 & 2 & 3\end{pmatrix} G\begin{pmatrix}\ell & 1 & 4\\ 1 & 2 & 3\end{pmatrix},\\ \ell\cdot v_3\;\ell\cdot(v_1 - v_2) &\propto G\begin{pmatrix}\ell & 1 & 2\\ 1 & 2 & 3\end{pmatrix} G\begin{pmatrix}\ell & 3 & 4\\ 1 & 2 & 3\end{pmatrix},\\ \hat{\ell}^2 &\propto G\begin{pmatrix}\ell & 1 & 2 & 3\end{pmatrix},\end{aligned} \tag{5.41}$$

   where the constants of proportionality depend only on the external momenta (here and in what follows we represent the external momenta p_i inside the Gram determinants with the corresponding labels i);

2. eq. (5.40) is just one possible choice to represent the numerator. For instance, one could swap the $\ell\cdot v_i$ factors inside the brackets in eq. (5.40) for $\ell\cdot p_i$ or rewrite them in terms of inverse propagators where possible. As long as the UV power-counting is satisfied one can choose different representations depending on the context.

5.3.4 Evanescent Integrands

The set of IR-finite integrals contains a noteworthy subset of convergent integrals which are manifestly of $\mathcal{O}(\epsilon)$ while containing no explicit appearances of ϵ (or d). We call these *evanescent* integrals. To find integrands giving rise to evanescent integrals, we start with the set of integrands of IR-finite integrals which are also UV-finite, and impose further restrictions on their coefficients. In particular we can split the numerator of the integrand

$$\mathcal{N} = \mathcal{N}_4 + \mathcal{N}_{d-4}\,, \tag{5.42}$$

where $\mathcal{N}_4 = \mathcal{N}|_{d=4}$, so that $\mathcal{N}_{d-4}$ vanishes exactly in four dimensions for any value of the loop momenta. If the integral $\mathcal{I}[\mathcal{N}]$ is finite then $\mathcal{I}[\mathcal{N}_4]$ is also finite as the procedure described above to determine UV- and IR-finite integrands could in principle be performed purely in four dimensions. Rewriting the equation above as

$$\mathcal{N}_{d-4} = \mathcal{N} - \mathcal{N}_4 \,, \tag{5.43}$$

we see that as $d \to 4$ the right-hand side has to vanish and therefore $\mathcal{N}_{d-4}$ can be at most of $\mathcal{O}(\epsilon)$. To find evanescent integrands we therefore require the integrand to vanish when all loop momenta are four-dimensional, that is $\mathcal{N}_4 = 0$.

For $(n > 4)$-point integrals, setting the $(d-4)$-dimensional components of each loop momentum to zero corresponds to fixing the extra components $\hat{\ell}_i = 0$ so that all ν_{ij} vanish identically. For the numerator to vanish as $d \to 4$ we require a vanishing coefficient for every monomial of the independent scalar products $\ell_i \cdot v_{j=1,\cdots,4}$. The truncated ideal of evanescent numerators is then the intersection of the IR-finite truncated ideal $\mathcal{W}$ with the one generated by the ν_{ij}.

For $(n \leq 4)$-point integrals we need to be more careful: we can still freely set to zero the coefficient of every monomial without a factor of ν_{ij}, as these are linearly independent and do not vanish as $d \to 4$. Conversely $\nu_{ij} \neq 0$ in four space-time dimensions, so evanescence of a term containing one of these factors is not guaranteed. Instead the $\hat{\ell}_i$ become linearly dependent if enough loops are present because they span a $(5-n)$-dimensional space. As a consequence, any Gram determinant with $m \geq 6 - n$ entries of the $\hat{\ell}_i$'s will automatically vanish. For instance, with $n = 4$ we need at least two loops to find an evanescent numerator via the factor

$$G\left(\hat{\ell}_1 \; \hat{\ell}_2\right) . \tag{5.44}$$

This is in accordance with the fact that for the one-loop box no evanescent numerator can be extracted from eq. (5.40). In general, within the space of polynomials defined by eq. (5.13), the ideal of evanescent numerators for $n \leq 4$ is given by the intersection of the IR-finite ideal with the ideal generated by all choices of the Gram determinant

$$G\begin{pmatrix} \hat{\ell}_{i_1} & \dots & \hat{\ell}_{i_{6-n}} \\ \hat{\ell}_{j_1} & \dots & \hat{\ell}_{j_{6-n}} \end{pmatrix} . \tag{5.45}$$

Evanescently-Finite Integrals Integrands can vanish in four dimensions even if they fail the UV-finiteness power-counting criterion, or if they fail to cancel all IR divergences revealed by the Landau equations. In dimensional regularization, these combinations can give rise to *evanescently finite* integrals. These are integrals which are finite, but where the finiteness depends on cancellation of a pole in ϵ (due to a UV or IR divergence) with a factor of ϵ that arises from the evanescence properties of the integrand. Their existence is special to dimensional regularization. We will not study them exhaustively, but provide explicit examples in section 5.4.

5.3.5 Example: Massless Pentagon

The massless pentagon, depicted in fig. 4.3, is the simplest one-loop case where evanescent integrals arise. Let us summarize the results of our procedure applied to the pentagon. We start by writing a UV-compatible ansatz for the numerator, here a rank-five polynomial in the variables

$$\hat{\ell}^2,\ \ell\cdot v_1,\ \ell\cdot v_2,\ \ell\cdot v_3,\ \ell\cdot v_4\,. \tag{5.46}$$

This polynomial has 166 independent monomials whose coefficients are unfixed rational functions of the independent Mandelstam variables, for instance the set $\{s_{12}, s_{23}, s_{34}, s_{45}, s_{51}\}$.

We proceed by listing all IR singularities. The list generalizes that for the box integral (see table 5.1): here we find a total of ten regions (five soft, five collinear). Requiring the numerator to vanish appropriately in each of the IR regions, we obtain a set of 141 IR-finite independent numerators. The ideal needs only six generators:

$$\begin{aligned}&\ell\cdot v_4\,\ell\cdot(v_1-v_2)\,,\quad (\ell-p_1)\cdot v_1\,\ell\cdot(v_2-v_3)\,,\quad \ell\cdot(v_1-v_2)\,\ell\cdot(v_3-v_4)\,,\\ &\ell\cdot(v_2-v_3)\,\ell\cdot v_4\,,\quad \ell\cdot(v_3-v_4)\,(\ell-p_1)\cdot v_1\,,\quad \hat{\ell}^2\,.\end{aligned} \tag{5.47}$$

The same ideal can equivalently be expressed in terms of the closely related set of Gram determinants using relations of the type (5.41). The result is

$$\begin{aligned} &G\begin{pmatrix}\ell\ 1\ 2\ 3\\ \ell\ 3\ 4\ 5\end{pmatrix}, \quad G\begin{pmatrix}\ell-p_1\ 2\ 3\ 4\\ \ell\quad 4\ 5\ 1\end{pmatrix}, \quad G\begin{pmatrix}\ell\ 3\ 4\ 5\\ \ell\ 5\ 1\ 2\end{pmatrix}, \\ &G\begin{pmatrix}\ell\ 4\ 5\ 1\\ \ell\ 1\ 2\ 3\end{pmatrix}, \quad G\begin{pmatrix}\ell\quad 5\ 1\ 2\\ \ell-p_1\ 2\ 3\ 4\end{pmatrix}, \quad G\Big(\ell\ 1\ 2\ 3\ 4\Big)\,. \end{aligned} \tag{5.48}$$

Turning to evanescent integrands, the further requirement that the numerator should vanish when the loop momenta are purely four-dimensional leads us to a subset of 40 evanescent integrals, whose numerators belong to the ideal generated by

$$\hat{\ell}^2 = G\Big(\ell\ 1\ 2\ 3\ 4\Big)/G\Big(1\ 2\ 3\ 4\Big)\,, \tag{5.49}$$

which is consistent with the well-known result,

$$\int d^dl \frac{G\Big(\ell\ 1\ 2\ 3\ 4\Big)}{\mathcal{D}_1\cdots\mathcal{D}_5} \propto (d-4)\times\int d^{d+2}l\frac{G\Big(1\ 2\ 3\ 4\Big)}{\mathcal{D}_1\cdots\mathcal{D}_5} = \mathcal{O}(\epsilon)\,. \tag{5.50}$$

5.4 Examples of Finite Ideals

In this section we present some explicit results. First, we apply our procedure to characterize the IR-finite integrals for the planar double box, and then show how a general conjecture for the all-loop ladder topology can be justified. We then move to consider the non-planar double box and another two-loop four-point graph which we refer to as the beetle graph. Both the non-planar double box and the beetle require dealing with powerlike IR singularities and allow us to illustrate aspects of our procedure.

5.4.1 Planar Double Box

In this section, we apply the procedures of section 2.3.6 to the massless planar double box integral. We parametrize the loop momenta as shown in fig. 5.2(a). All external momenta are outgoing and we label the edges from 1 to 7, so that their momenta read, in order of labels

$$\ell_1, \quad \ell_1-p_1, \quad \ell_1-p_{12}, \quad \ell_2, \quad \ell_2-p_{123}, \quad \ell_2-p_{12}, \quad \ell_1-\ell_2. \tag{5.51}$$

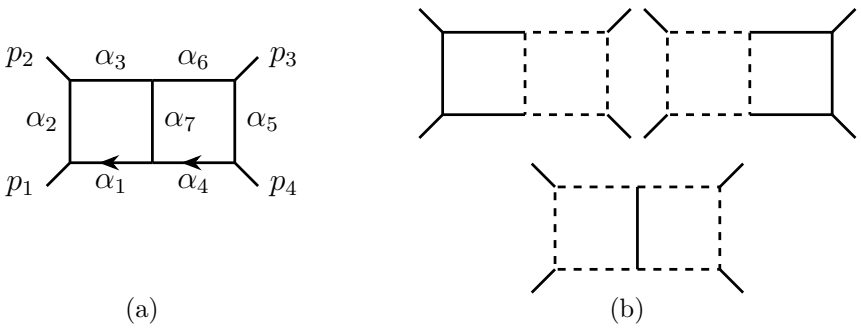

Figure 5.2: The planar double box graph (a) and and its sub-integrations (b).

We start by imposing UV-convergence constraints and then proceed to the IR analysis described in previous sections.

UV divergences

To avoid the overall UV divergence, the maximal allowed numerator rank is 5. Three distinct linear combinations of the loop momenta enter the denominators: ℓ_1, ℓ_2, and $(\ell_1 - \ell_2)$. Holding each one of them fixed in turn yields three possible sub-integrations over the remaining variable ℓ corresponding to the dashed lines in fig. 5.2(b). These give rise to the following constraints on the numerator:

$$\lim_{\rho\to\infty} \begin{cases} \rho^{-4}\,\mathcal{N}\,(\ell_1 = \text{const},\ \ell_2 = \rho\ell) = 0\,, \\ \rho^{-4}\,\mathcal{N}\,(\ell_1 = \rho\ell,\ \ell_2 = \text{const}) = 0\,, \\ \rho^{-8}\,\mathcal{N}\,(\ell_1 = \rho\ell,\ \ell_2 = \text{const} + \rho\ell) = 0\,. \end{cases} \tag{5.52}$$

The first and second constraints simply count the powers of ℓ_2 and ℓ_1 respectively, so the numerator has to be at most cubic in either of the loop momenta. The third constraint is automatically satisfied for numerators of rank five. Hence, a numerator for the double box yields a UV-finite integral if it is at most cubic in ℓ_1, at most cubic in ℓ_2, and has a total rank of at most five.

IR divergences

We start by identifying all reduced diagrams of the double box. We do this by computing the first Symanzik polynomial:

$$\mathcal{U} = (\alpha_1 + \alpha_2 + \alpha_3)(\alpha_4 + \alpha_5 + \alpha_6) + \alpha_7(\alpha_1 + \alpha_2 + \alpha_3 + \alpha_4 + \alpha_5 + \alpha_6)\,, \tag{5.53}$$

Table 5.2: One-loop reduced diagrams of the planar double box and corresponding Symanzik polynomials.

reduced graph	solution of $\mathcal{U} = 0$ (full graph)	Symanzik polynomials (reduced graph)
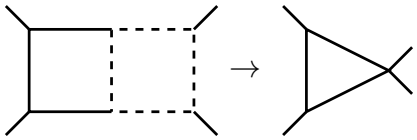	$\alpha_4 = \alpha_5 =$ $\alpha_6 = \alpha_7 = 0$	$\mathcal{U} = \alpha_1 + \alpha_2 + \alpha_3$ $\mathcal{F} = s\,\alpha_1\alpha_3$
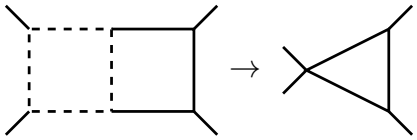	$\alpha_1 = \alpha_2 =$ $\alpha_3 = \alpha_7 = 0$	$\mathcal{U} = \alpha_4 + \alpha_5 + \alpha_6$ $\mathcal{F} = s\,\alpha_4\alpha_6$
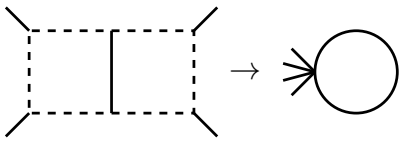	$\alpha_1 = \alpha_2 = \alpha_3 =$ $\alpha_4 = \alpha_5 = \alpha_6 = 0$	$\mathcal{U} = \alpha_7$ $\mathcal{F} = 0$

and setting $\mathcal{U} = 0$ term by term. This yields three solutions which we collect in table 5.2. These solutions describe the reduced diagrams of fig. 5.2(b). Because these diagrams already have only one loop, they represent all reduced diagrams of interest for solving the degenerate-case Landau equations: indeed, solving $\mathcal{U} = 0$ monomial by monomial for the reduced diagrams gives no further solutions with at least one α_i positive.

We now have to solve the parameter-space Landau equations for the original diagram and the three reduced diagrams. We start with the planar double box diagram itself. As the graph is planar, it is natural to express the second Symanzik polynomial $\mathcal{F}$ in terms of the independent Mandelstam invariants of consecutive external momenta, $s = (p_1 + p_2)^2$ and $t = (p_2 + p_3)^2$, so that $\mathcal{F}$ is subtraction-free:

$$\mathcal{F} = s\,[\alpha_1\alpha_3(\alpha_4 + \alpha_5 + \alpha_6) + \alpha_4\alpha_6(\alpha_1 + \alpha_2 + \alpha_3) + \alpha_7(\alpha_1 + \alpha_4)(\alpha_3 + \alpha_6)] + t\,\alpha_2\alpha_5\alpha_7\,. \tag{5.54}$$

We find ten solutions of $\mathcal{F} = 0$ monomial by monomial. They are listed in the first column of table 5.3. The last two solutions should be discarded as they nullify $\mathcal{U}$ as well. As explained in section 2.3.6 they will be considered in the analysis of the sub-integrations. For the remaining eight solutions, we evaluate the corresponding

Table 5.3: Non-degenerate solutions of the Landau equations for the planar double box.

solution of $\mathcal{F}=0$	momentum constraints	
$\alpha_3=\alpha_5=\alpha_6=0$	$\ell_1 \parallel p_1$	$\ell_2 \parallel p_1$
$\alpha_2=\alpha_3=\alpha_6=0$	$\ell_1 \parallel p_4$	$\ell_2 \parallel p_4$
$\alpha_1=\alpha_4=\alpha_5=0$	$(\ell_1-p_{12}) \parallel p_2$	$(\ell_2-p_{12}) \parallel p_2$
$\alpha_1=\alpha_2=\alpha_4=0$	$(\ell_1-p_{12}) \parallel p_3$	$(\ell_2-p_{12}) \parallel p_3$
$\alpha_3=\alpha_6=\alpha_7=0$	$\ell_1 \parallel p_1$	$\ell_2 \parallel p_4$
$\alpha_3=\alpha_4=\alpha_7=0$	$\ell_1 \parallel p_1$	$(\ell_2-p_{12}) \parallel p_3$
$\alpha_1=\alpha_6=\alpha_7=0$	$(\ell_1-p_{12}) \parallel p_2$	$\ell_2 \parallel p_4$
$\alpha_1=\alpha_4=\alpha_7=0$	$(\ell_1-p_{12}) \parallel p_2$	$(\ell_2-p_{12}) \parallel p_3$
$\alpha_1=\alpha_2=\alpha_3=\alpha_7=0$		—
$\alpha_4=\alpha_5=\alpha_6=\alpha_7=0$		—

loop momenta, recognizing the well-known double-collinear IR divergences of the planar double box. For example, the solution on the first line of table 5.3 gives,

$$\ell_1 = \frac{\alpha_2(\alpha_4+\alpha_7)}{(\alpha_1+\alpha_2)(\alpha_4+\alpha_7)+\alpha_4\alpha_7}\,p_1\,, \qquad \ell_2 = \frac{\alpha_2\alpha_7}{(\alpha_1+\alpha_2)(\alpha_4+\alpha_7)+\alpha_4\alpha_7}\,p_1\,, \tag{5.55}$$

describing a double-collinear IR divergence ($\ell_1 \parallel p_1$, $\ell_2 \parallel p_1$).

Computing all intersections of the surfaces associated with the singular configurations in table 5.2, or equivalently setting collinearity coefficients to zero or one, we reproduce the double-soft and soft-collinear IR sub-divergences. For example, intersecting ($\ell_1 \parallel p_1$, $\ell_2 \parallel p_1$) with ($\ell_1 \parallel p_1$, $\ell_2 \parallel p_4$) gives rise to the soft-collinear configuration ($\ell_1 \parallel p_1$, $\ell_2 = 0$) as it sets $\alpha_7 = 0$ in eq. (5.55). Similarly, intersecting ($\ell_1 \parallel p_1$, $\ell_2 \parallel p_1$) with ($\ell_1 \parallel p_4$, $\ell_2 \parallel p_4$) yields the double-soft divergence ($\ell_1 = 0$, $\ell_2 = 0$) setting $\alpha_2 = 0$ in eq. (5.55).

Notice that $\ell_1 = 0$ implies $\alpha_2\alpha_7 = 0$. This forbids the configuration ($\ell_1 = 0$, $\ell_2 \parallel p_1$) corresponding to a disconnected collinear diagram. More generally, the eight solutions of table 5.3 give rise to sub-divergences which are in agreement with the results presented in ref. [144].

Let us now turn to the reduced graphs of table 5.2. We repeat the same procedure: find all solutions of $\mathcal{F}=0$ monomial by monomial, and then compute the corresponding constraints on the loop momenta. The results of the reduced-graph analysis are given in table 5.4. The first two graphs produce the familiar

Table 5.4: Solutions of the Landau equations for the one-loop reduced diagrams of the planar double box.

reduced graph	solutions of $\mathcal{F} = 0$	momentum constraint
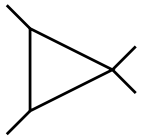	$\alpha_3 = 0$ $\alpha_1 = 0$	$\ell_1 \parallel p_1$ $(\ell_1 - p_{12}) \parallel p_2$
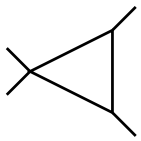	$\alpha_6 = 0$ $\alpha_4 = 0$	$\ell_2 \parallel p_4$ $(\ell_2 - p_{12}) \parallel p_3$
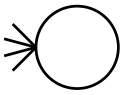	$\alpha_7 \neq 0$	$\ell_1 - \ell_2 = 0$

Table 5.5: Results of the double box numerator analysis.

rank	1	2	3	4	5
# finite integrals	0	2	18	89	247
# finite generators	0	2	4	4	0
# evanescent integrals	0	0	0	1	7
# evanescent generators	0	0	0	1	0

single-collinear divergences, as well as the single-soft divergences from intersections of solutions. The last graph gives rise to an additional single-soft configuration, which is integrable by power-counting even with a trivial numerator, therefore we discard it (if we allowed higher powers of denominators, it could in principle become divergent).

As we now have the full set of singular configurations for the loop momenta, we can proceed by imposing finiteness constraints on the UV-finite numerator ansatz, as described in section 5.3.2. Because all divergences (including sub-divergences) are logarithmic, it suffices to require that the numerator vanishes on all collinear configurations, as in the one-loop box case. In table 5.5 we list the numbers of linearly independent finite and evanescent ($\mathcal{O}(\epsilon)$) integrals up to a given rank, along with the number of the corresponding generators arising at each rank. We construct them in the next section.

Finding a Basis of Generators

Thus far, we have identified the truncated ideals corresponding to IR-finite and evanescent numerators for the double-box integral. We now turn to finding a compact and nice representation for the generators of these ideals. To do so we start by defining[6] the rank-one monomials,

$$\beta_1 = \ell_1 \cdot v_2\,, \quad \beta_2 = (\ell_1 - p_{12}) \cdot v_1\,, \quad \beta_3 = (\ell_2 - p_{12}) \cdot v_2\,, \quad \beta_4 = \ell_2 \cdot (v_2 - v_3)\,,$$
$$\beta_{12} = \ell_1 \cdot v_3\,, \quad \beta_{34} = (\ell_2 - p_{123}) \cdot (v_1 - v_2)\,. \tag{5.56}$$

These turn out to have simple representations in terms of Gram determinants. The β_i variables are rank-one numerators which vanish in the collinear region associated to the p_i; the β_{ij} are rank one which vanish in the collinear regions associated to both p_i and p_j. In addition, $\beta_1\beta_2$ and β_{12} vanish in all soft limits involving ℓ_1; by symmetry, $\beta_3\beta_4$ and β_{34} vanish in those involving ℓ_2.

Thanks to their properties we can use the βs together with the ν_{ij} as building blocks for the basis of the ideal of IR-finite numerators for the double box. We write down the simplest combinations that cancel all divergences, making sure not to repeat any lower rank basis element when writing higher rank ones. Starting at rank two, we find that only the combinations $\beta_{12}\,\beta_{34}$ and ν_{12} are IR-finite. In fact, they correspond to the desired rank-two generators. At rank three we have more options. For instance, we can tame the singularities associated with legs 1 and 2 using two different βs, and the ones of legs 3 and 4 with a single one: $\beta_1\,\beta_2\,\beta_{34}$. By symmetry we can also choose $\beta_{12}\,\beta_3\,\beta_4$. In addition, because the $\hat{\ell}_i$ vanish in any IR limit, we can write down two more rank-three generators, $\nu_{11}\,\beta_{34}$ and $\nu_{22}\,\beta_{12}$. Finally, at rank four we have the following options:

1. cancel the divergence on each corner separately using the product $\beta_1\,\beta_2\,\beta_3\,\beta_4$;

2. use β_1 and β_2 to remove the singularities associated with ℓ_1, and ν_{22} to remove those of ℓ_2, using the product $\beta_1\,\beta_2\,\nu_{22}$;

[6]These definitions depend both on the loop-momentum routing and the choice made for momentum conservation ($p_4 = -p_1 - p_2 - p_3$ in our case). Any changes will be reflected on the explicit form of the βs.

3. use the flipped version $\beta_3\,\beta_4\,\nu_{11}$;

4. use only the $\hat{\ell}$ components of the loop momenta, with the product $\nu_{11}\,\nu_{22}$.

Together, these options give us all four rank-four generators. Summarizing, we find the double box generators,

$$\begin{aligned}
&\text{rank two :} && \beta_{12}\,\beta_{34}\,, \quad \nu_{12}\,, \\
&\text{rank three :} && \beta_1\,\beta_2\,\beta_{34}\,, \quad \beta_{12}\,\beta_3\,\beta_4\,, \quad \nu_{11}\,\beta_{34}\,, \quad \nu_{22}\,\beta_{12}\,, \\
&\text{rank four :} && \beta_1\,\beta_2\,\beta_3\,\beta_4\,, \quad \nu_{11}\,\beta_3\,\beta_4\,, \quad \nu_{22}\,\beta_1\,\beta_2\,, \quad \nu_{11}\,\nu_{22}\,.
\end{aligned} \tag{5.57}$$

Using computational algebraic geometry, we have checked that this set of generators is non-redundant and indeed generates the entire truncated ideal of IR-finite numerators.

Because we have only three independent external momenta, we can look to Gram determinants built out of the $\hat{\ell}$ components of the available loop momenta to build evanescent generators ($\mathcal{O}(\epsilon)$). At two loops the only possible combination is,

$$G\left(\hat{\ell}_1\;\hat{\ell}_2\right) = \nu_{11}\,\nu_{22} - \nu_{12}^2 \propto G\left(\ell_1\;\ell_2\;p_1\;p_2\;p_3\right)\,. \tag{5.58}$$

This is indeed the only evanescent generator, as can be seen from the counting in table 5.5. The evanescent ideal is then generated by,

$$\nu_{11}\,\nu_{22} - \nu_{12}^2\,. \tag{5.59}$$

Every evanescent numerator is by definition also IR-finite, and this generator can be written in terms of the generators in eq. (5.57). In order to make the subset of evanescent numerators more manifest within the IR-finite ones, we could alternatively choose the rank-four generators for the planar double box to be,

$$\beta_1\,\beta_2\,\beta_3\,\beta_4\,, \quad \nu_{11}\,\beta_3\,\beta_4\,, \quad \nu_{22}\,\beta_1\,\beta_2\,, \quad \nu_{11}\,\nu_{22} - \nu_{12}^2\,. \tag{5.60}$$

Beyond evanescence, we can also form combinations of IR-finite integrands that for symmetry reasons give rise to identically vanishing integrals (*i.e.* to all orders in ϵ). We will not discuss these any further. We also leave the question of

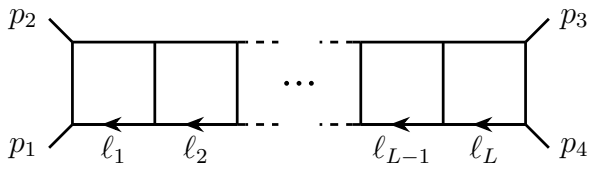

Figure 5.3: All-loop ladder integral.

combining local finiteness with integration-by-parts reduction to future investigation.

We can obtain examples of evanescently-finite integrands for the planar double box within the evanescent ideal by selecting UV-divergent numerators such as $(\nu_{11}\,\nu_{22} - \nu_{12}^2)\,\ell_1\cdot\ell_2$ or $(\nu_{11}\,\nu_{22} - \nu_{12}^2)\,\ell_1\cdot p_1\,\ell_2\cdot p_2$.

5.4.2 Ladder Integrals: an All-Loops Conjecture

Assuming that all integrals with ladder topologies have singularities that are at worst logarithmic in the IR (as is plausible), the reasoning in the previous section can be extended directly to all loop orders. In order to do so, we generalize eq. (5.56),

$$\begin{gathered}\beta_1 = \ell_1\cdot v_2\,, \quad \beta_2 = (\ell_1 - p_{12})\cdot v_1\,, \quad \beta_3 = (\ell_L - p_{12})\cdot v_2\,, \quad \beta_4 = \ell_L\cdot(v_2 - v_3)\,,\\ \beta_{12} = \ell_1\cdot v_3\,, \quad \beta_{34} = (\ell_L - p_{123})\cdot(v_1 - v_2)\,.\end{gathered} \tag{5.61}$$

Using these variables and defining the L-loop momenta as in fig. 5.3, our conjecture for the generators of the truncated ideal of IR-finite numerators takes the remarkably simple form,

$$\begin{aligned}&\text{rank two :} && \beta_{12}\,\beta_{34}\,, \quad \nu_{1,L}\,,\\ &\text{rank three :} && \beta_1\,\beta_2\,\beta_{34}\,, \quad \beta_{12}\,\beta_3\,\beta_4\,, \quad \nu_{1,i\neq L}\,\beta_{34}\,, \quad \nu_{L,i\neq 1}\,\beta_{12}\,,\\ &\text{rank four :} && \beta_1\,\beta_2\,\beta_3\,\beta_4\,, \quad \nu_{1,i\neq L}\,\beta_3\,\beta_4\,, \quad \nu_{L,i\neq 1}\,\beta_1\,\beta_2\,, \quad \nu_{1,i\neq L}\nu_{L,j\neq 1}\,.\end{aligned} \tag{5.62}$$

We thus have two conjectured generators at rank two, $2L$ generators at rank three, L^2 generators at rank four, with no additional generators beyond rank four. The larger number of generators is simply due to having more loop momenta at our disposal to build some of the ν_{ij} combinations. The role of the scattering-plane variables β is unchanged.

As to evanescent generators, we see that (see section 5.3.4) every Gram determinant involving at least two different $\hat{\ell}_i$ will automatically vanish as $D \to 4$. It follows that the truncated ideal of evanescent numerators is the intersection of the IR-finite one of eq. (5.62) with the one generated by the two-by-two Gram determinants,

$$G\begin{pmatrix}\hat{\ell}_{i_1} & \hat{\ell}_{i_2}\\ \hat{\ell}_{j_1} & \hat{\ell}_{j_2}\end{pmatrix} = \nu_{i_1 j_1}\,\nu_{i_2 j_2} - \nu_{i_1 j_2}\,\nu_{i_2 j_1}\,. \tag{5.63}$$

We can write out the intersection explicitly, finding that it is generated by the set,

$$\begin{aligned}
&\text{rank four :} && \nu_{1i}\,\nu_{Lj} - \nu_{1j}\,\nu_{Li}\,, \quad \nu_{1L}\,\nu_{p_1 h_1} - \nu_{1 h_1}\,\nu_{p_1 L}\,,\\
&\text{rank five :} && (\nu_{1p_1}\,\nu_{p_3 p_2} - \nu_{1p_2}\,\nu_{p_3 p_1})\,\beta_{34}\,, \quad (\nu_{Lh_1}\,\nu_{h_3 h_2} - \nu_{Lh_2}\,\nu_{h_3 h_1})\,\beta_{12}\,,\\
&\text{rank six :} && (\nu_{1p_1}\,\nu_{p_3 p_2} - \nu_{1p_2}\,\nu_{p_3 p_1})\,\beta_3\,\beta_4\,, \quad (\nu_{Lh_1}\,\nu_{h_3 h_2} - \nu_{Lh_2}\,\nu_{h_3 h_1})\,\beta_1\,\beta_2\,,\\
& && (\nu_{l_1 l_3}\,\nu_{l_2 l_4} - \nu_{l_1 l_4}\,\nu_{l_2 l_3})\beta_{12}\,\beta_{34}\,,\\
&\text{rank seven :} && (\nu_{l_1 l_3}\,\nu_{l_2 l_4} - \nu_{l_1 l_4}\,\nu_{l_2 l_3})\,\beta_{12}\,\beta_3\,\beta_4\,, \quad (\nu_{l_1 l_3}\,\nu_{l_2 l_4} - \nu_{l_1 l_4}\,\nu_{l_2 l_3})\,\beta_1\,\beta_2\,\beta_{34}\,,\\
&\text{rank eight :} && (\nu_{l_1 l_3}\,\nu_{l_2 l_4} - \nu_{l_1 l_4}\,\nu_{l_2 l_3})\,\beta_1\,\beta_2\,\beta_3\,\beta_4\,,
\end{aligned} \tag{5.64}$$

where the indices are defined as,

$$i, j = 1, \ldots, L, \quad p_r = 1, \ldots, L-1, \quad h_r = 2, \ldots, L, \quad l_r = 2, \ldots, L-1\,, \tag{5.65}$$

in order to avoid double-counting of lower-rank generators and are assumed to take values for which the corresponding generator is non-zero, *e.g.* the choice $l_1 = l_2 = l_3 = l_4 = 2$ is forbidden because most generators at ranks six, seven, and eight would vanish identically. The evanescent generators above can be written in terms of the IR-finite generators in eq. (5.62). From eq. (5.64) we find the following numbers of generators at each rank:

$$\begin{aligned}
&\text{rank four :} && (3L^2 - 9L + 8)/2\,,\\
&\text{rank five :} && (L-2)(L^2 - 4L + 5)\,,\\
&\text{rank six :} && (L-2)(L^3 - 9L + 16)/8\,,\\
&\text{rank seven :} && (L-2)(L-3)(L^2 - 5L + 8)/4\,,\\
&\text{rank eight :} && (L-2)(L-3)(L^2 - 5L + 8)/8\,.
\end{aligned} \tag{5.66}$$

We deduce that the rank-four generators are present for any number of loops, while those at ranks five and six require a minimum of three loops, and those at ranks

seven and eight first appear at four loops. All IR-finite and evanescent generators in eqs. (5.62) and (5.64) are UV finite.

We have verified the validity of this conjecture at two, three and four loops by explicit computation of the ideals.

5.4.3 Non-Planar Double Box

We next consider the non-planar double box integral. There are two important differences between the planar and non-planar double box integrals. In particular the non-planar one:

1. lacks a subtraction-free form (see section 2.3.6) for the $\mathcal{F}$ polynomial;
2. has power-like soft divergences: regions of the loop integration where the integrand scales as $\mathrm{d}\lambda\, \lambda^{-\alpha}$ with $\alpha > 1$.

For these reasons we believe the non-planar box to be an instructive example. We repeat the procedure outlined in the previous section, highlighting the role of power-like divergences along the way.

The loop momenta are parametrized as shown in fig. 5.4(a) with all external momenta outgoing and we label the edges from 1 to 7 so that their momenta read, in increasing order of labels,

$$\ell_1, \quad \ell_1 - p_1, \quad \ell_1 - p_{12}, \quad \ell_2, \quad \ell_2 - p_{123}, \quad \ell_2 - \ell_1 - p_3, \quad \ell_1 - \ell_2. \tag{5.67}$$

As before, we start by imposing UV-convergence constraints and proceed to the IR analysis afterwards.

UV divergences

The maximal allowed numerator rank is five and there are three distinct sub-integrations corresponding to the dashed lines in fig. 5.4(b). These give rise to the following constraints on the numerator:

$$\lim_{\rho\to\infty} \begin{cases} \rho^{-4}\,\mathcal{N}\left(\ell_1 = \text{const},\ \ell_2 = \rho\ell\right) = 0\,, \\ \rho^{-6}\,\mathcal{N}\left(\ell_1 = \rho\ell,\ \ell_2 = \text{const}\right) = 0\,, \\ \rho^{-6}\,\mathcal{N}\left(\ell_1 = \rho\ell,\ \ell_2 = \text{const} + \rho\ell\right) = 0\,. \end{cases} \tag{5.68}$$

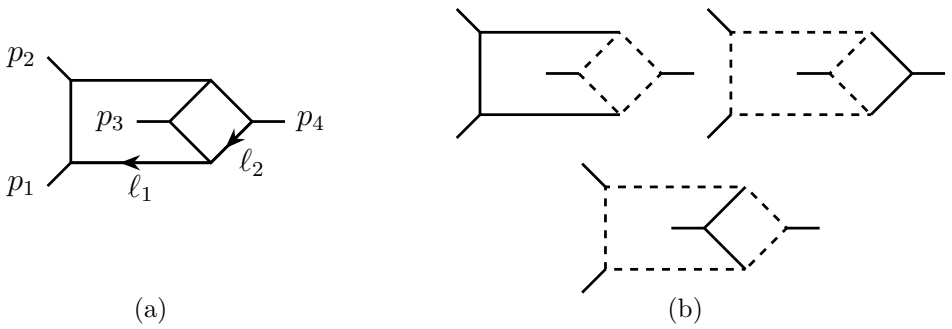

Figure 5.4: The non-planar double box graph (a) and its sub-integrations (b).

Overall, a UV-finite numerator for the non-planar double box should be at most of rank five, with maximum degrees of five and three in ℓ_1 and ℓ_2 respectively.

IR divergences

As before, the relevant reduced diagrams correspond to the zeros of the first Symanzik polynomial:

$$\mathcal{U} = (\alpha_1 + \alpha_2 + \alpha_3)(\alpha_4 + \alpha_5 + \alpha_6 + \alpha_7) + (\alpha_4 + \alpha_5)(\alpha_6 + \alpha_7), \tag{5.69}$$

and reproduce the sub-integrations of fig. 5.4(b). To solve the parameter-space Landau equations for the full diagram, we compute the second Symanzik polynomial:

$$\mathcal{F} = s\left[\alpha_1\alpha_3(\alpha_4 + \alpha_5 + \alpha_6 + \alpha_7) + \alpha_1\alpha_5\alpha_6 + \alpha_3\alpha_4\alpha_7\right] + t\,\alpha_2\alpha_5\alpha_7 - (s+t)\,\alpha_2\alpha_4\alpha_6\,. \tag{5.70}$$

Unlike the planar case, $\mathcal{F}$ is no longer a sum of positive terms for appropriate signs of the Mandelstam invariants. Therefore, we consider instead the most general linear combination of the Landau equations (2.82),

$$\begin{aligned}\sum_{e=1}^{E} w_e\alpha_e\frac{\partial}{\partial\alpha_e}\mathcal{F} = {} & s\,(w_1+w_3+w_4)\,\alpha_1\alpha_3\alpha_4 + s\,(w_1+w_3+w_5)\,\alpha_1\alpha_3\alpha_5 \\ & + s\,(w_1+w_3+w_6)\,\alpha_1\alpha_3\alpha_6 + s\,(w_1+w_3+w_7)\,\alpha_1\alpha_3\alpha_7 \\ & + s\,(w_1+w_5+w_6)\,\alpha_1\alpha_5\alpha_6 + s\,(w_3+w_4+w_7)\,\alpha_3\alpha_4\alpha_7 \\ & + t\,(w_2+w_5+w_7)\,\alpha_2\alpha_5\alpha_7 - (s+t)\,(w_2+w_4+w_6)\,\alpha_2\alpha_4\alpha_6\,,\end{aligned} \tag{5.71}$$

Table 5.6: Results of the non-planar double box numerator analysis.

rank	1	2	3	4	5
# finite integrals	0	0	9	65	230
# finite generators	0	0	9	8	0
# evanescent integrals	0	0	0	1	7
# evanescent generators	0	0	0	1	0

and require that each coefficient is strictly positive when $s, t > 0$. It is straightforward to check that the resulting system of linear inequalities is feasible: one possible solution is,

$$\vec{w} = (0, -1, 1, 0, 2, 0, 0)\,. \tag{5.72}$$

This means that a subtraction-free linear combination of the Landau equations exists, therefore we can find their solutions simply by setting $\mathcal{F}$ to zero term by term as usual; in other words, no divergences due to cancellations in $\mathcal{F}$ can occur (see also ref. [148, Appendix A]). For the reduced diagrams, $\mathcal{F}$ is subtraction-free itself, so their analysis does not pose any difficulty.

Solutions of the Landau equations correspond to double- and single-collinear IR divergences, all of which are logarithmic. However, if we take intersections of these solutions we find additional sub-divergences, two of which are power-like. These are the double-soft configurations $(\ell_1 = 0, \ell_2 = 0)$ and $(\ell_1 = p_1 + p_2, \ell_2 = -p_4)$, in accordance with ref. [144]. Therefore, unlike the planar case, cancellation of collinear configurations alone is insufficient. In principle, one has to expand the UV-finite ansatz to a certain sub-leading order in the vicinity of the power-like configurations, and require that these divergent contributions vanish. In practice however, we find that these additional constraints are satisfied automatically as long as all collinear divergences are canceled. We report the results of our analysis in table 5.6.

Finding a Basis of Generators

By analogy with the planar double box we can define a set of variables,

$$\begin{gathered}\beta_1 = \ell_1{\cdot}v_2\,, \quad \beta_2 = (\ell_1 - p_{12}){\cdot}v_1\,, \quad \beta_3 = (\ell_1 - \ell_2){\cdot}v_1\,, \quad \beta_3' = (\ell_1 - \ell_2){\cdot}v_2\,, \\ \beta_4 = \ell_2{\cdot}(v_1 - v_2)\,, \quad \beta_4' = \ell_2{\cdot}(v_2 - v_3)\,, \quad \beta_{12} = \ell_1{\cdot}v_3\,,\end{gathered} \tag{5.73}$$

which vanish on appropriate collinear and soft limits. In particular each β_S (and β'_S) vanishes on the collinear configurations involving the particles in S, and also vanishes on the soft limits involving the combinations of loop momenta in its definition. In terms of these quantities we find the generators

$$\begin{aligned}
&\text{rank three :} \quad \beta_{12}\,\beta_3\,\beta_4\,, \quad \beta_{12}\,\beta'_3\,\beta_4\,, \quad \beta_{12}\,\beta_3\,\beta'_4\,, \quad \beta_{12}\,\beta'_3\,\beta'_4\,, \quad \beta_{12}\,(\nu_{12}-\nu_{22})\,,\\
&\qquad\qquad \beta_3\,\nu_{12}\,, \quad \beta'_3\,\nu_{12}\,, \quad \beta_4\,(\nu_{11}-\nu_{12})\,, \quad \beta'_4\,(\nu_{11}-\nu_{12})\,,\\
&\text{rank four :} \quad \beta_1\,\beta_2\,\beta_3\,\beta_4\,, \quad \beta_1\,\beta_2\,\beta'_3\,\beta_4\,, \quad \beta_1\,\beta_2\,\beta_3\,\beta'_4\,, \quad \beta_1\,\beta_2\,\beta'_3\,\beta'_4\,,\\
&\qquad\qquad \beta_1\beta_2\,(\nu_{12}-\nu_{22})\,, \quad \nu_{12}\,(\nu_{11}-\nu_{12})\,, \quad \nu_{12}\,(\nu_{12}-\nu_{22})\,, \quad \nu_{11}\nu_{22}-\nu_{12}^2\,.
\end{aligned} \tag{5.74}$$

Just as for the planar double box, we have only three independent external and two loop momenta, so we expect a single evanascent generator. This is indeed the case: it is $G\left(\hat{\ell}_1\ \hat{\ell}_2\right) = \nu_{11}\,\nu_{22} - \nu_{12}^2$.

5.4.4 Two-Loop Beetle

In this section we briefly treat the "beetle" integral of fig. 5.5(a). We will not show the whole procedure here, but simply provide results for the IR-finite and evanescent truncated ideals.

This integral is of interest to us because it contains power-like double-collinear (see fig. 5.5(b)) and soft-collinear divergences, which did not appear in any of cases treated above. The presence of power-like divergences involving collinear configurations requires us to take into account eq. (5.30) for the first time in this chapter. In practice, as we will see shortly, this introduces a dependence on the Mandelstam variables s_{ij} in the set of generators for the ideal of locally finite numerators. To describe our results, we can define the set of rank-one monomials,

$$\begin{aligned}
&\beta_1 = \ell_1{\cdot}v_2\,, \quad \beta_{12} = \ell_1{\cdot}v_3\,, \quad \gamma_1 = \ell_2{\cdot}v_2\,, \quad \gamma_3 = (\ell_2-p_{12}){\cdot}v_2\,,\\
&\gamma_{12} = \ell_2{\cdot}v_3\,, \quad \gamma_{14} = \ell_2{\cdot}\,(v_2-v_3)\,, \quad \gamma_{34} = \ell_2{\cdot}\,(v_1-v_2)\,, \quad \gamma_{23} = (\ell_2-p_1){\cdot}v_1\,,
\end{aligned} \tag{5.75}$$

so that the β_S (respectively the γ_S) vanish on collinear configurations of ℓ_1 (respectively ℓ_2) involving the external momenta in S. In terms of these variables[7],

[7]The variables in eq. (5.75) are not all linearly independent. We express our results in terms of an overcomplete set for the sake of clarity.

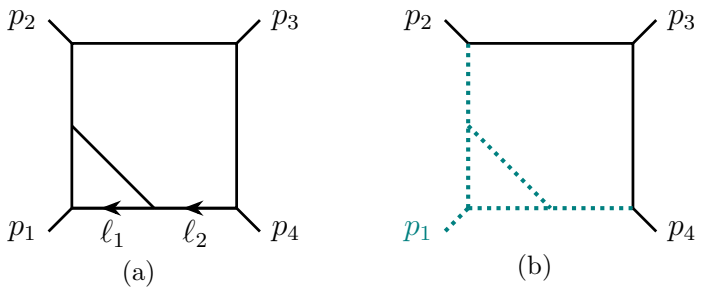

Figure 5.5: The beetle graph (a) and a collinear configuration leading to a power-like divergence (b). In (b) teal dotted edges are collinear to p_1.

we can express the set of generators as follows,

$$\begin{aligned}
\text{rank three}: \quad & \gamma_{12}\,\gamma_{34}\,(s_{12}\beta_1 + s_{13}\beta_{12})\,, \quad \gamma_{14}\,\gamma_{23}\,(s_{12}\beta_1 + s_{13}\beta_{12})\,, \\
& \beta_1\,\nu_{22}\,, \quad \beta_{12}\,\nu_{22}\,, \quad \gamma_1\,\nu_{12}\,, \quad \gamma_{12}\,\nu_{12}\,, \\
\text{rank four}: \quad & \beta_1\,\gamma_{12}\,\gamma_{34}\,(s_{12}\gamma_1 + s_{13}\gamma_{12})\,, \quad \beta_1\,\gamma_{14}\,\gamma_{23}\,(s_{12}\gamma_1 + s_{13}\gamma_{12})\,, \\
& \beta_{12}\,\gamma_{12}^2\,\gamma_{34}\,, \quad \beta_{12}\,\gamma_{12}\,\gamma_{23}\,\gamma_{14}\,, \\
& \beta_1\,\gamma_{23}\,[s_{23}\gamma_1^2 + (\gamma_1 + \gamma_{34})(s_{12}\gamma_1 + s_{13}\gamma_{12})]\,, \quad \nu_{12}\,\nu_{22}\,.
\end{aligned} \tag{5.76}$$

The polynomial $\beta_1 s_{12} + \beta_{12} s_{13}$ and its equivalent with $\beta \to \gamma$ are related to standard scalar products of loop and external momenta,

$$\beta_1 s_{12} + \beta_{12} s_{13} = 2p_1 \cdot \ell_1 \quad \text{and} \quad \gamma_1 s_{12} + \gamma_{12} s_{13} = 2p_1 \cdot \ell_2\,. \tag{5.77}$$

Finally we find that, within the UV power counting, there are no evanescent numerators for the beetle integral.

5.4.5 Two-Loop Four-Gluon Helicity Amplitudes

In this section, we present a simple but concrete application of the concepts and results discussed in previous sections. We focus on the leading-colour amplitudes for two-loop scattering of four gluons in pure Yang–Mills theory. Very compact expressions for the all-plus amplitude have been known for a long time [149] and expressions for all other helicity configurations were first computed in refs. [150] and [151]. Our goal here is not to obtain the most compact results, but rather to give a hint of how organising scattering amplitudes according to their IR structure

can offer a simpler representation. For our example, we make use of the rank-two IR-finite numerators of eq. (5.57),

$$f_1(p_1,p_2,p_3,p_4) = \beta_{12}\beta_{34}\,, \quad f_2(p_1,p_2,p_3,p_4) = \nu_{12}\,, \tag{5.78}$$

to write the bare four-gluon helicity amplitudes in a basis of 13 master integrals as follows,

$$\mathcal{A}^{0\to gggg}(\boldsymbol{\lambda}) = \Bigg[r_1^{\boldsymbol{\lambda}} \; \boxed{} \; [f_1(p_1,p_2,p_3,p_4)] + r_2^{\boldsymbol{\lambda}} \; \boxed{} \; [f_2(p_1,p_2,p_3,p_4)] +$$
$$r_3^{\boldsymbol{\lambda}} \; \boxed{} \; [f_1(p_4,p_1,p_2,p_3)] + r_4^{\boldsymbol{\lambda}} \; \boxed{} \; [f_2(p_4,p_1,p_2,p_3)] +$$
$$r_5^{\boldsymbol{\lambda}} \; \triangleleft \; + r_6^{\boldsymbol{\lambda}} \; \diamond \; + r_7^{\boldsymbol{\lambda}} \; \boxed{} \; + r_8^{\boldsymbol{\lambda}} \; \boxed{} \; + r_9^{\boldsymbol{\lambda}} \; \boxed{} \; +$$
$$r_{10}^{\boldsymbol{\lambda}} \; \bowtie \; + r_{11}^{\boldsymbol{\lambda}} \; \times \; + r_{12}^{\boldsymbol{\lambda}} \; \triangle \; + r_{13}^{\boldsymbol{\lambda}} \; \boxed{} \; \Bigg] \Phi(\boldsymbol{\lambda})\,. \tag{5.79}$$

Here, $\mathcal{A}^{0\to gggg}(\boldsymbol{\lambda})$ is the coefficient of the colour factor $N_c^2\,\mathrm{Tr}[T^{a_1}T^{a_2}T^{a_3}T^{a_4}]$ for the helicity configuration $\boldsymbol{\lambda} = \{\lambda_1,\lambda_2,\lambda_3,\lambda_4\}$ (N_c is the dimension of the Yang–Mills group and a_i is the colour index of the i–th gluon). The coefficients $r_i^{\boldsymbol{\lambda}}$ are rational functions of the space-time dimensions D and of the independent Mandelstam variables s_{12}, s_{23}. Finally, $\Phi(\boldsymbol{\lambda})$ is an overall spinor factor.

The first four integrals in eq. (5.79) are IR-finite, and contain the whole dependence on the double-box topology (the one with the largest number of propagators). The numerators of eq. (5.78) correspond to linear combinations of the chiral numerators presented in ref. [152]. The remaining nine integrals are chosen to match as closely as possible the IR singularities obtained from the Landau equations. Because our analysis is for the moment limited to IR-finite integrals we do not have a systematic way to select IR-divergent integrals. We postpone an investigation of this aspect to future work.

With the choice of master integrals adopted in eq. (5.79), we observe that all rational coefficients $r_i^{\boldsymbol{\lambda}}$ are regular in the limit $\epsilon \to 0$, implying that all divergences are contained in the integrals themselves.

The helicity configurations which vanish at tree-level have an overall factor of ϵ so that, so long as we are interested in the amplitudes only up to $\mathcal{O}(\epsilon^0)$, we can safely drop all IR-finite integrals. We then find,

$$\mathcal{A}^{0\to gggg}(+,+,+,+) = \epsilon\, C(\epsilon) \Bigg[\tilde{r}_5 \; + \tilde{r}_6 \; + \tilde{r}_7 \; + \tilde{r}_8 \; + \tilde{r}_9 \; + \tilde{r}_{10} \; + \tilde{r}_{11} \; + \tilde{r}_{12} \; + \tilde{r}_{13} \; \Bigg] \Phi(+,+,+,+)\,, \tag{5.80}$$

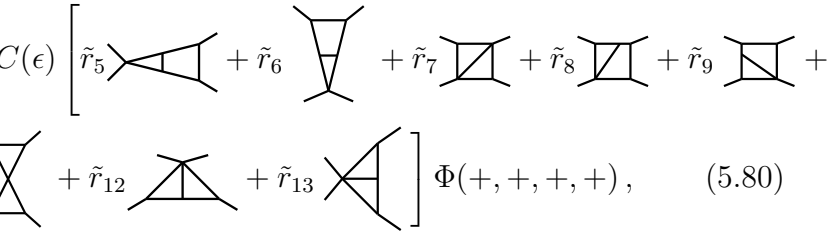

where we have defined the rational coefficients $\tilde{r}_i$ to make the overall factor of ϵ explicit, and where the ϵ-dependent coefficient $C(\epsilon)$ approaches a finite constant as $\epsilon \to 0$. We collect the explicit expressions for the coefficients in appendix C. A similar expression holds for the single-minus amplitude. Our choice of master integrals makes eq. (5.80) free of contributions related to the double box, the most complicated topology for this process.

6
Conclusions and Outlook

The main objective of this thesis was to present the calculation of state-of-the-art scattering amplitudes in massless QCD and emphasise some of the interesting structures appearing in their non-planar sector.

In particular in chapters 1 and 2 we gave a brief introduction and reviewed some of the methods employed in the computation of scattering amplitudes. Most of the methodology discussed is quite general, but here we specifically focused on computations based on the evaluation of Feynman diagrams.

In chapter 3 we described the structure and challenges of three-loop four-point QCD amplitudes for the processes

$$q\bar{q} \to Q\bar{Q}\,, \quad q\bar{q} \to gg\,, \quad gg \to gg$$

as well as all interactions obtained via crossing symmetry. As an outcome of these amplitudes we were able to verify the structure of the quadrupole contribution to the soft anomalous dimension in QCD, an intrinsically non-planar effect. Furthermore, the exact full-colour amplitudes obtained opened the door for the extraction of the three-loop QCD gluon Regge trajectory, an essential element of NNLL BFKL resummation.

In chapter 4 we turned our attention to the two-loop five-gluon amplitudes and addressed the explosion in complexity due to their sub-leading-colour corrections.

These amplitudes, together with the ones of other partonic channels presented in ref. [122] and recomputed independently in refs. [123, 124], provide the full double-virtual correction to the NNLO $pp \to jjj$ cross section. They also provide an opportunity for the direct study of special kinematic limits such as soft and collinear ones as well as the multi-Regge kinematics (MRK). Specifically the MRK limit of these amplitudes would allow the computation of the NNLL correction to the Lipatov vertex [107].

Finally, chapter 5 was devoted to the idea of leveraging knowledge of the IR divergences of gauge theory amplitudes to simplify their integrand representations. As a first step in this direction, we introduced a reduced set of IBP relations which preserve (most of) the IR structure of Feynman integrals. We also addressed the problem of the choice of master integrals with respect to such relations by looking at the space of integrals which are locally-finite, *i.e.* which have no IR divergences and are integrable (up to UV divergences). As a next step, it would be natural to extend these ideas to a comprehensive study of the types of integrals and integral relations needed to faithfully represent at the integral level the UV and IR divergent contributions to scattering amplitudes.

Appendices

A Constants

A.1 Cusp and Collinear Anomalous Dimensions in QCD

In this appendix, we list the perturbative expansions of the cusp anomalous dimension and of the quark and gluon collinear anomalous dimensions,

$$\gamma^{\rm K} = \sum_{n=0} \left(\frac{\alpha_s}{4\pi}\right)^{n+1} \gamma_n^{\rm K}, \qquad \gamma^{g/q} = \sum_{n=0} \left(\frac{\alpha_s}{4\pi}\right)^{n+1} \gamma_n^{q/g}. \tag{A.1}$$

The required expansion coefficients of the cusp anomalous dimension read [70–72]

$$\begin{aligned}
\gamma_0^{\rm K} &= 4\,, \\
\gamma_1^{\rm K} &= \left(\frac{268}{9} - \frac{4\pi^2}{3}\right) C_A - \frac{40}{9}\, n_f\,, \\
\gamma_2^{\rm K} &= C_A^2 \left(\frac{490}{3} - \frac{536\pi^2}{27} + \frac{44\pi^4}{45} + \frac{88}{3}\,\zeta_3\right) + C_A n_f \left(\frac{80\pi^2}{27} - \frac{836}{27} - \frac{112}{3}\,\zeta_3\right) \\
&\quad + C_F n_f \left(32\zeta_3 - \frac{110}{3}\right) - \frac{16}{27}\, n_f^2\,.
\end{aligned} \tag{A.2}$$

The required expansion coefficients of the quark collinear anomalous dimension are [78]

$$\begin{aligned}
\gamma_0^q &= -3C_F\,, \\
\gamma_1^q &= C_F^2 \left(-\frac{3}{2} + 2\pi^2 - 24\zeta_3\right) + C_F C_A \left(-\frac{961}{54} - \frac{11\pi^2}{6} + 26\zeta_3\right) + C_F n_f \left(\frac{65}{27} + \frac{\pi^2}{3}\right),
\end{aligned}$$

$$
\begin{aligned}
\gamma_2^q = {} & C_F^3 \left(-\frac{29}{2} - 3\pi^2 - \frac{8\pi^4}{5} - 68\zeta_3 + \frac{16\pi^2}{3}\,\zeta_3 + 240\zeta_5\right) \\
& + C_F^2 C_A \left(-\frac{151}{4} + \frac{205\pi^2}{9} + \frac{247\pi^4}{135} - \frac{844}{3}\,\zeta_3 - \frac{8\pi^2}{3}\,\zeta_3 - 120\zeta_5\right) \\
& + C_F C_A^2 \left(-\frac{139345}{2916} - \frac{7163\pi^2}{486} - \frac{83\pi^4}{90} + \frac{3526}{9}\,\zeta_3 - \frac{44\pi^2}{9}\,\zeta_3 - 136\zeta_5\right) \\
& + C_F^2 n_f \left(\frac{2953}{54} - \frac{13\pi^2}{9} - \frac{14\pi^4}{27} + \frac{256}{9}\,\zeta_3\right) \\
& + C_F C_A n_f \left(-\frac{8659}{729} + \frac{1297\pi^2}{243} + \frac{11\pi^4}{45} - \frac{964}{27}\,\zeta_3\right) \\
& + C_F n_f^2 \left(\frac{2417}{729} - \frac{10\pi^2}{27} - \frac{8}{27}\,\zeta_3\right)\,,
\end{aligned}
\tag{A.3}
$$

while for the gluon collinear anomalous dimension [79] they read

$$
\begin{aligned}
\gamma_0^g &= -\beta_0\,, \\
\gamma_1^g &= C_A^2 \left(-\frac{692}{27} + \frac{11}{3}\zeta_2 + 2\zeta_3\right) + C_A n_f \left(\frac{128}{27} - \frac{2}{3}\zeta_2\right) + 2C_F n_f\,, \\
\gamma_2^g &= C_A^3 \left(\frac{-97186}{729} + \frac{6109}{81}\zeta_2 + \frac{122}{3}\zeta_3 - \frac{319}{3}\zeta_4 - \frac{40}{3}\zeta_2\zeta_3 \; - 16\zeta_5\right) \\
&\quad + C_A^2 n_f \left(\frac{30715}{1458} - \frac{1198}{81}\zeta_2 + \frac{356}{27}\zeta_3 + \frac{82}{3}\zeta_4\right) - \frac{11}{9} C_F n_f^2 - C_F^2 n_f \\
&\quad + C_A C_F n_f \left(\frac{1217}{27} - 2\zeta_2 - \frac{152}{9}\zeta_3 - 8\zeta_4\right) + C_A n_f^2 \left(-\frac{269}{1458} + \frac{20}{27}\zeta_2 - \frac{56}{27}\zeta_3\right).
\end{aligned}
\tag{A.4}
$$

A.2 Impact Factors for the High-Energy Limit

In this appendix we provide expressions for the QCD quark and gluon impact factors up to two loops and up to the relevant order in ϵ. They read

$$
\begin{aligned}
\mathcal{I}_1^q = {} & \frac{4 - \frac{\zeta_2}{2}}{N_c} + N_c \left(\frac{7\zeta_2}{2} + \frac{13}{18}\right) - \frac{5n_f}{9} \\
& + \epsilon \left[N_c \left(-\frac{\zeta_2}{6} + \frac{10\zeta_3}{3} + \frac{40}{27}\right) + \frac{1}{N_c} \left(-\frac{3\zeta_2}{4} - \frac{7\zeta_3}{3} + 8\right) + n_f \left(\frac{\zeta_2}{6} - \frac{28}{27}\right) \right] \\
& + \epsilon^2 \left[N_c \left(-\frac{13\zeta_2}{36} + \frac{35\zeta_4}{16} - \frac{7\zeta_3}{9} + \frac{242}{81}\right) + \frac{1}{N_c} \left(-2\zeta_2 - \frac{47\zeta_4}{16} - \frac{7\zeta_3}{2} + 16\right) \right. \\
& \qquad \left. + n_f \left(\frac{5\zeta_2}{18} + \frac{7\zeta_3}{9} - \frac{164}{81}\right) \right] \\
& + \epsilon^3 \left[N_c \left(-\frac{26\zeta_2\zeta_3}{3} - \frac{20\zeta_2}{27} - \frac{47\zeta_4}{48} + \frac{36\zeta_5}{5} - \frac{91\zeta_3}{54} + \frac{1456}{243}\right) \right.
\end{aligned}
$$

$$
\begin{aligned}
&+\frac{1}{N_c}\left(\frac{7\zeta_2\zeta_3}{6}-4\zeta_2-\frac{141\zeta_4}{32}-\frac{31\zeta_5}{5}-\frac{28\zeta_3}{3}+32\right)\\
&+n_f\left(\frac{14\zeta_2}{27}+\frac{47\zeta_4}{48}+\frac{35\zeta_3}{27}-\frac{976}{243}\right)\Bigg]\\
&+\epsilon^4\Bigg[\frac{1}{N_c}\left(\frac{7\zeta_2\zeta_3}{4}-8\zeta_2-\frac{47\zeta_4}{4}-\frac{93\zeta_5}{10}+\frac{49\zeta_3^2}{18}-\frac{56\zeta_3}{3}-\frac{949\pi^6}{120960}+64\right)\\
&+N_c\left(\frac{7\zeta_2\zeta_3}{18}-\frac{121\zeta_2}{81}-\frac{611\zeta_4}{288}-\frac{31\zeta_5}{15}-\frac{91\zeta_3^2}{18}-\frac{280\zeta_3}{81}-\frac{977\pi^6}{120960}+\frac{8744}{729}\right)\\
&+n_f\left(-\frac{7\zeta_2\zeta_3}{18}+\frac{82\zeta_2}{81}+\frac{235\zeta_4}{144}+\frac{31\zeta_5}{15}+\frac{196\zeta_3}{81}-\frac{5840}{729}\right)\Bigg]+\mathcal{O}(\epsilon^5)\,,
\end{aligned}
\tag{A.5}
$$

$$
\begin{aligned}
\mathcal{I}_2^q=&-\frac{3N_c^2\zeta_2}{2\epsilon^2}+N_c^2\left(\frac{87\zeta_2}{4}+\frac{25\zeta_4}{16}+\frac{41\zeta_3}{9}+\frac{22537}{2592}\right)+\frac{1}{N_c^2}\left(\frac{21\zeta_2}{4}-\frac{83\zeta_4}{16}-\frac{15\zeta_3}{2}+\frac{255}{32}\right)\\
&+N_cn_f\left(-4\zeta_2-\frac{23\zeta_3}{9}-\frac{650}{81}\right)+\frac{n_f}{N_c}\left(-\zeta_2-\frac{19\zeta_3}{9}-\frac{505}{81}\right)+\frac{25n_f^2}{54}+\frac{19\zeta_2}{2}\\
&-\frac{47\zeta_4}{8}-\frac{205\zeta_3}{18}+\frac{28787}{648}\\
&+\epsilon\Bigg[N_c^2\left(\frac{161\zeta_2\zeta_3}{6}+\frac{4055\zeta_2}{144}+\frac{587\zeta_4}{12}+\frac{49\zeta_5}{2}+\frac{898\zeta_3}{27}+\frac{911797}{15552}\right)+n_f^2\left(\frac{140}{81}-\frac{5\zeta_2}{18}\right)\\
&+\frac{1}{N_c^2}\left(\frac{49\zeta_2\zeta_3}{6}+\frac{325\zeta_2}{16}-\frac{201\zeta_4}{16}-3\zeta_5-\frac{166\zeta_3}{3}+\frac{2157}{64}\right)\\
&+N_cn_f\left(-\frac{61\zeta_2}{36}-\frac{247\zeta_4}{24}-\frac{85\zeta_3}{27}-\frac{36031}{972}\right)-\frac{5507\zeta_3}{54}+\frac{746543}{3888}\\
&+\frac{n_f}{N_c}\left(-\frac{13\zeta_2}{4}-\frac{83\zeta_4}{24}-\frac{17\zeta_3}{27}-\frac{11983}{486}\right)+13\zeta_2\zeta_3+\frac{115\zeta_2}{8}-\frac{1283\zeta_4}{48}+\frac{121\zeta_5}{2}\Bigg]\\
&+\epsilon^2\Bigg[N_c^2\left(-\frac{3613\zeta_2\zeta_3}{18}+\frac{5131\zeta_2}{864}+\frac{31811\zeta_4}{288}+\frac{94\zeta_5}{5}-\frac{293\zeta_3^2}{18}+\frac{12007\zeta_3}{648}+\frac{3251\pi^6}{120960}\right.\\
&\left.+\frac{23246941}{93312}\right)+N_cn_f\left(\frac{625\zeta_2\zeta_3}{18}+\frac{1475\zeta_2}{108}-\frac{779\zeta_4}{72}-\frac{143\zeta_5}{5}+\frac{1993\zeta_3}{81}-\frac{805855}{5832}\right)\\
&+\frac{1}{N_c^2}\left(10\zeta_2\zeta_3+\frac{2287\zeta_2}{32}-\frac{5627\zeta_4}{64}-\frac{9\zeta_5}{2}+\frac{1255\zeta_3^2}{18}-\frac{6205\zeta_3}{24}+\frac{7193\pi^6}{120960}+\frac{13575}{128}\right)\\
&+\frac{n_f}{N_c}\left(\frac{31\zeta_2\zeta_3}{9}-\frac{45\zeta_2}{4}-\frac{503\zeta_4}{144}-\frac{151\zeta_5}{15}+\frac{623\zeta_3}{81}-\frac{227023}{2916}\right)\\
&+n_f^2\left(-\frac{53\zeta_2}{54}+\frac{5\zeta_4}{48}-\frac{35\zeta_3}{27}+\frac{404}{81}\right)+\frac{1613\zeta_2\zeta_3}{36}+\frac{197\zeta_2}{24}-\frac{27175\zeta_4}{144}+\frac{791\zeta_5}{30}\\
&+\frac{1621\zeta_3^2}{18}-\frac{170951\zeta_3}{324}+\frac{17\pi^6}{70}+\frac{16114247}{23328}\Bigg]+\mathcal{O}(\epsilon^3)\,,
\end{aligned}
\tag{A.6}
$$

$$\begin{aligned}\mathcal{I}_1^g = {} & N_c\left(4\zeta_2 - \frac{67}{18}\right) + \frac{5n_f}{9} + \epsilon\left[N_c\left(\frac{17\zeta_3}{3} + \frac{11\zeta_2}{12} - \frac{202}{27}\right) + n_f\left(-\frac{\zeta_2}{6} + \frac{28}{27}\right)\right] \\ & + \epsilon^2\left[N_c\left(\frac{41\zeta_4}{8} + \frac{77\zeta_3}{18} + \frac{67\zeta_2}{36} - \frac{1214}{81}\right) + n_f\left(-\frac{7\zeta_3}{9} - \frac{5\zeta_2}{18} + \frac{164}{81}\right)\right] \\ & + \epsilon^3\left[N_c\left(-\frac{59\zeta_2\zeta_3}{6} + \frac{67\zeta_5}{5} + \frac{517\zeta_4}{96} + \frac{469\zeta_3}{54} + \frac{101\zeta_2}{27} - \frac{7288}{243}\right)\right. \\ & \left. + n_f\left(-\frac{47\zeta_4}{48} - \frac{35\zeta_3}{27} - \frac{14\zeta_2}{27} + \frac{976}{243}\right)\right] \\ & + \epsilon^4\left[N_c\left(-\frac{\pi^6}{4320} - \frac{70\zeta_3^2}{9} - \frac{77\zeta_2\zeta_3}{36} + \frac{341\zeta_5}{30} + \frac{3149\zeta_4}{288} + \frac{1414\zeta_3}{81} + \frac{607\zeta_2}{81} - \frac{43736}{729}\right)\right. \\ & \left. + n_f\left(\frac{7\zeta_2\zeta_3}{18} - \frac{31\zeta_5}{15} - \frac{235\zeta_4}{144} - \frac{196\zeta_3}{81} - \frac{82\zeta_2}{81} + \frac{5840}{729}\right)\right] + \mathcal{O}(\epsilon^5)\,,\end{aligned} \tag{A.7}$$

$$\begin{aligned}\mathcal{I}_2^g = {} & -\frac{3N_c^2\zeta_2}{2\epsilon^2} + N_c^2\left(\frac{9\zeta_4}{4} + \frac{88\zeta_3}{9} + \frac{335\zeta_2}{18} - \frac{26675}{648}\right) + N_c n_f\left(\frac{2\zeta_3}{9} - \frac{25\zeta_2}{9} + \frac{2063}{216}\right) \\ & + \frac{n_f}{N_c}\left(2\zeta_3 - \frac{55}{24}\right) - \frac{25n_f^2}{162} \\ & + \epsilon\left[N_c^2\left(22\zeta_2\zeta_3 - 39\zeta_5 + \frac{275\zeta_4}{4} + \frac{1865\zeta_3}{18} + \frac{3191\zeta_2}{72} - \frac{98671}{648}\right)\right. \\ & + N_c n_f\left(-\frac{19\zeta_4}{2} - \frac{157\zeta_3}{9} - \frac{871\zeta_2}{108} + \frac{149033}{3888}\right) \\ & \left. + \frac{n_f}{N_c}\left(3\zeta_4 + \frac{19\zeta_3}{3} + \frac{\zeta_2}{4} - \frac{1711}{144}\right) + n_f^2\left(\frac{5\zeta_2}{54} - \frac{140}{243}\right)\right] \\ & + \epsilon^2\left[N_c^2\left(-\frac{4733\pi^6}{30240} - \frac{659\zeta_3^2}{18} - \frac{8987\zeta_2\zeta_3}{36} - \frac{187\zeta_5}{5} + \frac{16103\zeta_4}{64} + \frac{121859\zeta_3}{324} + \frac{71263\zeta_2}{648}\right.\right. \\ & \left. - \frac{6140957}{11664}\right) + N_c n_f\left(\frac{781\zeta_2\zeta_3}{18} + \frac{104\zeta_5}{5} - \frac{5803\zeta_4}{144} - \frac{5698\zeta_3}{81} - \frac{1645\zeta_2}{72} + \frac{3197809}{23328}\right) \\ & + \frac{n_f}{N_c}\left(-2\zeta_2\zeta_3 + 14\zeta_5 + \frac{19\zeta_4}{2} + \frac{197\zeta_3}{9} + \frac{55\zeta_2}{24} - \frac{42727}{864}\right) \\ & \left. + n_f^2\left(-\frac{5\zeta_4}{144} + \frac{35\zeta_3}{81} + \frac{53\zeta_2}{162} - \frac{404}{243}\right)\right] + \mathcal{O}(\epsilon^3)\,.\end{aligned} \tag{A.8}$$

B

Spinor Helicity Formulas and Conventions

Below are collected some conventions and identities involved in the spinor helicity formalism. We start by defining the anti-symmetric Levi-Civita tensors

$$\epsilon^{\alpha\beta} = -\epsilon_{\alpha\beta} = \begin{pmatrix} 0 & 1 \\ -1 & 0 \end{pmatrix} \quad \text{and} \quad \epsilon^{\dot{\alpha}\dot{\beta}} = -\epsilon_{\dot{\alpha}\dot{\beta}} = \begin{pmatrix} 0 & 1 \\ -1 & 0 \end{pmatrix} , \tag{B.1}$$

which lower/raise spinor indices and satisfy

$$\epsilon_{\alpha\beta}\epsilon^{\beta\gamma} = \delta_{\alpha}^{\gamma} . \tag{B.2}$$

The σ matrices are connected by the relation

$$\overline{\sigma}^{\mu,\dot{\alpha}\alpha} = \epsilon^{\alpha\beta}\epsilon^{\dot{\alpha}\dot{\beta}}\sigma^{\mu}_{\beta\dot{\beta}} \tag{B.3}$$

and satisfy the following set of identities

$$\sigma^{\mu}_{\alpha\dot{\alpha}}\sigma_{\mu,\beta\dot{\beta}} = 2\epsilon_{\alpha\beta}\epsilon_{\dot{\alpha}\dot{\beta}} , \tag{B.4}$$

$$\sigma^{\mu}_{\alpha\dot{\alpha}}\overline{\sigma}_{\mu}^{\dot{\beta}\beta} = 2\delta_{\alpha}^{\beta}\delta_{\dot{\alpha}}^{\dot{\beta}} , \tag{B.5}$$

$$\{\sigma^{\mu}, \overline{\sigma}^{\nu}\}_{\alpha}{}^{\beta} = 2\eta^{\mu\nu}\delta_{\alpha}^{\beta} , \tag{B.6}$$

$$\mathrm{Tr}(\sigma^{\mu}\overline{\sigma}^{\nu}) = \mathrm{Tr}(\overline{\sigma}^{\mu}\sigma^{\nu}) = 2\eta^{\mu\nu} . \tag{B.7}$$

The Dirac γ-matrices can be written in the spinor representation in terms of (2.12) in the following way:

$$\gamma^{\mu} = \begin{pmatrix} 0 & \sigma^{\mu}_{\alpha\dot{\beta}} \\ \overline{\sigma}^{\mu,\dot{\alpha}\beta} & 0 \end{pmatrix} , \tag{B.8}$$

where γ^μ is a 4 by 4 matrix and the entries are identified as $(1,2,3,4) = (1,2,\dot{1},\dot{2})$, where undotted indices α and β take the first two components and dotted indices $\dot{\alpha}$ and $\dot{\beta}$ take the second two components

This allows us to define the quantities

$$p_{\alpha\dot{\alpha}} = p_\mu \sigma^\mu_{\alpha\dot{\alpha}} = |p\rangle_\alpha [p|_{\dot{\alpha}}, \quad p^{\dot{\alpha}\alpha} = p_\mu \overline{\sigma}^{\mu,\dot{\alpha}\alpha} = |p]^{\dot{\alpha}} \langle p|^\alpha \tag{B.9}$$

and, using (B.3) and (B.4), one can see by direct computation that the inverse relations are

$$p^\mu = \frac{1}{2}\sigma^\mu_{\alpha\dot{\alpha}} p^{\dot{\alpha}\alpha} = \frac{1}{2}\sigma^\mu_{\alpha\dot{\alpha}} |p]^{\dot{\alpha}} \langle p|^\alpha, \quad p^\mu = \frac{1}{2}\overline{\sigma}^{\mu,\dot{\alpha}\alpha} p_{\alpha\dot{\alpha}} = \frac{1}{2}\overline{\sigma}^{\mu,\dot{\alpha}\alpha} |p\rangle_\alpha [p|_{\dot{\alpha}} \,. \tag{B.10}$$

C

Rational Coefficients of the All-Plus Amplitude

In this section we list the rational coefficients for the all-plus gluon amplitude of eq. (5.80). In terms of the variable $x = -s_{13}/s_{12}$ we find,

$$\begin{aligned}
\tilde{r}_5^+ &= \frac{1}{x} - \frac{1}{x^2} + \left(\frac{55}{6x^2} - \frac{193}{6x} - \frac{10}{x-1} - 1\right)\epsilon + \left(-\frac{92}{3x^2} + \frac{218}{3x} + \frac{82}{x-1} + \frac{49}{6}\right)\epsilon^2 \\
&\quad + \left(\frac{151}{3x^2} - \frac{205}{3x} - \frac{513}{2(x-1)} - 25\right)\epsilon^3 , \\
\tilde{r}_6^+ &= -\frac{1}{x^2} + x + \frac{3}{x} - 3 + \left(-10x^3 + 6x^2 + \frac{55}{6x^2} + \frac{191x}{6} - \frac{9}{2x} - \frac{65}{2}\right)\epsilon \\
&\quad + \left(82x^3 - \frac{1175x^2}{6} - \frac{92}{3x^2} + \frac{403x}{3} + \frac{50}{x} - \frac{239}{6}\right)\epsilon^2 \\
&\quad + \left(-\frac{513x^3}{2} + \frac{1453x^2}{2} + \frac{151}{3x^2} - \frac{4295x}{6} - \frac{133}{x} + \frac{657}{2}\right)\epsilon^3 , \\
\tilde{r}_7^+ &= 6 - \frac{6}{x} + \left(3x + \frac{55}{x} - 55\right)\epsilon + \left(-\frac{79x}{2} - \frac{184}{x} + 184\right)\epsilon^2 + \left(\frac{291x}{2} + \frac{302}{x} - 302\right)\epsilon^3 , \\
\tilde{r}_8^+ &= -\frac{1}{x^2} + \frac{2}{x} - 1 + \left(\frac{55}{6x^2} - x - \frac{118}{3x} + \frac{247}{6}\right)\epsilon + \left(-\frac{92}{3x^2} + \frac{49x}{6} + \frac{87}{x} - \frac{253}{2}\right)\epsilon^2 \\
&\quad + \left(\frac{151}{3x^2} - 25x - \frac{221}{3x} + \frac{1205}{6}\right)\epsilon^3 , \\
\tilde{r}_9^+ &= -\frac{1}{x^2} + \frac{2}{x} - 1 + \left(10x^2 + \frac{55}{6x^2} + \frac{8}{3x} - \frac{131}{6}\right)\epsilon + \left(-62x^2 - \frac{92}{3x^2} + \frac{213x}{2} + \frac{107}{3x} - \frac{99}{2}\right)\epsilon^2 \\
&\quad + \left(\frac{305x^2}{2} + \frac{151}{3x^2} - 357x - \frac{383}{3x} + \frac{1691}{6}\right)\epsilon^3 , \\
\tilde{r}_{10}^+ &= \frac{1}{x^2} - \frac{1}{x} + \left(-\frac{55}{6x^2} + \frac{193}{6x} - \frac{5}{x-1} - 41\right)\epsilon + \left(\frac{92}{3x^2} - \frac{218}{3x} + \frac{11}{x-1} + \frac{767}{6}\right)\epsilon^2
\end{aligned}$$

$$+\left(-\frac{151}{3x^2}+\frac{x}{2}+\frac{231}{4(x-1)}+\frac{205}{3x}-\frac{117}{2}\right)\epsilon^3\,,$$

$$\begin{aligned}
\tilde{r}_{11}^{+} &= \frac{1}{x^2}-x-\frac{3}{x}+3+\left(-5x^3-3x^2-\frac{55}{6x^2}+\frac{43x}{6}+\frac{9}{2x}+\frac{11}{2}\right)\epsilon \\
&+\left(11x^3+\frac{317x^2}{6}+\frac{92}{3x^2}-\frac{382x}{3}-\frac{50}{x}+\frac{497}{6}\right)\epsilon^2 \\
&+\left(\frac{231x^3}{4}-\frac{853x^2}{4}-\frac{151}{3x^2}+\frac{3433x}{12}+\frac{133}{x}-\frac{853}{4}\right)\epsilon^3\,, \\
\tilde{r}_{12}^{+} &= \frac{6}{x^2}-\frac{12}{x}+6+\left(30x^2-\frac{55}{x^2}+21x+\frac{92}{x}-118\right)\epsilon+\left(-126x^2+\frac{184}{x^2}-19x-\frac{221}{x}+368\right)\epsilon^2 \\
&+\left(\frac{51x^2}{2}-\frac{302}{x^2}-198x+\frac{199}{x}-182\right)\epsilon^3\,, \\
\tilde{r}_{13}^{+} &= \frac{6}{x}-\frac{6}{x^2}+\left(\frac{55}{x^2}-30x+\frac{30}{x-1}-\frac{73}{x}+129\right)\epsilon+\left(-\frac{184}{x^2}+186x-\frac{126}{x-1}+\frac{331}{x}-604\right)\epsilon^2 \\
&+\left(\frac{302}{x^2}-\frac{915x}{2}+\frac{51}{2(x-1)}-\frac{707}{x}+\frac{1431}{2}\right)\epsilon^3\,.
\end{aligned} \tag{C.1}$$

Terms of $\mathcal{O}(\epsilon^4)$ do not contribute to the finite part of the amplitude. The overall coefficient reads,

$$C(\epsilon)=\frac{16}{(-3+2\epsilon)^2(-1+2\epsilon)^2(-2+3\epsilon)(-1+3\epsilon)}\,. \tag{C.2}$$

References

[1] V. N. Gribov. "Quantization of Nonabelian Gauge Theories". In: *Nucl. Phys. B* 139 (1978). Ed. by J. Nyiri, p. 1.

[2] L. D. Faddeev and V. N. Popov. "Feynman Diagrams for the Yang-Mills Field". In: *Phys. Lett. B* 25 (1967). Ed. by Jong-Ping Hsu and D. Fine, pp. 29–30.

[3] Steven Weinberg. *The quantum theory of fields. Vol. 2: Modern applications*. Cambridge University Press, Aug. 2013.

[4] C. A. Baker et al. "Improved Experimental Limit on the Electric Dipole Moment of the Neutron". In: *Physical Review Letters* 97.13 (2006). URL: http://dx.doi.org/10.1103/PhysRevLett.97.131801.

[5] C. Abel et al. "Measurement of the Permanent Electric Dipole Moment of the Neutron". In: *Physical Review Letters* 124.8 (Feb. 2020). URL: http://dx.doi.org/10.1103/PhysRevLett.124.081803.

[6] Gerard 't Hooft and M. J. G. Veltman. "Regularization and Renormalization of Gauge Fields". In: *Nucl. Phys. B* 44 (1972), pp. 189–213.

[7] C. Becchi, A. Rouet, and R. Stora. "Renormalization of Gauge Theories". In: *Annals Phys.* 98 (1976), pp. 287–321.

[8] I. V. Tyutin. "Gauge Invariance in Field Theory and Statistical Physics in Operator Formalism". In: (1975). arXiv: 0812.0580 [hep-th].

[9] William E. Caswell. "Asymptotic Behavior of Nonabelian Gauge Theories to Two Loop Order". In: *Phys. Rev. Lett.* 33 (1974), p. 244.

[10] D. R. T. Jones. "Two Loop Diagrams in Yang-Mills Theory". In: *Nucl. Phys. B* 75 (1974), p. 531.

[11] O. V. Tarasov, A. A. Vladimirov, and A. Yu. Zharkov. "The Gell-Mann-Low Function of QCD in the Three Loop Approximation". In: *Phys. Lett. B* 93 (1980), pp. 429–432.

[12] S. A. Larin and J. A. M. Vermaseren. "The Three loop QCD Beta function and anomalous dimensions". In: *Phys. Lett. B* 303 (1993), pp. 334–336. arXiv: hep-ph/9302208.

[13] T. van Ritbergen, J. A. M. Vermaseren, and S. A. Larin. "The Four loop beta function in quantum chromodynamics". In: *Phys. Lett. B* 400 (1997), pp. 379–384. arXiv: hep-ph/9701390.

[14] M. Czakon. "The Four-loop QCD beta-function and anomalous dimensions". In: *Nucl. Phys. B* 710 (2005), pp. 485–498. arXiv: hep-ph/0411261.

[15] Particle Data Group et al. "Review of Particle Physics". In: *Progress of Theoretical and Experimental Physics* 2022.8 (Aug. 2022). _eprint: https://academic.oup.com/ptep/article-pdf/2022/8/083C01/49175539/ptac097.pdf, p. 083C01. URL: https://doi.org/10.1093/ptep/ptac097.

[16] H. Lehmann, K. Symanzik, and W. Zimmermann. "On the formulation of quantized field theories". In: *Nuovo Cim.* 1 (1955), pp. 205–225.

[17] H. Lehmann, K. Symanzik, and W. Zimmermann. "On the formulation of quantized field theories. II". In: *Nuovo Cim.* 6 (1957), pp. 319–333.

[18] Niklas Beisert et al. "Review of AdS/CFT Integrability: An Overview". In: *Lett. Math. Phys.* 99 (2012), pp. 3–32. arXiv: 1012.3982 [hep-th].

[19] Ruth Britto et al. "Direct proof of tree-level recursion relation in Yang-Mills theory". In: *Phys. Rev. Lett.* 94 (2005), p. 181602. arXiv: hep-th/0501052.

[20] Frits A. Berends and W. T. Giele. "Recursive Calculations for Processes with n Gluons". In: *Nucl. Phys. B* 306 (1988), pp. 759–808.

[21] Zvi Bern et al. "One loop n point gauge theory amplitudes, unitarity and collinear limits". In: *Nucl. Phys. B* 425 (1994), pp. 217–260. arXiv: hep-ph/9403226.

[22] Zvi Bern et al. "Fusing gauge theory tree amplitudes into loop amplitudes". In: *Nucl. Phys. B* 435 (1995), pp. 59–101. arXiv: hep-ph/9409265.

[23] R. Keith Ellis et al. "Masses, fermions and generalized D-dimensional unitarity". In: *Nucl. Phys. B* 822 (2009), pp. 270–282. arXiv: 0806.3467 [hep-ph].

[24] R. Keith Ellis et al. "One-loop calculations in quantum field theory: from Feynman diagrams to unitarity cuts". In: *Phys.Rept.* 518 (2012), pp. 141–250. arXiv: 1105.4319 [hep-ph].

[25] R. E. Cutkosky. "Singularities and discontinuities of Feynman amplitudes". In: *J. Math. Phys.* 1 (1960), pp. 429–433.

[26] Zvi Bern, Abilio De Freitas, and Lance J. Dixon. "Two loop helicity amplitudes for gluon-gluon scattering in QCD and supersymmetric Yang-Mills theory". In: *JHEP* 03 (2002), p. 018. arXiv: hep-ph/0201161.

[27] S. Abreu et al. "Two-Loop Four-Gluon Amplitudes from Numerical Unitarity". In: *Phys. Rev. Lett.* 119.14 (2017), p. 142001. arXiv: 1703.05273 [hep-ph].

[28] Tiziano Peraro and Lorenzo Tancredi. "Physical projectors for multi-leg helicity amplitudes". In: *JHEP* 07 (2019), p. 114. arXiv: 1906.03298 [hep-ph].

[29] Tiziano Peraro and Lorenzo Tancredi. "Tensor decomposition for bosonic and fermionic scattering amplitudes". In: *Phys. Rev. D* 103.5 (2021), p. 054042. arXiv: 2012.00820 [hep-ph].

[30] Gavin Cullen, Maciej Koch-Janusz, and Thomas Reiter. "Spinney: A Form Library for Helicity Spinors". In: *Comput. Phys. Commun.* 182 (2011), pp. 2368–2387. arXiv: 1008.0803 [hep-ph].

[31] S. Catani and M. H. Seymour. "The Dipole formalism for the calculation of QCD jet cross-sections at next-to-leading order". In: *Phys. Lett. B* 378 (1996), pp. 287–301. arXiv: hep-ph/9602277.

[32] S. Catani and M. H. Seymour. "A General algorithm for calculating jet cross-sections in NLO QCD". In: *Nucl. Phys. B* 485 (1997). [Erratum: Nucl.Phys.B 510, 503–504 (1998)], pp. 291–419. arXiv: hep-ph/9605323.

[33] Stefano Catani. "The Singular behavior of QCD amplitudes at two loop order". In: *Phys. Lett. B* 427 (1998), pp. 161–171. arXiv: hep-ph/9802439.

[34] Alexander C. Edison and Stephen G. Naculich. "SU(N) group-theory constraints on color-ordered five-point amplitudes at all loop orders". In: *Nucl. Phys. B* 858 (2012), pp. 488–501. arXiv: 1111.3821 [hep-th].

[35] Stefan Weinzierl. *Feynman Integrals*. Jan. 2022. arXiv: 2201.03593 [hep-th].

[36] A. von Manteuffel and C. Studerus. "Reduze 2 - Distributed Feynman Integral Reduction". In: (2012). arXiv: 1201.4330 [hep-ph].

[37] S. Laporta. "High precision calculation of multiloop Feynman integrals by difference equations". In: *Int. J. Mod. Phys. A* 15 (2000), pp. 5087–5159. arXiv: hep-ph/0102033.

[38] Francis Brown. "The Massless Higher-Loop Two-Point Function". In: *Communications in Mathematical Physics* 287.3 (Feb. 2009), pp. 925958. URL: http://dx.doi.org/10.1007/s00220-009-0740-5.

[39] Francis C. S. Brown. *On the periods of some Feynman integrals*. 2010. arXiv: 0910.0114 [math.AG].

[40] Erik Panzer. "Algorithms for the symbolic integration of hyperlogarithms with applications to Feynman integrals". In: *Comput. Phys. Commun.* 188 (2015), pp. 148–166. arXiv: 1403.3385 [hep-th].

[41] A. V. Kotikov. "Differential equations method: New technique for massive Feynman diagrams calculation". In: *Phys. Lett. B* 254 (1991), pp. 158–164.

[42] Nima Arkani-Hamed et al. "Local Integrals for Planar Scattering Amplitudes". In: *JHEP* 06 (2012), p. 125. arXiv: 1012.6032 [hep-th].

[43] Johannes M. Henn. "Multiloop integrals in dimensional regularization made simple". In: *Phys. Rev. Lett.* 110 (2013), p. 251601. arXiv: 1304.1806 [hep-th].

[44] A. V. Kotikov. "The property of maximal transcendentality: calculation of master integrals". In: *Theor. Math. Phys.* 176 (2013), pp. 913–921. arXiv: 1212.3732 [hep-ph].

[45] Kuo-Tsai Chen. "Iterated path integrals". In: *Bull.Am.Math.Soc.* 83 (1977), pp. 831–879.

[46] A. B. Goncharov. *Multiple polylogarithms, cyclotomy and modular complexes*. 2011. arXiv: 1105.2076 [math.AG].

[47] A. B. Goncharov et al. "Classical Polylogarithms for Amplitudes and Wilson Loops". In: *Phys. Rev. Lett.* 105 (15 2010), p. 151605. URL: https://link.aps.org/doi/10.1103/PhysRevLett.105.151605.

[48] F. J. Dyson. "The S matrix in quantum electrodynamics". In: *Phys. Rev.* 75 (1949), pp. 1736–1755.

[49] Steven Weinberg. "High-energy behavior in quantum field theory". In: *Phys. Rev.* 118 (1960), pp. 838–849.

[50] Y. Hahn and W. Zimmermann. "An elementary proof of Dyson's power counting theorem". In: *Commun. Math. Phys.* 10 (1968), pp. 330–342.

[51] W. Zimmermann. "The power counting theorem for Minkowski metric". In: *Commun. Math. Phys.* 11 (1968), pp. 1–8.

[52] Noboru Nakanishi. "General Integral Formula of Perturbation Term in the Quantized Field Theory". In: *Prog. Theor. Phys.* 17.3 (1957), pp. 401–418.

[53] Noboru Nakanishi. *Graph Theory and Feynman Integrals*. Gordon and Breach, 1971.

[54] L. D. Landau. "On analytic properties of vertex parts in quantum field theory". In: *Nucl. Phys.* 13.1 (1959), pp. 181–192.

[55] James Daniel Bjorken. "Experimental tests of Quantum electrodynamics and spectral representations of Green's functions in perturbation theory". PhD thesis. Stanford U., 1959.

[56] Noboru Nakanishi. "Ordinary and Anomalous Thresholds in Perturbation Theory". In: *Prog. Theor. Phys.* 22.1 (1959), pp. 128–144.

[57] Sebastian Mizera. "Crossing symmetry in the planar limit". In: *Phys. Rev. D* 104.4 (2021), p. 045003. arXiv: `2104.12776 [hep-th]`.

[58] Richard John Eden et al. *The analytic S-matrix*. Cambridge: Cambridge Univ. Press, 1966.

[59] Sebastian Mizera and Simon Telen. "Landau discriminants". In: *JHEP* 08 (2022), p. 200. arXiv: `2109.08036 [math-ph]`.

[60] Thomas Becher and Matthias Neubert. "Infrared singularities of scattering amplitudes in perturbative QCD". In: *Phys. Rev. Lett.* 102 (2009). [Erratum: Phys.Rev.Lett. 111, 199905 (2013)], p. 162001. arXiv: `0901.0722 [hep-ph]`.

[61] Thomas Becher and Matthias Neubert. "On the Structure of Infrared Singularities of Gauge-Theory Amplitudes". In: *JHEP* 06 (2009). [Erratum: JHEP 11, 024 (2013)], p. 081. arXiv: `0903.1126 [hep-ph]`.

[62] Einan Gardi and Lorenzo Magnea. "Factorization constraints for soft anomalous dimensions in QCD scattering amplitudes". In: *JHEP* 03 (2009), p. 079. arXiv: `0901.1091 [hep-ph]`.

[63] Einan Gardi and Lorenzo Magnea. "Infrared singularities in QCD amplitudes". In: *Nuovo Cim. C* 32N5-6 (2009). Ed. by Mario Greco, pp. 137–157. arXiv: `0908.3273 [hep-ph]`.

[64] Christian W. Bauer et al. "An Effective field theory for collinear and soft gluons: Heavy to light decays". In: *Phys. Rev. D* 63 (2001), p. 114020. arXiv: `hep-ph/0011336`.

[65] Christian W. Bauer, Dan Pirjol, and Iain W. Stewart. "Soft collinear factorization in effective field theory". In: *Phys. Rev. D* 65 (2002), p. 054022. arXiv: `hep-ph/0109045`.

[66] Christian W. Bauer et al. "Hard scattering factorization from effective field theory". In: *Phys. Rev. D* 66 (2002), p. 014017. arXiv: `hep-ph/0202088`.

[67] M. Beneke et al. "Soft collinear effective theory and heavy to light currents beyond leading power". In: *Nucl. Phys. B* 643 (2002), pp. 431–476. arXiv: hep-ph/0206152.

[68] Bakul Agarwal et al. "Four-loop collinear anomalous dimensions in QCD and N=4 super Yang-Mills". In: *Phys. Lett. B* 820 (2021), p. 136503. arXiv: 2102.09725 [hep-ph].

[69] Øyvind Almelid, Claude Duhr, and Einan Gardi. "Three-loop corrections to the soft anomalous dimension in multileg scattering". In: *Phys. Rev. Lett.* 117.17 (2016), p. 172002. arXiv: 1507.00047 [hep-ph].

[70] G. P. Korchemsky and A. V. Radyushkin. "Renormalization of the Wilson Loops Beyond the Leading Order". In: *Nucl. Phys. B* 283 (1987), pp. 342–364.

[71] S. Moch, J. A. M. Vermaseren, and A. Vogt. "The Three loop splitting functions in QCD: The Nonsinglet case". In: *Nucl. Phys. B* 688 (2004), pp. 101–134. arXiv: hep-ph/0403192.

[72] A. Vogt, S. Moch, and J. A. M. Vermaseren. "The Three-loop splitting functions in QCD: The Singlet case". In: *Nucl. Phys. B* 691 (2004), pp. 129–181. arXiv: hep-ph/0404111.

[73] Andrey Grozin et al. "Three Loop Cusp Anomalous Dimension in QCD". In: *Phys. Rev. Lett.* 114.6 (2015), p. 062006. arXiv: 1409.0023 [hep-ph].

[74] Johannes M. Henn, Gregory P. Korchemsky, and Bernhard Mistlberger. "The full four-loop cusp anomalous dimension in $\mathcal{N} = 4$ super Yang-Mills and QCD". In: *JHEP* 04 (2020), p. 018. arXiv: 1911.10174 [hep-th].

[75] Tobias Huber et al. "The four-loop cusp anomalous dimension from the $N = 4$ Sudakov form factor". In: *Phys. Lett. B* 807 (2020), p. 135543. arXiv: 1912.13459 [hep-th].

[76] Andreas von Manteuffel, Erik Panzer, and Robert M. Schabinger. "Cusp and collinear anomalous dimensions in four-loop QCD from form factors". In: *Phys. Rev. Lett.* 124.16 (2020), p. 162001. arXiv: 2002.04617 [hep-ph].

[77] V. Ravindran, J. Smith, and W. L. van Neerven. "Two-loop corrections to Higgs boson production". In: *Nucl. Phys. B* 704 (2005), pp. 332–348. arXiv: hep-ph/0408315.

[78] S. Moch, J. A. M. Vermaseren, and A. Vogt. "The Quark form-factor at higher orders". In: *JHEP* 08 (2005), p. 049. arXiv: hep-ph/0507039.

[79] S. Moch, J.A.M. Vermaseren, and A. Vogt. "Three-loop results for quark and gluon form-factors". In: *Phys. Lett. B* 625 (2005), pp. 245–252. arXiv: hep-ph/0508055.

[80] Giulio Falcioni et al. "Scattering amplitudes in the Regge limit and the soft anomalous dimension through four loops". In: (Nov. 2021). arXiv: 2111.10664 [hep-ph].

[81] Fabrizio Caola et al. "Three-loop helicity amplitudes for four-quark scattering in massless QCD". In: *JHEP* 10 (2021), p. 206. arXiv: 2108.00055 [hep-ph].

[82] Fabrizio Caola et al. "Three-Loop Gluon Scattering in QCD and the Gluon Regge Trajectory". In: *Phys. Rev. Lett.* 128.21 (2022), p. 212001. arXiv: 2112.11097 [hep-ph].

[83] Fabrizio Caola et al. "Three-loop helicity amplitudes for quark-gluon scattering in QCD". In: *JHEP* 12 (2022), p. 082. arXiv: 2207.03503 [hep-ph].

[84] C. Studerus. "Reduze-Feynman Integral Reduction in C++". In: *Comput.Phys.Commun.* 181 (2010), pp. 1293–1300. arXiv: 0912.2546 [physics.comp-ph].

[85] S. Laporta. "High precision calculation of multiloop Feynman integrals by difference equations". In: *Int.J.Mod.Phys.* A15 (2000), pp. 5087–5159. arXiv: hep-ph/0102033 [hep-ph].

[86] Andreas von Manteuffel and Robert M. Schabinger. "A novel approach to integration by parts reduction". In: *Phys. Lett.* B744 (2015), pp. 101–104. arXiv: 1406.4513 [hep-ph].

[87] Andreas von Manteuffel and Robert M. Schabinger. "Quark and gluon form factors to four-loop order in QCD: the N_f^3 contributions". In: *Phys. Rev.* D95.3 (2017), p. 034030. arXiv: 1611.00795 [hep-ph].

[88] Tiziano Peraro. "Scattering amplitudes over finite fields and multivariate functional reconstruction". In: *JHEP* 12 (2016), p. 030. arXiv: 1608.01902 [hep-ph].

[89] Tiziano Peraro. "FiniteFlow: multivariate functional reconstruction using finite fields and dataflow graphs". In: *JHEP* 07 (2019), p. 031. arXiv: 1905.08019 [hep-ph].

[90] Janusz Gluza, Krzysztof Kajda, and David A. Kosower. "Towards a Basis for Planar Two-Loop Integrals". In: *Phys. Rev. D* 83 (2011), p. 045012. arXiv: 1009.0472 [hep-th].

[91] Robert M. Schabinger. "A New Algorithm For The Generation Of Unitarity-Compatible Integration By Parts Relations". In: *JHEP* 01 (2012), p. 077. arXiv: 1111.4220 [hep-ph].

[92] Harald Ita. "Two-loop Integrand Decomposition into Master Integrals and Surface Terms". In: *Phys. Rev.* D94.11 (2016), p. 116015. arXiv: 1510.05626 [hep-th].

[93] Kasper J. Larsen and Yang Zhang. "Integration-by-parts reductions from unitarity cuts and algebraic geometry". In: *Phys. Rev.* D93.4 (2016), p. 041701. arXiv: 1511.01071 [hep-th].

[94] Janko Böhm et al. "Complete sets of logarithmic vector fields for integration-by-parts identities of Feynman integrals". In: *Phys. Rev. D* 98.2 (2018), p. 025023. arXiv: 1712.09737 [hep-th].

[95] Bakul Agarwal and Andreas Von Manteuffel. "On the two-loop amplitude for $gg \to ZZ$ production with full top-mass dependence". In: *PoS* RADCOR2019 (2019), p. 008. arXiv: 1912.08794 [hep-ph].

[96] Johannes Henn et al. "Constructing d-log integrands and computing master integrals for three-loop four-particle scattering". In: *JHEP* 04 (2020), p. 167. arXiv: 2002.09492 [hep-ph].

[97] Piotr Bargiela et al. "Three-loop helicity amplitudes for diphoton production in gluon fusion". In: (Nov. 2021). arXiv: 2111.13595 [hep-ph].

[98] Taushif Ahmed, Johannes Henn, and Bernhard Mistlberger. "Four-particle scattering amplitudes in QCD at NNLO to higher orders in the dimensional regulator". In: *JHEP* 12 (2019), p. 177. arXiv: 1910.06684 [hep-ph].

[99] Johannes M. Henn and Bernhard Mistlberger. "Four-Gluon Scattering at Three Loops, Infrared Structure, and the Regge Limit". In: *Phys. Rev. Lett.* 117.17 (2016), p. 171601. arXiv: 1608.00850 [hep-th].

[100] E. Remiddi and J.A.M. Vermaseren. "Harmonic polylogarithms". In: *Int.J.Mod.Phys.* A15 (2000), pp. 725–754. arXiv: hep-ph/9905237 [hep-ph].

[101] D Maitre. "HPL, a mathematica implementation of the harmonic polylogarithms". In: *Comput. Phys. Commun.* 174 (2006), pp. 222–240. arXiv: hep-ph/0507152.

[102] Fabio Cascioli, Philipp Maierhofer, and Stefano Pozzorini. "Scattering Amplitudes with Open Loops". In: *Phys.Rev.Lett.* 108 (2012), p. 111601. arXiv: 1111.5206 [hep-ph].

[103] Federico Buccioni et al. "OpenLoops 2". In: *Eur. Phys. J. C* 79.10 (2019), p. 866. arXiv: 1907.13071 [hep-ph].

[104] Simon Caron-Huot. "When does the gluon reggeize?" In: *JHEP* 05 (2015), p. 093. arXiv: 1309.6521 [hep-th].

[105] Simon Caron-Huot, Einan Gardi, and Leonardo Vernazza. "Two-parton scattering in the high-energy limit". In: *JHEP* 06 (2017), p. 016. arXiv: 1701.05241 [hep-ph].

[106] P. D. B. Collins. *An Introduction to Regge Theory and High-Energy Physics*. Cambridge Monographs on Mathematical Physics. Cambridge, UK: Cambridge Univ. Press, May 2009.

[107] L. N. Lipatov. "Reggeization of the Vector Meson and the Vacuum Singularity in Nonabelian Gauge Theories". In: *Sov. J. Nucl. Phys.* 23 (1976), pp. 338–345.

[108] E. A. Kuraev, L. N. Lipatov, and Victor S. Fadin. "Multi - Reggeon Processes in the Yang-Mills Theory". In: *Sov. Phys. JETP* 44 (1976), pp. 443–450.

[109] Victor S. Fadin and L. N. Lipatov. "Radiative corrections to QCD scattering amplitudes in a multi - Regge kinematics". In: *Nucl. Phys. B* 406 (1993), pp. 259–292.

[110] Vladimir N. Gribov. *Strong interactions of hadrons at high emnergies: Gribov lectures on Theoretical Physics*. Ed. by Yuri L. Dokshitzer and Julia Nyiri. Cambridge University Press, Oct. 2012.

[111] V. N. Gribov. *The theory of complex angular momenta: Gribov lectures on theoretical physics*. Cambridge Monographs on Mathematical Physics. Cambridge University Press, June 2007.

[112] Vittorio Del Duca et al. "High-energy QCD amplitudes at two loops and beyond". In: *Phys. Lett. B* 732 (2014), pp. 233–240. arXiv: 1311.0304 [hep-ph].

[113] Vittorio Del Duca et al. "Analyzing high-energy factorization beyond next-to-leading logarithmic accuracy". In: *JHEP* 02 (2015), p. 029. arXiv: 1409.8330 [hep-ph].

[114] Vittorio Del Duca and E. W. Nigel Glover. "The High-energy limit of QCD at two loops". In: *JHEP* 10 (2001), p. 035. arXiv: hep-ph/0109028.

[115] Vittorio Del Duca and E. W. N. Glover. "Testing high-energy factorization beyond the next-to-leading-logarithmic accuracy". In: *JHEP* 05 (2008), p. 056. arXiv: 0802.4445 [hep-th].

[116] V. S. Fadin. "Particularities of the NNLLA BFKL". In: *AIP Conf. Proc.* 1819.1 (2017). Ed. by Marcella Capua et al., p. 060003. arXiv: 1612.04481 [hep-ph].

[117] V. S. Fadin and L. N. Lipatov. "Reggeon cuts in QCD amplitudes with negative signature". In: *Eur. Phys. J. C* 78.6 (2018), p. 439. arXiv: 1712.09805 [hep-ph].

[118] Giulio Falcioni et al. "Disentangling the Regge cut and Regge pole in perturbative QCD". In: (Dec. 2021). arXiv: 2112.11098 [hep-ph].

[119] Victor S. Fadin, R. Fiore, and M. I. Kotsky. "Gluon Regge trajectory in the two loop approximation". In: *Phys. Lett. B* 387 (1996), pp. 593–602. arXiv: hep-ph/9605357.

[120] J. Blumlein, V. Ravindran, and W. L. van Neerven. "On the gluon Regge trajectory in O alpha-s**2". In: *Phys. Rev. D* 58 (1998), p. 091502. arXiv: hep-ph/9806357.

[121] Vittorio Del Duca, Robin Marzucca, and Bram Verbeek. "The gluon Regge trajectory at three loops from planar Yang-Mills theory". In: (Nov. 2021). arXiv: 2111.14265 [hep-ph].

[122] Bakul Agarwal et al. "Five-Parton Scattering in QCD at Two Loops". In: (Nov. 2023). arXiv: 2311.09870 [hep-ph].

[123] Giuseppe De Laurentis et al. "Double-Virtual NNLO QCD Corrections for Five-Parton Scattering: The Gluon Channel". In: (Nov. 2023). arXiv: 2311.10086 [hep-ph].

[124] Giuseppe De Laurentis, Harald Ita, and Vasily Sotnikov. "Double-Virtual NNLO QCD Corrections for Five-Parton Scattering: The Quark Channels". In: (Nov. 2023). arXiv: 2311.18752 [hep-ph].

[125] Costas G. Papadopoulos, Damiano Tommasini, and Christopher Wever. "The Pentabox Master Integrals with the Simplified Differential Equations approach". In: *JHEP* 04 (2016), p. 078. arXiv: 1511.09404 [hep-ph].

[126] T. Gehrmann, J.M. Henn, and N.A. Lo Presti. "Pentagon functions for massless planar scattering amplitudes". In: *JHEP* 10 (2018), p. 103. arXiv: 1807.09812 [hep-ph].

[127] Samuel Abreu, Ben Page, and Mao Zeng. "Differential equations from unitarity cuts: nonplanar hexa-box integrals". In: *JHEP* 01 (2019), p. 006. arXiv: 1807.11522 [hep-th].

[128] D. Chicherin et al. "Analytic result for the nonplanar hexa-box integrals". In: *JHEP* 03 (2019), p. 042. arXiv: 1809.06240 [hep-ph].

[129] Samuel Abreu et al. "The two-loop five-point amplitude in $\mathcal{N} = 4$ super-Yang-Mills theory". In: *Phys. Rev. Lett.* 122.12 (2019), p. 121603. arXiv: 1812.08941 [hep-th].

[130] D. Chicherin et al. "All Master Integrals for Three-Jet Production at Next-to-Next-to-Leading Order". In: *Phys. Rev. Lett.* 123.4 (2019), p. 041603. arXiv: 1812.11160 [hep-ph].

[131] Dmitry Chicherin and Vasily Sotnikov. "Pentagon Functions for Scattering of Five Massless Particles". In: *JHEP* 20 (2020), p. 167. arXiv: 2009.07803 [hep-ph].

[132] Philipp Maierhöfer, Johann Usovitsch, and Peter Uwer. "Kira—A Feynman integral reduction program". In: *Comput. Phys. Commun.* 230 (2018), pp. 99–112. arXiv: 1705.05610 [hep-ph].

[133] Jonas Klappert et al. "Integral reduction with Kira 2.0 and finite field methods". In: *Comput. Phys. Commun.* 266 (2021), p. 108024. arXiv: 2008.06494 [hep-ph].

[134] Janko Boehm et al. "IBP reduction coefficients made simple". In: *JHEP* 12 (2020), p. 054. arXiv: 2008.13194 [hep-ph].

[135] Bakul Agarwal et al. "Two-loop leading colour QCD corrections to $q\bar{q} \to \gamma\gamma g$ and $qg \to \gamma\gamma q$". In: *JHEP* 04 (2021), p. 201. arXiv: 2102.01820 [hep-ph].

[136] Bakul Agarwal et al. "Two-loop helicity amplitudes for diphoton plus jet production in full color". In: (May 2021). arXiv: 2105.04585 [hep-ph].

[137] Wolfram Decker et al. SINGULAR *4-2-0 — A computer algebra system for polynomial computations*. http://www.singular.uni-kl.de. 2020.

[138] Zvi Bern, Lance J. Dixon, and David A. Kosower. "One loop corrections to five gluon amplitudes". In: *Phys. Rev. Lett.* 70 (1993), pp. 2677–2680. arXiv: hep-ph/9302280 [hep-ph].

[139] Zvi Bern, Lance J. Dixon, and David A. Kosower. "One loop corrections to two quark three gluon amplitudes". In: *Nucl. Phys. B* 437 (1995), pp. 259–304. arXiv: hep-ph/9409393.

[140] S. Badger et al. "Analytic form of the full two-loop five-gluon all-plus helicity amplitude". In: *Phys. Rev. Lett.* 123.7 (2019), p. 071601. arXiv: 1905.03733 [hep-ph].

[141] S. Abreu et al. "Leading-color two-loop QCD corrections for three-jet production at hadron colliders". In: *JHEP* 07 (2021), p. 095. arXiv: 2102.13609 [hep-ph].

[142] Stefano Catani. "The singular behaviour of QCD amplitudes at two-loop order". In: *Physics Letters B* 427.12 (May 1998), pp. 161171. URL: http://dx.doi.org/10.1016/S0370-2693(98)00332-3.

[143] https://zenodo.org/records/10227683.

[144] Charalampos Anastasiou and George Sterman. "Removing infrared divergences from two-loop integrals". In: *JHEP* 07 (2019), p. 056. arXiv: 1812.03753 [hep-ph].

[145] George F. Sterman. "Mass Divergences in Annihilation Processes. 1. Origin and Nature of Divergences in Cut Vacuum Polarization Diagrams". In: *Phys. Rev. D* 17 (1978), p. 2773.

[146] Stephen B. Libby and George F. Sterman. "Jet and Lepton Pair Production in High-Energy Lepton-Hadron and Hadron-Hadron Scattering". In: *Phys. Rev. D* 18 (1978), p. 3252.

[147] Stephen B. Libby and George F. Sterman. "Mass Divergences in Two Particle Inelastic Scattering". In: *Phys. Rev. D* 18 (1978), p. 4737.

[148] Einan Gardi et al. "The on-shell expansion: from Landau equations to the Newton polytope". In: *JHEP* 07 (2023), p. 197. arXiv: 2211.14845 [hep-th].

[149] Z. Bern, Lance J. Dixon, and D. A. Kosower. "A Two loop four gluon helicity amplitude in QCD". In: *JHEP* 01 (2000), p. 027. arXiv: hep-ph/0001001.

[150] Z. Bern, A. De Freitas, and Lance J. Dixon. "Two loop amplitudes for gluon fusion into two photons". In: *JHEP* 09 (2001), p. 037. arXiv: hep-ph/0109078.

[151] E. W. Nigel Glover, C. Oleari, and M. E. Tejeda-Yeomans. "Two loop QCD corrections to gluon-gluon scattering". In: *Nucl. Phys. B* 605 (2001), pp. 467–485. arXiv: hep-ph/0102201.

[152] Simon Caron-Huot and Kasper J. Larsen. "Uniqueness of two-loop master contours". In: *JHEP* 10 (2012), p. 026. arXiv: 1205.0801 [hep-ph].